

3-18-2019

Cationic Cobalt (II) Hydroformylation

Drew Michael Hood

Louisiana State University and Agricultural and Mechanical College, dhood4@lsu.edu

Follow this and additional works at: https://digitalcommons.lsu.edu/gradschool_dissertations



Part of the [Inorganic Chemistry Commons](#)

Recommended Citation

Hood, Drew Michael, "Cationic Cobalt (II) Hydroformylation" (2019). *LSU Doctoral Dissertations*. 4882.
https://digitalcommons.lsu.edu/gradschool_dissertations/4882

This Dissertation is brought to you for free and open access by the Graduate School at LSU Digital Commons. It has been accepted for inclusion in LSU Doctoral Dissertations by an authorized graduate school editor of LSU Digital Commons. For more information, please contact gradetd@lsu.edu.

CATIONIC COBALT (II) HYDROFORMYLATION

A Dissertation

Submitted to the Graduate Faculty of the
Louisiana State University and
Agricultural and Mechanical College
in partial fulfillment of the
requirements for the degree of
Doctor of Philosophy

in

The Department of Chemistry

by
Drew Michael Hood
B.S. McNeese State University, 2014
May 2019

Acknowledgments

First and foremost I would like to thank my wonderful wife Leiflyn Gamborg who could not have been more supportive during this entire process. I love you and I could not have done any of this without you. To my advising professor, Dr. George Stanley, you have been the best teacher a student could ask for and I will always appreciate the knowledge and guidance you have given me. I must also thank Dr. George Stanley for the continued financial support throughout my graduate career. To my lab mate Ryan Johnson, you helped to make this whole process more enjoyable. I will always look back on the days of us working in the lab fondly. To Marshall Moulis, thank you for all the training and companionship you provided at the beginning of my graduate career. To my father, mother, father in-law and mother in-law you have all been very supportive of my endeavors and this entire process has been made easier by your support. To everyone mentioned above I cannot say how much I appreciate everything you have done for me.

I would like to thank the members of my committee, Dr. Weiwei Xie, Dr. Gerald Schneider, and Dr. Ingmar Schoegl for your patience and flexibility. I thank Dr. Connie David in the Mass Spec facility, Dr. Thomas Weldeghiorghis in the NMR facility, and Dr. Frank Fronczek in the X-ray crystallography lab for each of their assistance in analysis of various materials and understanding of the processes. Thank you for your time and your attribution to my research. Finally I must thank all of the sources that have funded this work including the Louisiana Board of Regents, the LSU LIFT2 fund, Dow chemical, and Exxon Mobil.

Table of Contents

Acknowledgments.....	ii
List of Abbreviations	v
Abstract.....	vii
Chapter 1. Hydroformylation of Olefins.....	1
1.1. Discovery of Hydroformylation.....	1
1.2. Applications of Aldehyde Products	4
1.3. Cobalt Based Hydroformylation	7
1.4. Rhodium Based Hydroformylation.....	8
1.5. References.....	11
Chapter 2. Discovery and Characterization of a Cationic Cobalt (II) Hydroformylation Catalyst	14
2.1. Introduction.....	14
2.2. Discovery of Cationic Cobalt Hydroformylation Catalyst	16
2.3. Cationic Cobalt Pre-catalyst Characterization	19
2.4. Cationic Cobalt Catalyst Characterization.....	28
2.5. References.....	46
Chapter 3. Catalyst Modifications	48
3.1. Introduction.....	48
3.2. Effects of Complex Charge on Catalytic Activity	49
3.3. Alternative Ligands.....	51
3.4. Effects of Modifying Chelating Bisphosphine Ligands.....	55
3.5. References.....	60
Chapter 4. Reaction Condition Optimization.....	62
4.1. Introduction.....	62
4.2. Effects of Varying Temperature	63
4.3. Effects of Pressure	66
4.4. Solvent Effects	68
4.5. Catalyst Stability	71
4.6. References.....	78
Chapter 5. Hydroformylation using Cationic Cobalt Catalysts with Different Alkenes	80
5.1. Introduction.....	80
5.2. Alfa Olefin Hydroformylation	82
5.3. Internal and Branched Olefin Hydroformylation.....	86
5.4. References.....	90
Chapter 6. Experimental Procedures.....	91
6.1. General Considerations.....	91

6.2. General Hydroformylation Procedure.....	94
6.3. [Co(acac)(dioxane) _x]BF ₄ Synthesis.....	95
6.4. [Co(acac)(ligand)]BF ₄ Synthesis.....	96
6.5. Co(acac) ₂ DPPBz Synthesis.....	96
6.6. [CoDPPBz](BF ₄) ₂ Synthesis.....	97
Vita.....	98

List of Abbreviations

DEPBz	1,2-Bis(diethylphosphino)benzene
DPPBz	1,2-Bis(diphenylphosphino)benzene
dppm	1,2-Bis(diphenylphosphino)methane
dppe	1,2-Bis(diphenylphosphino)ethane
depe	1,2-Bis(diethylphosphino)ethane
d(i-Pr)pe	1,2-Bis(di-i-propylphosphino)ethane
d(Cy)pe	1,2-Bis(dicyclohexylphosphino)ethane
dppp	1,2-Bis(diphenylphosphino)propane
dppb	1,2-Bis(diphenylphosphino)butane
dppNaph	1,8-(Diphenylphosphino)naphthalene
PPh ₃	Triphenylphosphine
PBu ₃	Tri-n-butylphosphine
biphenphos	6,6'-[(3,3'-Di-t-butyl-5,5'-dimethoxy-1,1'-biphenyl-2,2'-diyl)bis(oxy)] bis(dibenzo[d,f][1,3,2]dioxaphosphin)
iso	Isomerization
hydro	Hydrogenation
L:B	Linear to branch ratio
psi	Pounds per square inch
TOF	Turn over frequency
mL	Milliliter
M	Molar
mM	Millimolar
NMR	Nuclear magnetic resonance

Ppm	Parts per million
EPR	Electron paramagnetic resonance
MS	Mass spectrometry
GC/MS	Gas chromatography mass spectrometry
FTIR	Fourier-transform infrared spectroscopy
CO	Carbon monoxide
min	Minute
hr	Hour
<i>meso</i>	<i>mesomeric</i>
<i>rac</i>	<i>racemic</i>

Abstract

While investigating a bimetallic cobalt hydroformylation catalyst a new class of monometallic cationic cobalt (II) hydroformylation catalyst were discovered. These newly discovered catalyst proved to be very unique with high hydroformylation activity under mild conditions. The pre-catalyst were characterized using various methods including NMR, EPR, MS, and X-ray crystallography. Similarly the active catalyst was also investigated using NMR, EPR, FTIR, and X-ray crystallography. Various catalyst modifications were investigated for their effects on hydroformylation activity. Likewise various reaction parameters were probed to determine their effect on hydroformylation activity. Finally the best cationic cobalt (II) catalyst were directly compared to industry standards for various alkenes to establish an idea of the industrial application of this catalyst system.

Chapter 1. Hydroformylation of Olefins

1.1. Discovery of Hydroformylation

In 1938 Otto Roelen was working on Fischer-Tropsch synthesis in the laboratories of Ruhrchemie AG at Oberhausen, Germany. In an attempt to increase the chain length of Fischer-Tropsch products he recycled the primarily generated alkene (olefin) and passed a mixture of the alkene and synthesis gas with ethylene over a fixed bed of cobalt containing catalyst. The products that Roelen observed were not the longer chained alkenes but contained trace amounts of aldehydes – a product not produced via Fischer-Tropsch catalysis. Roelen had just discovered a new reaction that he called the “oxo reaction,” also known as hydroformylation. The catalyst was later identified as $\text{HCo}(\text{CO})_4$ that was generated from reaction of cobalt metal with H_2/CO . This reaction would prove to be one of the first industrially important homogeneously catalyzed reactions.¹

Hydroformylation is a reaction in which an alkene and a mixture of hydrogen and carbon monoxide (synthesis gas) react to produce an aldehyde depicted in Figure 1.1. Since the catalyst is dissolved in the same phase as the reagents it is considered a homogeneous reaction. If the aldehyde produced is the one position it is said to be linear or normal. If the resulting aldehyde is not in the one position it is said to be branched or iso. The linear to branched (L:B) or normal to iso ratio is of great importance in hydroformylation as the linear products generally have a higher market value. Side reactions include alkene isomerization and alkene hydrogenation both of which are usually not desired as they tend result in lower value products than the starting reagents.² Alkene isomerization can be important when working with internal alkenes as the isomerization can move the double bond to the 1-position, leading to a better chance of getting the linear aldehyde product.

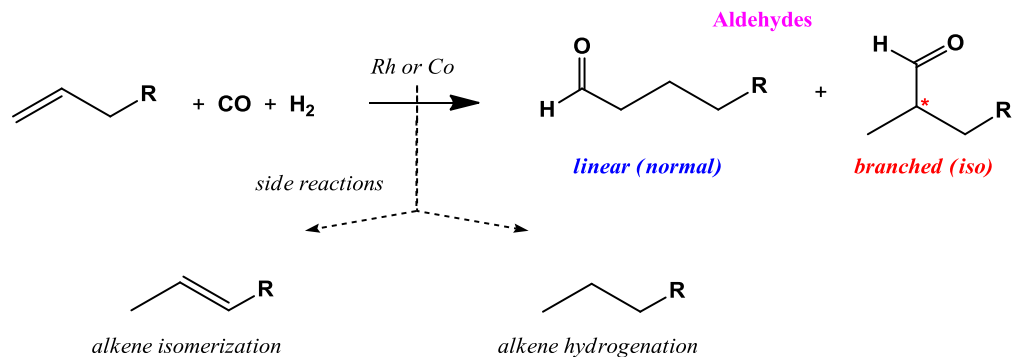


Figure 1.1. Hydroformylation catalysis

The original hydroformylation catalyst discovered by Roelen was $\text{HCo}(\text{CO})_4$, formed from cobalt metal under the high temperature and H_2/CO pressure that Roelen used. The mechanism developed by Heck and Brewslow depicts the formation of the active catalyst followed by the catalytic cycle illustrated in Figure 1.2.³

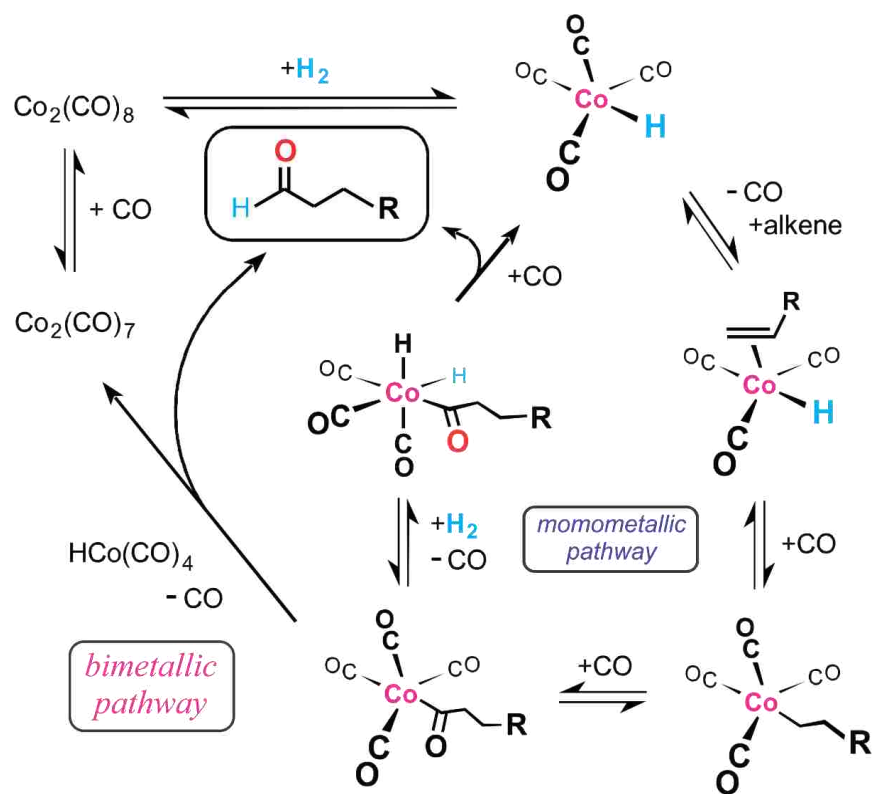


Figure 1.2. Heck and Brewslow's catalytic cycle for hydroformylation by $\text{HCo}(\text{CO})_4$.

The cycle involves the dissociation of a carbonyl group from the active species and the addition of an alkene. The hydride then undergoes a migratory insertion with the alkene to form an alkyl followed by the addition of a carbonyl. The alkyl then undergoes a migratory insertion with the carbonyl forming an acyl group followed by the addition of another carbonyl. Then a carbonyl must dissociate followed by the oxidative addition of hydrogen to generate a dihydride complex. Then the acyl and one of the hydrides undergo a reductive elimination to produce the aldehyde followed by the addition of a carbonyl to regenerate the starting catalyst. The bimetallic pathway is considered a minor one and is of little importance here. This catalytic cycle is still the accepted general catalytic pathway by which all metals proceed during hydroformylation.

Work with other unmodified metals produced an activity hierarchy for metal centers with the most active for hydroformylation on the left (Rh) and the least active on the right (Ni).



Additionally other metals have been claimed to have activity towards hydroformylation including Mo, Cr, Mn, and Tc. Furthermore; platinum has been shown to be of particular interest in asymmetric hydroformylation. However; rates and lifetimes for metals other than rhodium, cobalt are very low and, therefore; only rhodium and cobalt are used in commercial hydroformylation plants.³

In addition to metals, alkenes were also tested for their hydroformylation activity. The series shown in Figure 1.3 shows the effect of double bond placement and alkene structure on hydroformylation activity. Clearly moving the double bond internally decreases activity, as well as increasing the alkene's steric bulk via branching. The resulting effect is that linear terminal olefins are the most active and internal branched are the least active for hydroformylation regardless of the catalyst used.⁴

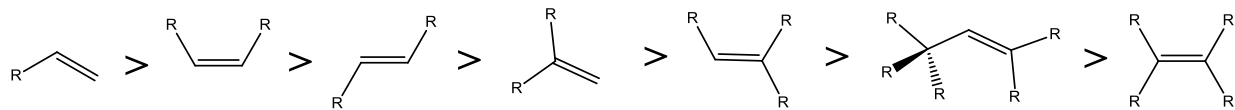


Figure 1.3. Alkene activity for all hydroformylation catalyst

1.2. Applications of aldehyde products.

Initially hydroformylation was of little importance industrially since alkene sources were limited to natural resources or Fischer-Tropsch synthesis neither of which allowed for cheap large scale production. However; this would not last as in the late 1940's, approximately 10 years after Roelen's discovery two major changes to the chemical industry paved the way for large scale hydroformylation. The first was the growth of the petrochemical industry that produced cheap alkene feedstocks that offered increased availability and quality. The second was the development of the polyvinylchloride (PVC) and detergent industries that would rely heavily on hydroformylation products. The combination of cheap alkene feedstocks and a growing market to sell aldehyde-derived products dramatically increased the value of hydroformylation as a large-scale industrial process. The market did grow into an industry that produced 10.4 million metric tons of product in 2008 making it one of the largest homogeneously catalyzed reactions in industry.^{1,2}

Currently the uses for aldehyde products stretch far beyond PVC and detergents, albeit both industries are still large and account for a significant portion of the market. Aldehydes from hydroformylation are usually converted to carboxylic acids, esters, amines or alcohols - all of which find uses in a broad range of industries (Figure1.4).²

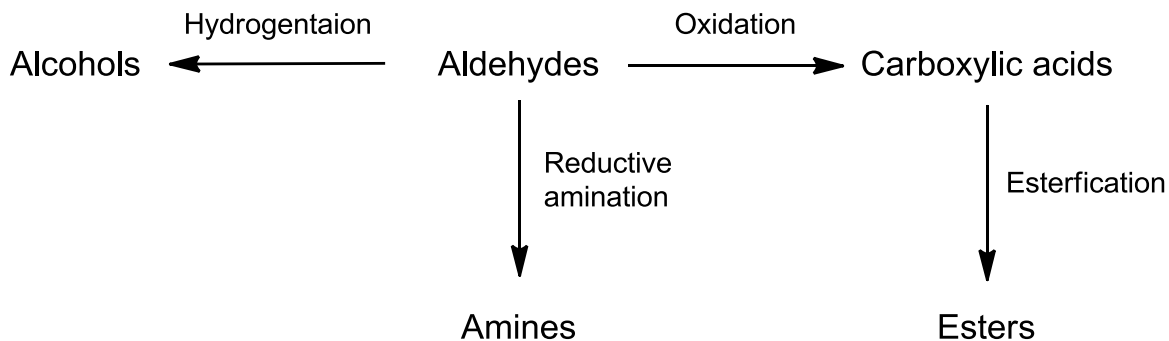


Figure 1.4. Products derived from aldehydes

The largest single product is 2-ethyl hexanol (2-EH), which is produced via aldol condensation of *n*-butyraldehyde, the product of propylene hydroformylation. 2-ethyl hexanol is used along with isononyl alcohol and phthalic anhydride as plasticizers for polyvinyl chloride plastics.⁶

There are a few major hydroformylation processes that are worth mentioning in more detail. The first being the production of linear aldehydes namely the production of *n*-butanal, which is mainly used to produce 2-ethyl-hexanol that is mostly converted into plasticizers. This process is usually carried out using a triphenylphosphine (PPh₃) rhodium catalyst because of the high catalyst activity under low syngas pressure and the high linear to branch selectivity of the catalyst. The high linear to branch is required because the butanal is subjected to aldol condensation to produce a longer chain alcohol. Branched aldehydes will not self-condensate so starting with a linear aldehyde is important for this chemistry.

Another major hydroformylation process is the conversion of isooctenes to isononanol for plasticizer products. This process relies on the high activity of the unmodified cobalt catalyst, HCo(CO)₄, to hydroformylate far less reactive internal and branched alkenes that make up a large portion of the alkene feed. This process does not require a condensation step and produces plasticizers with lower pour points than 2-ethyl-hexanol plasticizers - a feature that is desirable in some plastic applications. Unfortunately in order to maintain the stability and activity of

$\text{HCo}(\text{CO})_4$ the reaction conditions used for this process are harsh with temperatures of about 150-180°C and pressures of about 250 to 350 bar (3625-5076 psig). $\text{HCo}(\text{CO})_4$ readily decomposes to cobalt metal as the temperature increases. The CO partial pressure needs to be increased logarithmically as the temperature increases for this catalyst system. Such high-pressure conditions drastically increase the cost of building and maintaining a chemical plant based on $\text{HCo}(\text{CO})_4$. ExxonMobil runs the high-pressure $\text{HCo}(\text{CO})_4$ catalyst technology in its Baton Rouge plant.

The third major hydroformylation process is the production of detergent grade alcohols from internal linear olefins. This was developed by Shell and is tied to their Shell Higher Olefin Process (SHOP) in which ethylene is first oligomerized into a broad distribution of 1-alkenes (C_4 to C_{40}). The 1-alkenes are separated and the middle fraction marketed as longer chain alpha-olefins. The short and longer chain 1-alkenes are metathesized to generate a C_{12-18} mixture of internal alkenes. These are then hydroformylated and converted into linear alcohols with long chain lengths for the production of detergents. A phosphine modified cobalt catalyst, $\text{HCo}(\text{CO})_3(\text{PR}_3)$, is employed that gives 8:1 L:B aldehydes and alcohols despite the alkene feed having internal double bonds. This is because both the $\text{HCo}(\text{CO})_4$ and phosphine-modified, $\text{HCo}(\text{CO})_3(\text{PR}_3)$, catalysts are very active at alkene isomerization. 1-alkenes, as mentioned earlier are the most active for hydroformylation, so when the catalyst isomerizes an internal double bond to the 1-position, this hydroformylates much more quickly and produces the linear product. The Shell phosphine-modified cobalt catalyst uses a large sterically bulky alkylated phosphine that that favors the linear product.

While the pressure required for this process is much lower than for unmodified cobalt at approximately 50 to 150 bar (725-2175 psig) the temperature requirements are higher at

approximately 180-220°C. The higher linear to branch ratio is needed by Shell because linear detergents make the best surfactants in addition to being biodegradable.⁶

Many other processes are employed to produce a large array of products on smaller scales. Several ingredients in the perfume industry are produced via hydroformylation such as 2-methyl-undecanal a highly desired fragrance used in the famous Chanel No5.⁷ Lubricants are another sector in which hydroformylation is employed to produce products such as 1-tridecanol. Although like many lubricants, 1-tridecanol has other alternative uses such as an ingredient in surfactants, ink solvents, and pesticides. Aldehydes produced via hydroformylation indirectly have application across the entire chemical industry.⁶

1.3. Cobalt Based Hydroformylation

The $\text{HCo}(\text{CO})_4$ catalyst, often referred to as the unmodified or high-pressure cobalt catalyst, was used for the first generation of industrial hydroformylation processes with differences between industrial processes being limited mainly to how the catalyst is recycled. Difficulty with catalyst recycle was one of the caveats of the unmodified cobalt carbonyl catalyst and is usually a significant problem with most homogeneously catalyzed reactions. However; the process also suffered from harsh reaction conditions requiring temperatures of 160 to 250°C and pressures from 20 to 35 MPa (2900-5076 psig, 200-300 bar). Nevertheless this technology is used by several companies for many years and is in use today here in Baton Rouge at the ExxonMobil petrochemical complex due the high catalyst activity toward internal branched alkenes that they use and the extent to which the technology is well developed.^{1,6,8}

The need for a better catalyst that operated under milder conditions and with higher linear to branched (L:B) aldehyde regioselectivity was apparent and in the 1960s researchers at Shell discovered a phosphine-modified cobalt catalyst that had better L:B selectivity and operated

under milder conditions. Shell replaced one of the carbonyls with a phosphine ligand, which stabilized the catalyst with respect to decomposition to cobalt metal. The new catalyst runs under lower pressures of 50 to 150 bar (725-2175 psig) and temperatures of 160-200°C. Importantly, the phosphine-modified cobalt catalyst produced higher L:B ratios of 8:1 for the aldehydes produced, compared to only 2 to 3:1 for $\text{HCo}(\text{CO})_4$.⁸

The donating phosphine ligand not only stabilizes the Co-CO bonding, which resists decomposition to cobalt metal, but it also makes the hydride more hydridic and active for hydrogenation of aldehyde to alcohol. This is Shell's desired product, so the aldehyde hydrogenation activity is highly desired. However, the increased hydrogenation activity of the $\text{HCo}(\text{CO})_3(\text{PR}_3)$ catalyst also increases the highly undesired side reaction of hydrogenation of alkene to alkane. The much lower activity of the phosphine-modified cobalt catalyst necessitates running with high catalyst concentrations, which Shell has engineered its reactors to handle. This process is currently run by Shell in Geismar, LA and is tightly associated to the Shell Higher Olefin Process (SHOP, discussed earlier). Aside from the Shell work, and a few examples in the literature, very little research has been done on modified cobalt hydroformylation catalysts to date.^{1,2,6,8,9}

1.4. Rhodium Based Hydroformylation

In the 1960's Osborn, Young, and Wilkinson discovered that catalysts from rhodium instead of cobalt not only yielded much higher activity, but under significantly milder conditions.¹⁰⁻¹² This discovery spawned the third generation of hydroformylation processes that would be known as the low pressure oxo processes (LPO). The new process combined the more active rhodium metal center with excess PPh_3 to generate a highly active and selective hydroformylation catalyst system. This new rhodium phosphine catalyst allowed for

temperatures in the range of 60-150°C and pressures from 10 to 20 bar (147-294 psig). Additionally the rhodium phosphine catalyst gave L:B ratios that were >9:1 and could be tuned by changing the PPh₃ concentration. Another major advantage of rhodium phosphine catalyst was the lower production of side products. The first commercial process was launched in 1974 and Rh/PPh₃ technology now accounts for about 75% of the hydroformylation market.¹

Rhodium based catalysts have been shown to be significantly more active than cobalt based catalysts – a reactivity difference of 1000 is often stated. Despite this the accepted catalytic cycle essentially mirrors that of Heck’s proposed cycle for cobalt based catalyst, shown in Figure 1.5.

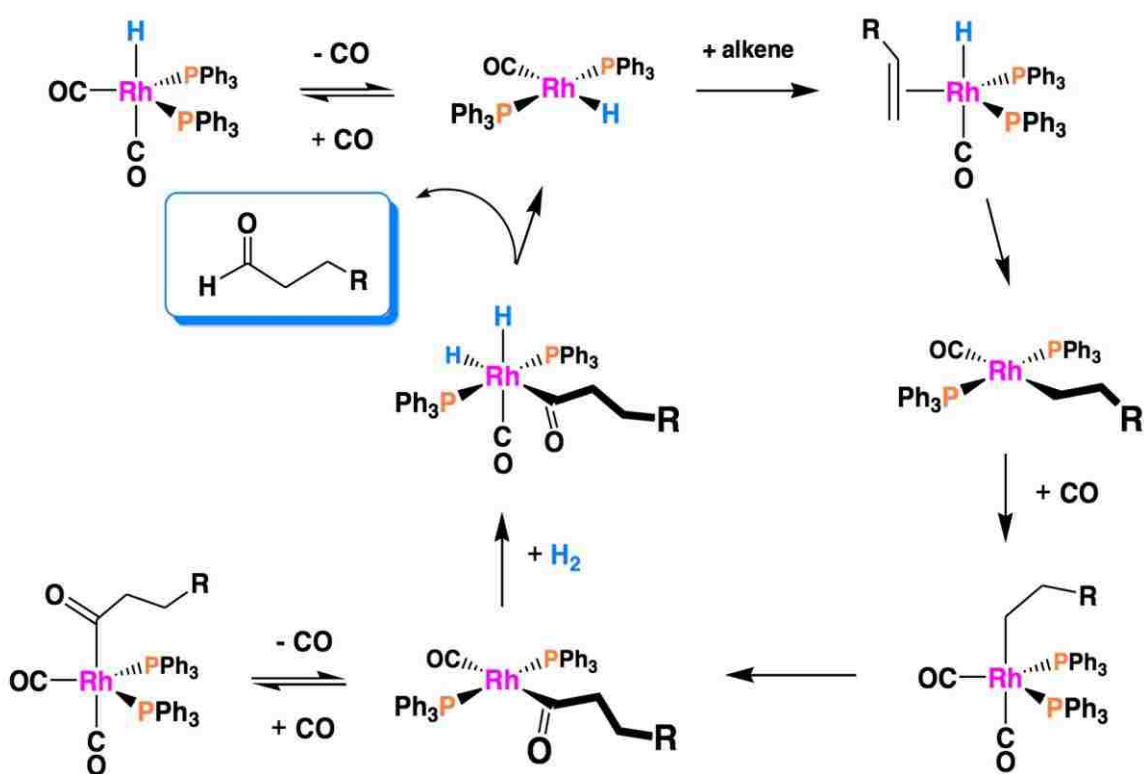


Figure 1.5. Catalytic cycle for rhodium hydroformylation

One key feature seen in this mechanism is the fact that two phosphines are bound at the same time. This is believed to be the key species that gives rise to the higher linear to branch ratio (L:B) seen with rhodium hydroformylation. Figure 1.6 details the different catalyst species that can exist in solution depending on the PPh₃ and CO concentrations as well as the respective activity of each catalyst.

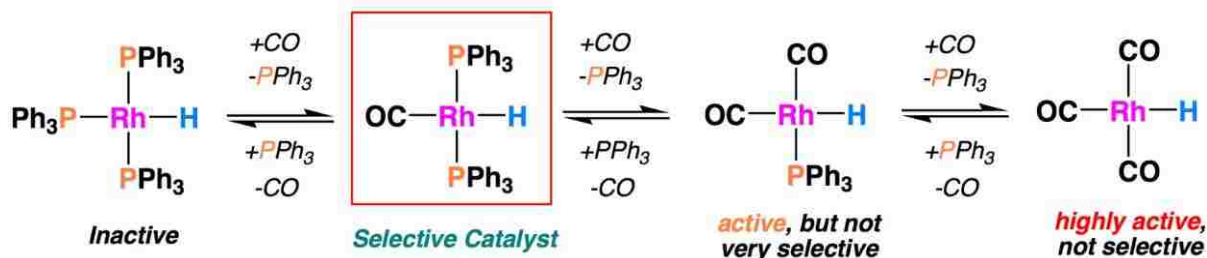


Figure 1.6. PPh₃/CO equilibrium for the rhodium catalyst

Extensive research has been done on the phosphine-modified rhodium hydroformylation catalyst since the initial observations by Wilkinson - in fact almost all current hydroformylation literature revolves around trying to develop new and better ligands for rhodium hydroformylation. The low pressure conditions and high activity make it relatively easy to study by academic researchers. Arguably the most successful alternative ligands to PPh₃ have been bisphosphine chelating ligands, the most popular of which are shown in Figure 1.7. One common trait among the different ligands are their large bite angles and steric factors that favor catalysts that are highly selective for linear aldehydes.¹³⁻¹⁹

All of the ligands shown in Figure 1.7 are very active and selective under mild conditions, however; excess ligand is still needed and since the ligands are significantly more expensive than PPh₃ they are not very competitive for commercial applications. This is amplified when considering degradation of ligand by impurities in the alkene feed as well as metal centered ligand degradation reactions are common in rhodium based hydroformylation. These

reactions further increase the amount of ligand and catalyst needed to keep a reactor running and therefore have to be considered when evaluating cost.

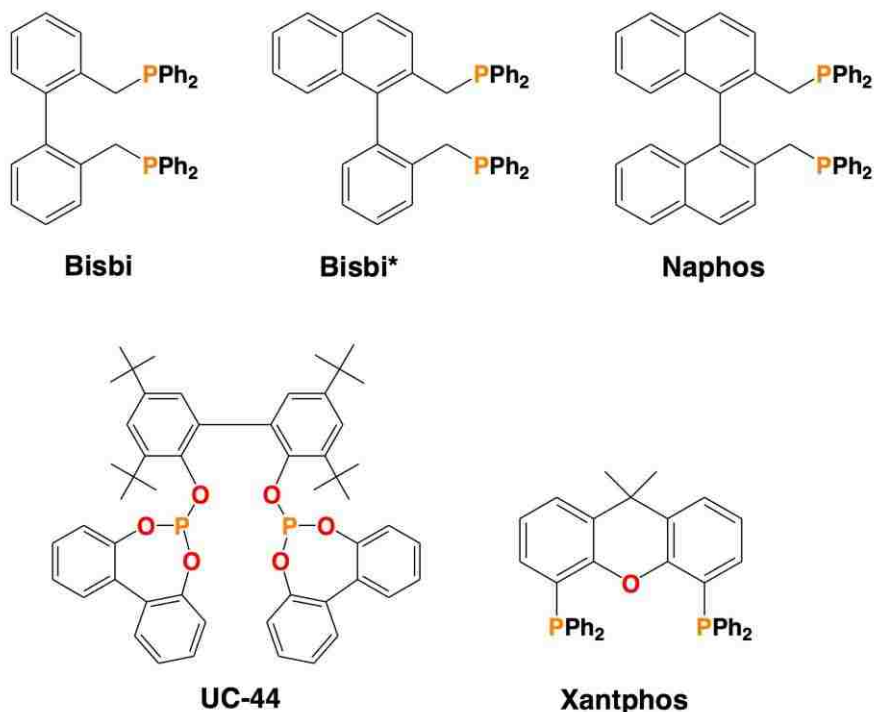


Figure 1.7. Commercially designed chelating phosphine ligands

UC-44 is a bisphosphite, not a phosphine, making it unique among the ligands depicted in Figure 1.7. Phosphite ligands produce the most active ligand-modified rhodium catalysts, while still achieving high aldehyde linear selectivity. Interestingly rhodium phosphite catalyst are also reasonably good isomerization catalysts. Even when using an internal alkene high linear selectivity can be achieved thanks to the isomerization activity of the catalyst. Unfortunately the phosphorus oxygen bonds on the phosphite are prone to hydrolysis and will even react with the aldehyde product. They are also susceptible to Rh-induced oxidative cleavage reactions. This leads to short catalyst lifetimes and greatly hinders industrial applications of this technology.²⁰⁻²²

1.5. References

1. Cornils, B.; Herrmann, W. A. *Applied Homogeneous Catalysis with Organometallic Compounds*. Wiley: 2002.

2. Franke, R.; Selent, D.; Borner, A. Applied Hydroformylation. *Chem. Rev.* **2012**, 112, 5675.
3. Pruchnik, F.P. *Organometallic Chemistry of Transition Elements*. Plenum Press: 1990.
4. Heck, R. F.; Breslow, D. S., The Reaction of Cobalt Hydrotetracarbonyl with Olefins. *J. Am. Chem. Soc.* **1961**, 83, 4023.
5. Botteghi, C.; Ganzerla, R.; Lenarda, M.; Moretti, G. Advances in the hydroformylation of olefins containing functional groups. *J. Mol. Catal.* **1987**, 40, 129.
6. Bhaduri, S.; Mukesh, D. *Homogeneous Catalysis: Mechanisms and Industrial Applications*. Wiley: 2014.
7. Surburg, H.; Panten, J. *Common Fragrance and Flavor Materials*. Wiley:2006.
8. Hebrard, F.; Kalck, P. Cobalt-Catalyzed Hydroformylation of Alkenes: Generation and Recycling of the Carbonyl Species, and Catalytic Cycle. *Chem. Rev.* **2009**, 109, 4272.
9. Tucci, E.R. Organophosphorus Complexes of Cobalt Carbonyl as Hydroformylation Catalyst. *I&CE*. **1969**, 8, 286.
10. Osborn, J. A.; Wilkinson, G.; Young, J. F., Mild Hydroformylation of Olefins using Rhodium Catalysts. *Chem. Commun.* **1965**, 0, 17.
11. Evans, D.; Osborn, J. A., Hydroformylation of Alkenes by Use of Rhodium Complex Catalysts. *J. Chem. Soc. A.* **1968**, 0, 3133.
12. Brown, C. K.; Wilkinson, G., Homogeneous Hydroformylation of Alkenes with Hydridocarbonyltris(triphenylphosphine)rhodium(I) as Catalyst. *J. Chem. Soc. A.* **1970**, 0, 2753.
13. Gillespie, J.; Dodds D.L.; Kamer P.J.C., Rational design of diphosphorus ligands – a route to superior catalysts. *Dalton Trans.*, **2010**, 39, 2751.
14. Dierkes, P. and van Leeuwen, P.W.N.M. The bite angle makes the difference: a practical ligand parameter for diphosphine ligands. *Dalton Trans.*, **1999**, 1519.
15. Van Leeuwen, P.W.N.M., Kamer, P.C.J., Reek, J.N.H., and Dierkes, P., Ligand Bite Angle Effects in Metal-catalyzed C–C Bond Formation. *Chem. Rev.*, **2000**. 100, 2741.
16. Kamer, P.C.J., van Leeuwen, P.W.N.M., and Reek, J.N.H. Wide Bite Angle Diphosphines: Xantphos Ligands in Transition Metal Complexes and Catalysis. *Acc. Chem. Res.* **2001**, 34, 895.

17. Kranenburg, M., van der Burgt, Y.E.M., Kamer, P.C.J., van Leeuwen, P.W.N.M., Goubitz, K., and Fraanje, J., New Diphosphine Ligands Based on Heterocyclic Aromatics Inducing Very High Regioselectivity in Rhodium-Catalyzed Hydroformylation: Effect of the Bite Angle. *Organometallics*, **1995**, 14, 3081.
18. Bahrmann, H., Bergrath, K., Kleiner, H.-J., Lappe, P., Naumann, C., Peters, D., and Regnat, D., Synthesis of linear aldehydes from internal olefins in water. *J. Organomet. Chem.*, **1996**, 520, 97.
19. Garrou, P.E. Transition-metal-mediated phosphorus-carbon bond cleavage and its relevance to homogeneous catalyst deactivation. *Chem. Rev.*, **1985**, 85, 171.
20. Gerrard, W. and Hudson, H.R. *Organic Phosphorus Compounds*, Wiley-Interscience, 1973, pp. 41–42.
21. Johnson, B., Keck-Antoine, K., Dejolier, B., Allen, N., Ortuoste, N., and Edge, M. Impact of improved phosphite hydrolytic stability on the processing stabilization of polypropylene. *J. Vinyl Add. Tech.*, **2005**, 11, 136.
22. Aksnes, G. and Aksnes, D. Kinetics and Mechanism of the Reaction of Tripropyl Phosphite with Water in Acetonitrile. *Acta Chim. Scand.*, **1964**, 18, 1623.

Chapter 2. Discovery and Characterization of a Cationic Cobalt (II) Hydroformylation Catalyst

2.1. Introduction

The Stanley group has previously set out to further rhodium hydroformylation by making a bimetallic catalyst where two rhodium centers work together to produce superior catalytic activity. Partial success was found using the P4 ligand depicted in Figure 2.1. The dirhodium catalyst hydroformylation system based on the P4 ligand was seen to have higher activities and selectivities than traditional Rh/PPh₃ catalysts, without the need for excess ligand.^{1,2} However; the original P4-ligand had too weak of a chelate effect leading to loss of one of the rhodium centers and catalyst deactivation. A new version of P4 was designed the synthesized in an attempt to improve the chelating ability of the P4 ligand and make a more robust dirhodium hydroformylation catalyst.³ The original ligand is now referred to by the group as the old P4 ligand and the subsequently modified ligand is known as the new P4-Ph (or et,ph-P4-Ph) ligand (Figure 2.1) due to the much stronger chelating 1,2-phenylene groups. Work is currently underway with the new P4 ligand dirhodium dicationic catalyst, which does appear to have a much stronger chelate, but now suffers from rhodium-induced ligand degradation reactions.

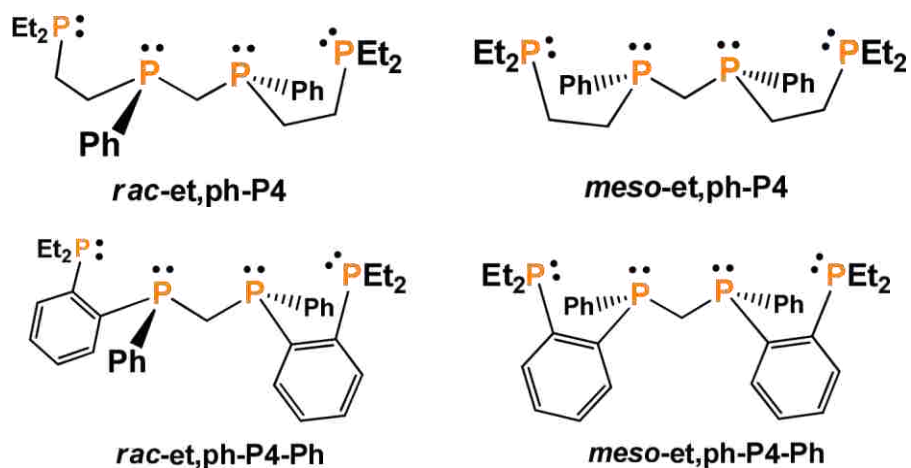


Figure 2.1. Old (top) and new (bottom) P₄ ligands

After the success the Stanley group had with the bimetallic rhodium hydroformylation catalyst a bimetallic cobalt catalyst was proposed. Given that the rhodium bimetallic catalyst was better than the monometallic systems, perhaps the bimetallic cobalt complex would show bimetallic cooperativity that would make it superior to monometallic cobalt catalysts. Ranelka Fernando in our group did extensive DFT calculations on both the dirhodium and proposed dicobalt dicationic catalysts. She calculated a mechanism for the dicobalt P₄ catalyst that was very similar to the dirhodium catalyst, which is shown in Figure 2.2. The dicobalt catalyst was calculated to have a higher activation barrier than the dirhodium system, but that was expected.

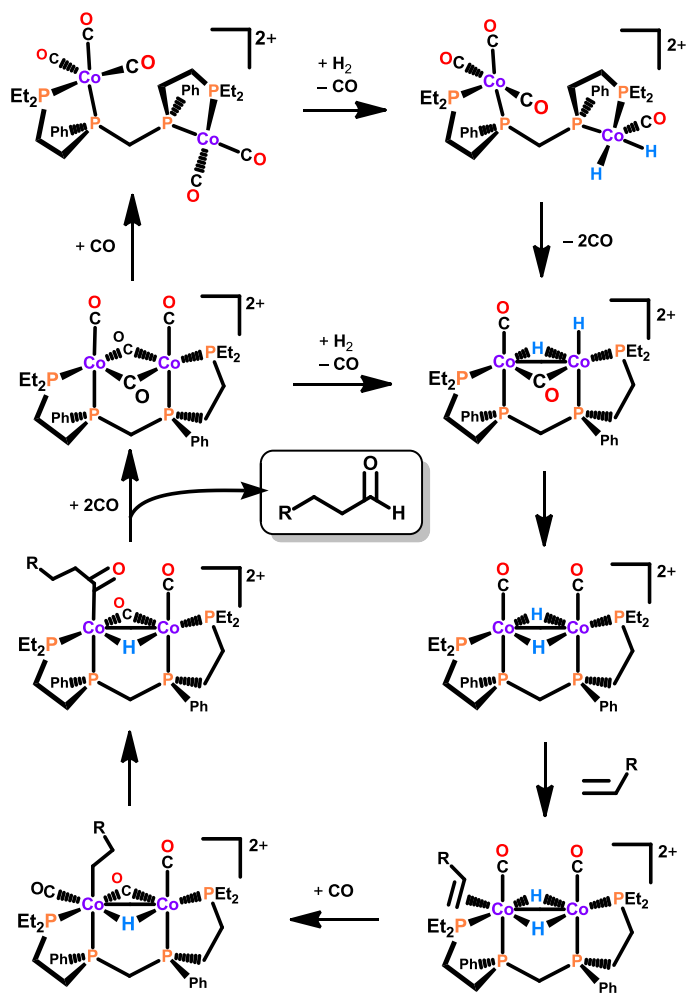


Figure 2.2. Proposed dicobalt hydroformylation mechanism based on DFT calculations.

Initially the group wanted to synthesize a cobalt starting material that had cobalt centers in the plus one oxidation state, in direct analogy to the dirhodium catalyst. Therefore; preparing a dicobalt precursor based on the new P4-Ph ligand with cobalt centers in the +1 oxidation state was my first goal.

2.2. Discovery of Cationic Cobalt Hydroformylation Catalyst

Despite many attempts to develop a Co(+1) starting material no real progress was achieved. At this point I decided to develop a starting material that would form a catalyst precursor Co(+2) oxidation states. Co(+2) starting materials are far more common than Co(+1). Success was achieved by protonating off one acetylacetonate (acac) ligand from $\text{Co}(\text{acac})_2$ with

HBF_4 in 1,4-dioxane to form $[\text{Co}(\text{acac})(\text{dioxane})_4](\text{BF}_4)$ depicted in Figure 2.3. This new starting material was used to produce a dicationic dicobalt complex with the new P4-Ph ligand shown in Figure 2.4.

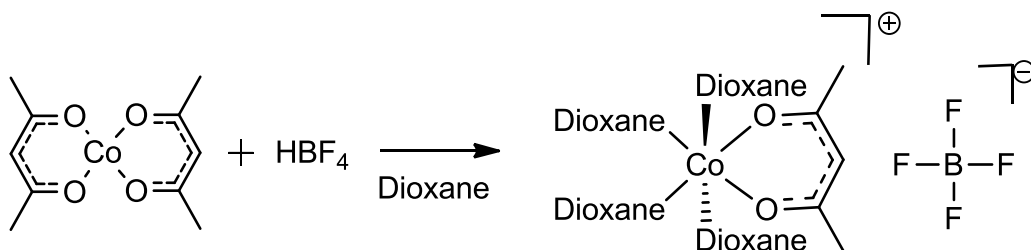


Figure 2.3. Synthesis of $[\text{Co}(\text{acac})(\text{dioxane})_4](\text{BF}_4)$ starting material.

The Co(II) starting material, $[\text{Co}(\text{acac})(\text{dioxane})_4](\text{BF}_4)$, proved to be an excellent entry point for preparing the dicobalt P4-Ph complexes, $[\text{Co}_2(\text{acac})_2(\text{rac- or meso- P4-Ph})](\text{BF}_4)_2$ (Figure 2.4). Both the *rac*- and *meso*-dicobalt catalyst precursors proved to be rather active hydroformylation catalysts for 1-hexene, although the L:B aldehyde regioselectivity was low, ranging between 0.8 and 1.1. There was also extensive alkene isomerization and some hydrogenation of the aldehyde product to alcohol detailed in Table 2.1.

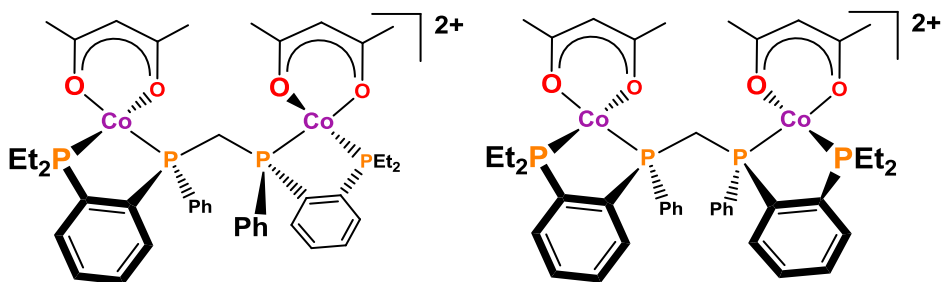


Figure 2.4. *Rac* (left) and *meso* (right) $[\text{Co}_2(\text{acac})_2(\text{P4-Ph})](\text{BF}_4)_2$

Table 2.1. Hydroformylation of 1-Hexene using Dicobalt P4-Ph Catalysts

Catalyst	Time	Aldehyde (TON)	Alcohol (TON)	Isomer (%)	Hydro (%)
[Co ₂ (acac) ₂ (<i>mixed</i> - P4-Ph)](BF ₄) ₂	10 min	355	N/A	56.4	1.0
	2 hr	734	85	15.5	2.0
[Co ₂ (acac) ₂ (<i>meso</i> - P4-Ph)](BF ₄) ₂	10 min	383	N/A	52.3	0.9
	2 hr	785	105	8.6	2.0
[Co ₂ (acac) ₂ (<i>rac</i> - P4-Ph)](BF ₄) ₂	10 min	316	N/A	57.7	0.8
	2 hr	653	86	23.5	1.8

Reactions were run at 160°C under 450psig of ; 1:1 H₂/Co in tetraethylene glycol dimethyl ether (t-glyme) with 1 M 1-hexene , 1 mM catalyst, and 0.1 M toluene. Aldehyde L:B = 0.9 for all runs.

The catalytic results from the *rac*- and *meso*-dicobalt catalyst precursors were very similar, which is very different from what we observe for the dirhodium system where the *racemic*-dirhodium catalyst is far more active and selective than the *meso*-diastereomer.¹⁻³ This indicates that the dicobalt catalyst system is operating in an open-mode form with the metal centers not cooperating. Studying the monometallic analog, therefore, became very important.

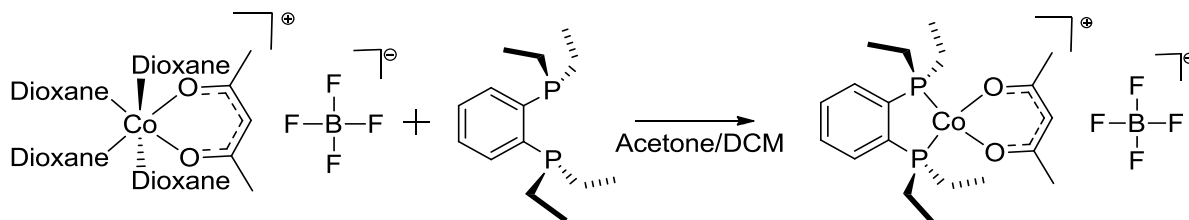


Figure 2.5. Monometallic catalyst synthesis

The monometallic catalyst precursor, [Co(acac){(Et₂P)₂-1,2-C₆H₄}] (BF₄) or [Co(acac)(DEPBz)](BF₄), was prepared in high yield as shown in Figure 2.5. The monometallic catalyst was then tested for hydroformylation to verify that the bimetallic systems were truly acting as two monometallic catalyst. Table 2.2 clearly shows that the *meso* and *racemic* bimetallic systems were acting as monometallic systems since the bimetallic and monometallic

ligands show no significant difference in catalytic activity. Furthermore, the monometallic catalysts avoid all the problems with the P4-Ph ligand discussed in Ryan Johnson's dissertation.

Table 2.2. Hydroformylation of 1-Hexene: Comparison of the Bimetallic and Monometallic Catalyst Analogs

Catalyst	Time	Aldehyde (TON)	Alcohol (TON)	Isomer (%)	Hydro (%)
[Co(acac){(Et ₂ P) ₂ -1,2-C ₆ H ₄]}(BF ₄)	10 min	425	10	51.8	1.1
	2 hr	779	114	8.4	2.0
[Co ₂ (acac) ₂ (<i>meso</i> - P4-Ph)](BF ₄) ₂	10 min	383	N/A	52.3	0.9
	2 hr	785	105	8.6	2.0
[Co ₂ (acac) ₂ (<i>rac</i> - P4-Ph)](BF ₄) ₂	10 min	316	N/A	57.7	0.8
	2 hr	653	86	23.5	1.8

Reactions were run at 160°C under 450 psig (31 bar) of 1:1 H₂/CO in tetraethylene glycol dimethyl ether (t-glyme) with 1 M 1-hexene, 2 mM Cobalt, and 0.1 M toluene. Aldehyde L:B = 0.9 for all runs.

2.3. Cationic Cobalt Pre-catalyst Characterization

With the monometallic nature of the newly discovered catalyst confirmed attention was shifted to understating the nature of the catalyst. Initially attention was focused on characterizing the catalyst precursor using nuclear magnetic resonance (NMR), electron paramagnetic resonance spectroscopy (EPR), high resolution electrospray mass spectrometry (MS), and single crystal X-ray diffraction. The catalyst precursor chosen for analysis was [Co(acac)DPPBz](BF₄), where DPPBz = (Ph₂P)₂-1,2-C₆H₄, due to the complex's better solubility and purity compared to the DEPbz-based cobalt precursor.

Nuclear magnetic resonance spectroscopy (NMR) is a powerful tool that gives detailed information on the electronic environment of a selected atom. NMR can be done for almost any type of atom so long as the system is diamagnetic, that is that all of the electrons are spin-paired. Unfortunately cobalt in the +2 oxidation state is always paramagnetic with one unpaired electron

for low spin complexes and three unpaired electrons for high spin complexes. The paramagnetic nature of the metal center not only makes the cobalt NMR silent but also makes any atom directly bound NMR silent as well. Additionally NMR signals for ligand atoms further away from the metal are broadened and often paramagnetically shifted. Chemical shifts and resonance broadening for atoms and molecules not directly associated with the paramagnetic molecule can also be affected. This phenomenon is exploited in the application of the Evan's method that quantifies the paramagnetic shift to differentiate spin states.^{4,5}

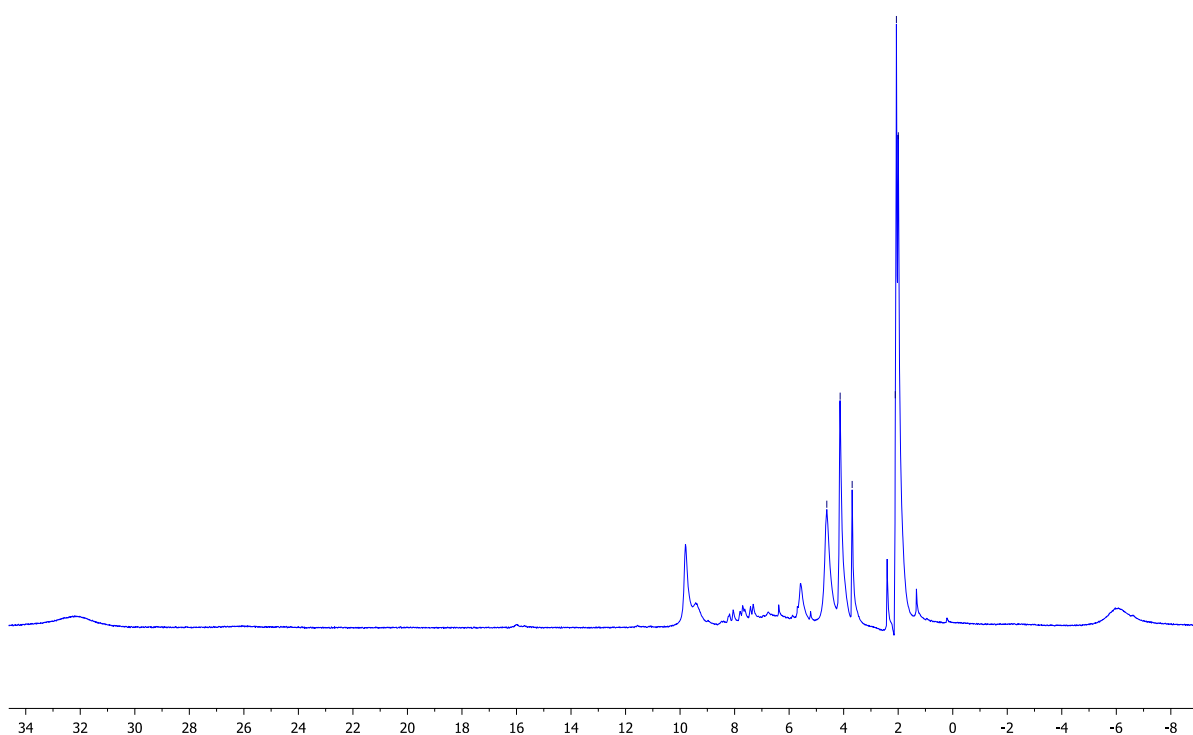


Figure 2.6. ^1H NMR of $[\text{Co}(\text{acac})(\text{DPPBz})](\text{BF}_4)$ in acetone- d_6 .

^{31}P , ^{13}C and ^1H NMR were collected on the catalyst precursor and while broadened and paramagnetically shifted signals were observed for the proton and carbon NMRs no signal was observed for the phosphorus atoms directly coordinated to the cobalt center. This is consistent with the fact that the catalyst precursor should be a paramagnetic cobalt in the +2 oxidation state. The proton NMR was consistent with a paramagnetic complex since the peaks were shifted and

broadened as seen in Figure 2.6. Additional structural detail can be inferred based on the peaks present in the ^1H spectra. The largest peak with a chemical shift of 2.1 ppm along with the peaks at 32.2, 9.8, 2.4, 2.1, 2.0, and 1.3 are all attributed to the acetylacetonate on the metal complex since they correspond well to paramagnetic metal acetylacetonate peaks in the literature.⁶ Some residual protic acetone is most likely present and is contributing to the large height of main peak at 2.1 ppm. The second group of large peaks at 4.6, 4.1, and 3.7 ppm are most likely related to the aromatic groups on the DPPBz bisphosphine ligand given that a similar splitting pattern is seen with the free DPPBz ligand in Figure 2.7. The acac and DPPBz ligand peaks shifted unequally, which could indicate stronger paramagnetic coupling between the cobalt and acac ligand. Prof. Stanley's DFT calculations on $[\text{Co}(\text{acac})(\text{DMPBz})]^+$ (methyl groups on the bisphosphine ligand) show more spin density on the acac through its higher energy π -system. The other peaks present are more difficult to assign and could be impurities formed during the acid synthesis of the $[\text{Co}(\text{acac})(\text{dioxane})_4]\text{BF}_4$ dioxane salt.

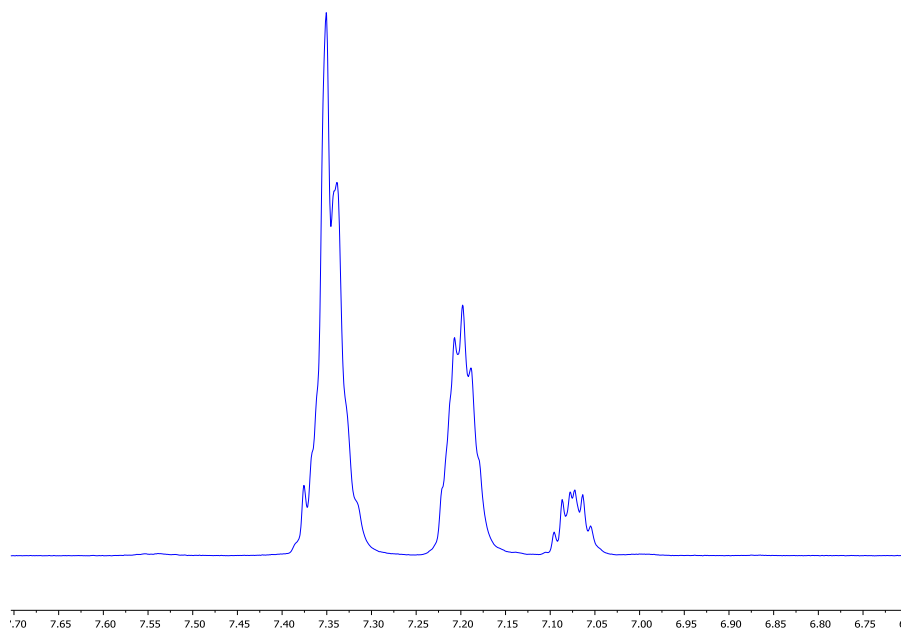


Figure 2.7. ^1H NMR of DPPBz ligand in acetone- d_6 .

The ^{13}C NMR of $[\text{Co}(\text{acac})(\text{DPPBz})](\text{BF}_4)$ in CDCl_3 is shown in Figure 2.8. Another ^{13}C NMR was taken using acetonitrile- d_3 as well that was identical (excluding the solvent peaks), however; the chloroform spectra was chosen since it is less crowded. Peaks for the solvent chloroform are clearly visible at 77.0 ppm. The aromatic carbons on the ligand appear as peaks around 128 ppm and 134 ppm. The acetylacetonate peaks are also visible at 0.0 ppm for the methyl carbons, 137 ppm for the ketone carbons and 144 ppm for the center carbon. All of the peaks are constant with the proposed precatalyst complex.

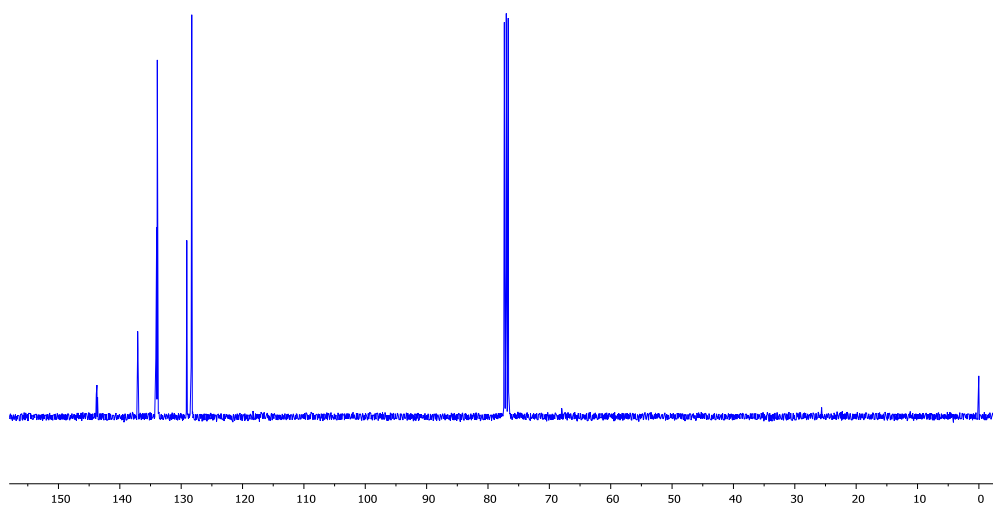


Figure 2.8. ^{13}C NMR of $[\text{Co}(\text{acac})(\text{DPPBz})](\text{BF}_4)$ in CDCl_3 .

Electron paramagnetic resonance spectroscopy (EPR) is in many ways is a mirror technique to NMR. EPR, unlike NMR, provides direct information on the unpaired electrons and their surroundings in a paramagnetic system. Information such as complex geometry, spin-coupling to other nuclei, and the number of unpaired electrons can all be evaluated. The number of unpaired electrons provides important insight into the spin state of a complex and, therefore, metal-ligand bond strengths. Low temperatures of >20 K as well as dilute samples in glassing solvents are required for good EPR spectra. Just like in NMR this can be somewhat limiting since not all solvents form glasses. Tetraethylene glycol dimethyl ether (t-glyme), the solvent

used for hydroformylation reactions, does not form a glass when frozen so another solvent system had to be used for the EPR study.⁷

EPR is not as commonly used as NMR and collecting spectrum usually requires more in-depth knowledge than we had. For this reason we collaborated with Dr. David Vinyard from the LSU Biological Sciences department. Dr. Vinyard is an expert in EPR and helped tremendously with the collection and interpretation of the EPR spectra presented. In Figure 2.9 the X-band EPR spectrum of $[\text{Co}(\text{acac})(\text{DPPBz})](\text{BF}_4)$ in frozen 2-methyl-THF solution is shown. The spectrum was recorded at 5.5 ± 0.2 K using $4 \mu\text{W}$ microwave power. Experimental data is shown in black and the simulation is shown in red.

The EPR spectrum is nearly axial with $g = [2.41, 2.29, 2.01]$ which is consistent with low-spin ($S = 1/2$) Co(II). Hyperfine interactions were simulated by Dr. David Vinyard from the $I = 7/2$ ^{59}Co (100%) using principal values of 0, 0, and 275 MHz, as well as from two equivalent $I = 1/2$ ^{31}P (100%) using principal values of 0, 0, and 350 MHz. Anisotropic line broadening was simulated using the H-strain tensor [500, 520, 30] MHz to account for unresolved hyperfine interactions. The simulated EPR spectrum matches well to the experimental data and fits our proposed complex well with a low spin cobalt in the +2 oxidation state and two equivalent phosphorus coordinated in a square planer geometry.

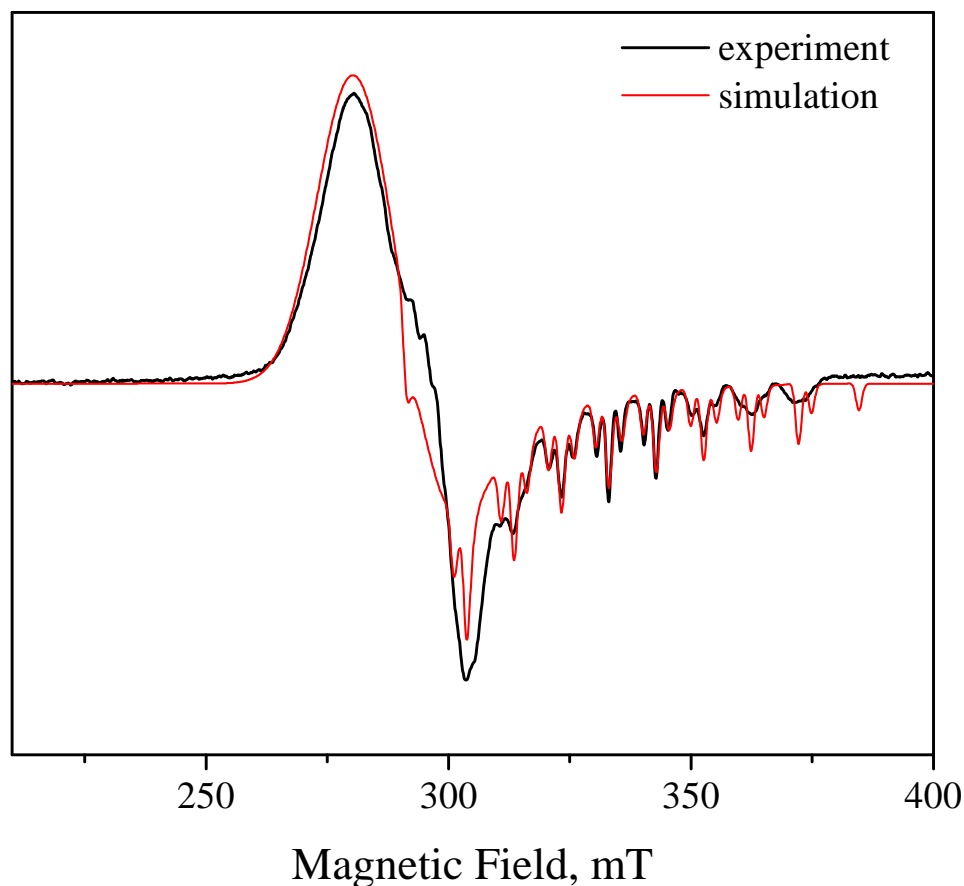


Figure 2.9. EPR spectrum of $[\text{Co}(\text{acac})(\text{DPPBz})](\text{BF}_4)$ at 5.5 K.

High resolution electrospray mass spectrometry was employed in lieu of elemental analysis to avoid residual solvent issues. The mass spec results for $[\text{Co}(\text{acac})(\text{DPPBz})](\text{BF}_4)$ are shown in Figure 2.10. The top graph shows the entire mass spectrometry window, while the bottom chart is a more detailed expansion of the region around the main peak. The major species are assigned with their calculated exact masses with the experimental masses for the parent peak listed. In the bottom spectrum the calculated isotopic distribution intensity pattern is in blue offset from the red experimental peaks. The parent peak and fragments assigned correspond well with the proposed $[\text{Co}(\text{acac})(\text{DPPBz})]^+$ complex. The next two largest peaks correspond to an oxidized free ligand and a bis-acetylacetonate complex that most likely formed during the analysis. The cluster of small high molecular weight peaks are most likely due to complex

aggregates also forming during the electrospray process. Unfortunately the catalyst precursor purity cannot be evaluated using this technique due to reactions occurring during analysis. .

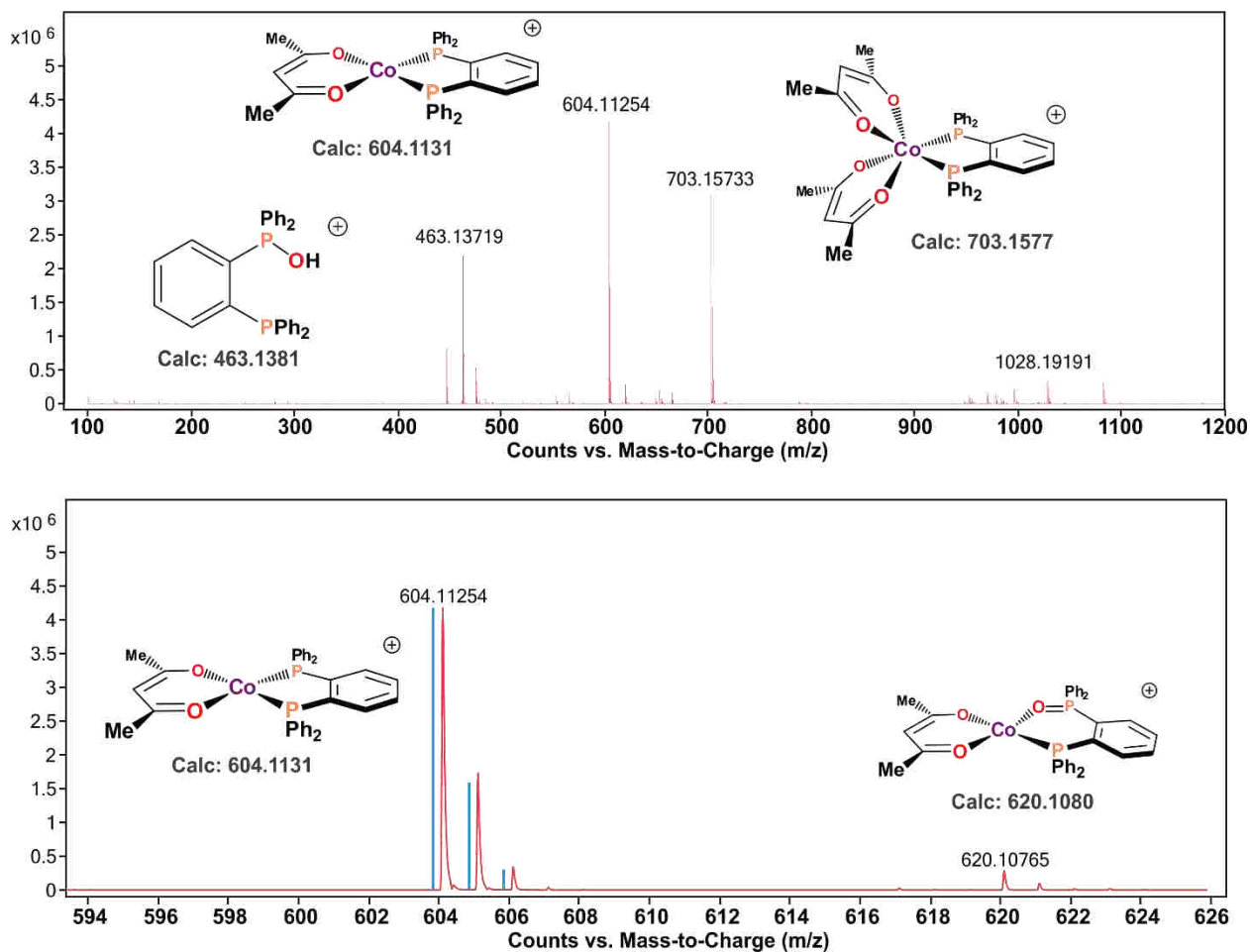


Figure 2.10. High resolution electrospray mass spectrum of $[\text{Co}(\text{acac})(\text{DPPBz})]^+$.

In Figure 2.11 the mass spectrometry results for the $[\text{Co}(\text{acac})(\text{dppe})](\text{BF}_4)$, $\text{dppe} = \text{Ph}_2\text{PCH}_2\text{CH}_2\text{PPh}_2$, are shown with the entire mass spectrometry window shown at the top and at the bottom a more detailed view of the parent peak region is shown. The major species are assigned with their calculated exact masses with the experimental masses for the parent peak listed. In the bottom spectrum the calculated isotopic distribution intensity pattern is in blue

offset from the red experimental peaks. Just like with $[\text{Co}(\text{acac})(\text{DPPBz})]^+$ the main peak corresponds to the expected complex and peaks for an oxidized free ligand along with a bis-acetylacetonate complex are observed. Again the precatalyst purity cannot be evaluated using this technique due to reactions occurring during electrospray analysis. However, the high degree of correlation between the two spectra supports our catalyst precursor composition, despite the use of different ligands.

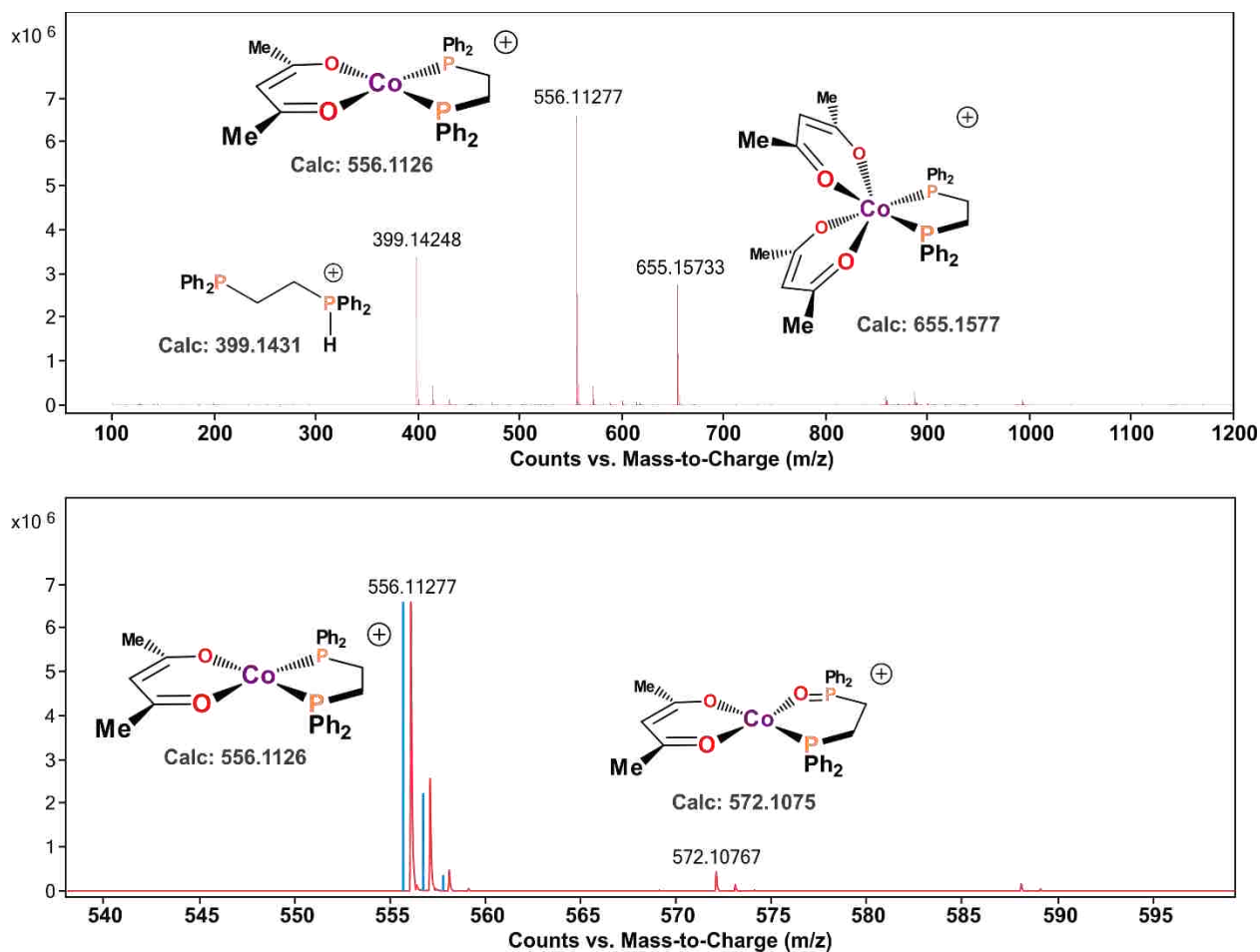


Figure 2.11. High resolution electrospray mass spectrum of $[\text{Co}(\text{acac})(\text{dppe})]^+$.

X-ray crystallography is one of the most powerful analytical techniques available to chemist providing an exact molecular structure and composition that makes up the crystal. The bond distances, bond angles and exact positioning of the atoms in a structure can be directly

viewed. Single-crystal X-ray diffraction is the best method for determining the exact chemical structure of a material.⁷

Luckily our collaborator at Exxon Mobil, Dr. Alex Carpenter, was able to get a crystal from a sample of catalyst precursor that we provided. In Figure 2.12 a thermal ellipsoid plot of [Co(acac)(DPPBz)(THF)](BF₄) using 50% probability ellipsoids is depicted with the BF₄ counter anion and hydrogen atoms omitted for clarity. Only the first carbon atom of the phenyl rings on the phosphorus centers are shown for clarity. There is a mirror plane passing through the acac C2 atom, the cobalt center, and oxygen atom of the THF, which relates the front and back atoms of the structure as shown. This structure was collected and analyzed by Dr. Alex Carpenter at Exxon Mobil's research facility in Baytown, TX.

The crystal structure agrees well with the picture presented by the EPR and MS data verifying that the precatalyst is [Co(acac)(DPPBz)(THF)](BF₄) with a square planer complex. Alternative analytical techniques such as elemental analysis could be used to potentially better quantify the precatalyst purity. However, these techniques often have problems when the material also has solvent molecules present – either as solvates or weakly coordinated to the metal center. The only way to truly guaranty precatalyst purity is to develop a high-yield crystal growth procedure. Since crystals are typically completely pure substances whose exact structure can be determined by X-ray crystallography.

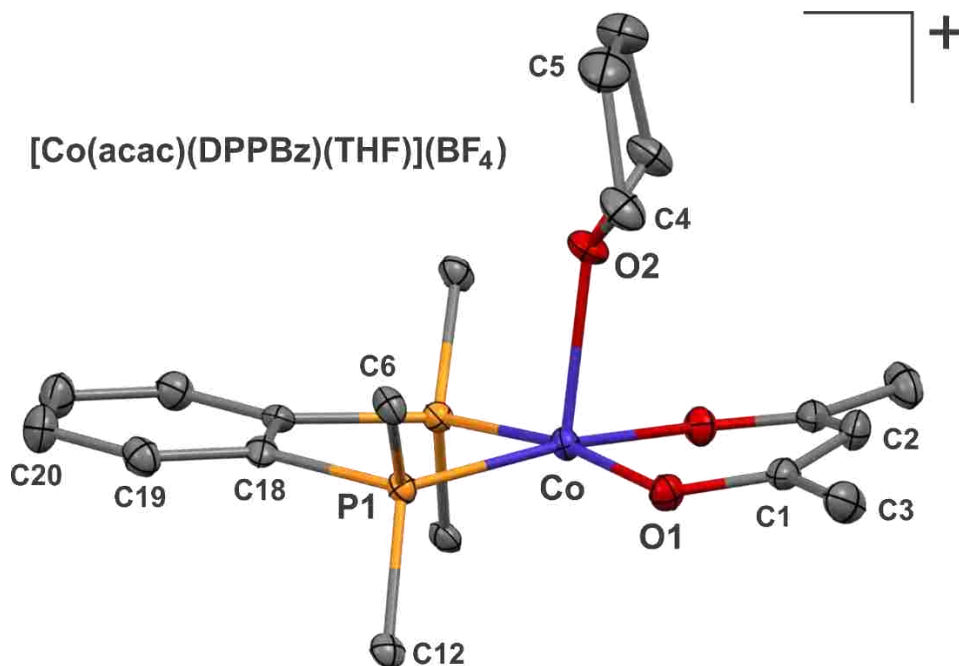


Figure 2.12. Thermal ellipsoid plot of $[\text{Co}(\text{acac})(\text{DPPBz})(\text{THF})]^+$. Hydrogen atoms and BF_4^- counter anion omitted for clarity. Only the first carbon atom of the terminal phenyl rings attached to the phosphorous atoms is shown for clarity.

2.4. Cationic Cobalt Catalyst Characterization

After the pre-catalyst was thoroughly characterized attention was redirected to characterizing the active catalyst. Since $[\text{Co}(\text{acac})(\text{DPPBz})(\text{THF})](\text{BF}_4)$ was used most extensively for the pre-catalyst characterization, the DPPBz-based complex was again used to generate the active hydride-carbonyl catalyst, which was studied by NMR, EPR, IR and single-crystal X-ray diffraction.

EPR was again employed with the help of Dr. David Vinyard in an attempt to probe the geometry and ligand structure of the active catalyst. Initially an EPR sample was prepared by collecting a sample from a hydroformylation reaction running under normal conditions specifically 30 bar of 1:1 $\text{H}_2:\text{CO}$ at 140°C in t-glyme. The autoclave was cooled, mostly depressurized, and a catalyst sample removed. The sample was diluted with 2-methyl tetrahydrofuran (2-MTHF) in a 4 mm quartz EPR tube under atmospheric pressure inside of the

glovebox before being frozen in liquid nitrogen and transferred to the EPR cryostat for further cooling to run the EPR experiment.

The resulting X-band EPR spectrum of what we propose as $[\text{HCo}(\text{CO})_x(\text{DPPBz})](\text{BF}_4)_x$, $x = 2$ or 3 , is shown in Figure 2.13. The spectrum was recorded at 7.0 ± 0.2 K using 2 mW microwave power. The experimental data is shown in black and the simulation is shown in red. The EPR spectrum is rhombic with $g = [6.02, 3.56, 3.24]$ consistent with high-spin ($S = 3/2$) Co(II). Hyperfine interactions were simulated by Dr. David Vinyard from the $I = 7/2$ ^{59}Co (100%) using principal values of 685, 640, and 0 MHz. Anisotropic line broadening was simulated using the H-strain tensor [600, 850, 1230] MHz to account for unresolved hyperfine interactions. Dr. David Vinyard's simulation is in good agreement with raw data and indicated a cobalt (II) high spin trigonal bipyramidal or square pyramidal structure correlating to a $17e^-$ dicarbonyl species discussed later where the unpaired electrons are only coupled to the cobalt metal center. The high spin nature seen in this EPR is strange as all of the ligands bound to the cobalt are traditionally strong field ligands, which would normally produce a low spin complex.⁵

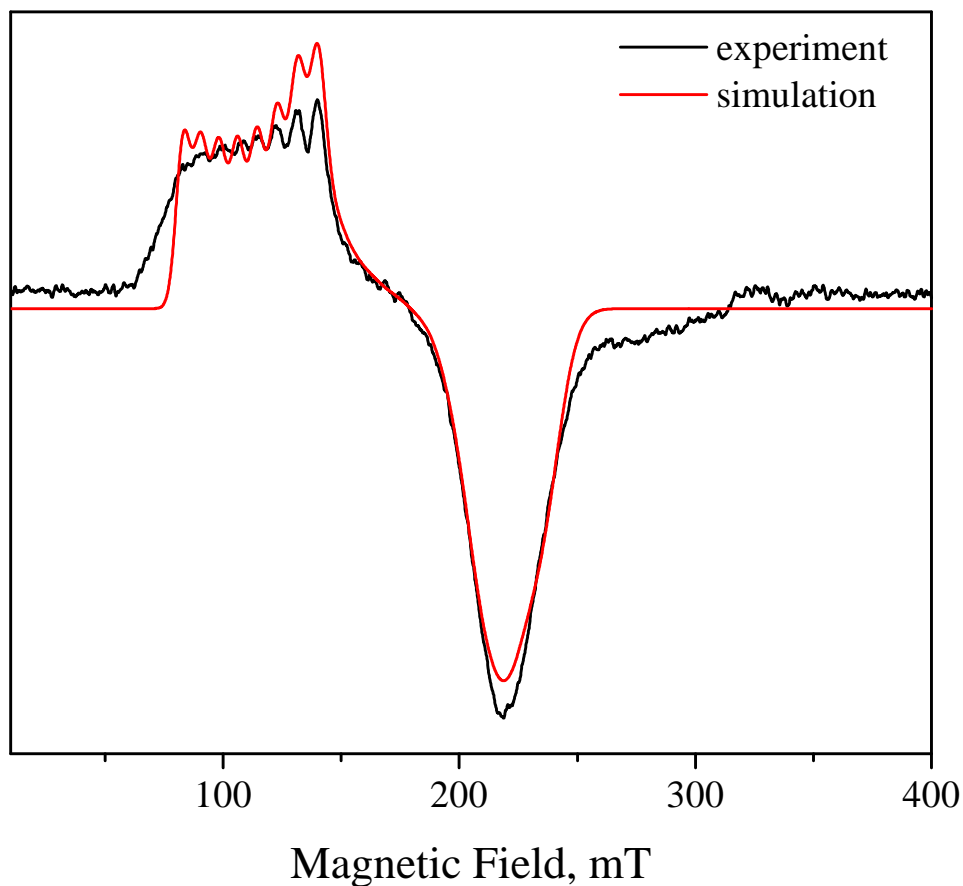


Figure 2.13. EPR spectrum of $[\text{HCo}(\text{CO})_2(\text{DPPBz})](\text{BF}_4)$ at 7 K (low pressure).

Since the data collected from the first EPR was not under H_2/CO pressure, another sample was prepared under pressure in the hopes that a more accurate catalyst representation would be observed. The sample was prepared by adding the catalyst precursor to a high pressure 4 mm quartz EPR tube (Wilmad) along with approximately 2 mL of 2-methyl-THF. The tube was flushed with 1:1 H_2/CO and then pressurized to 27 bar with 1:1 $\text{H}_2:\text{CO}$. Next the pressurized quartz EPR tube was heated in an oil bath to 140°C to activate the catalyst, then cooled to room temperature. Finally the EPR tube was frozen in liquid nitrogen and transferred to the EPR cryostat for the EPR experiment.

In Figure 2.14 the X-band EPR spectrum of $[\text{HCo}(\text{CO})_x(\text{DPPBz})](\text{BF}_4)$, $x = 2-3$, sample prepared under H_2/CO is shown. The spectrum was recorded at 6.7 ± 0.2 K using 1 mW microwave power. Experimental data is shown in black and the simulation is shown in red. The EPR spectrum is rhombic with $g = [6.06, 3.41, 3.12]$ consistent with high-spin ($S = 3/2$) Co(II). Hyperfine interactions simulated by Dr. David Vinyard are from the $I = 7/2$ ^{59}Co (100%) using principal values of 720, 650, and 0 MHz. Anisotropic line broadening was simulated using the H-strain tensor [740, 1850, 1400] MHz to account for unresolved hyperfine interactions. The small signal around 325 mT is an organic radical impurity often seen in samples. The hyperfines are dampened compared to the signal in Figure 2.12 which is most likely due a more diverse pool of catalyst species that would be present at higher temperatures and pressures specifically a mixture of the $17e^-$ dicarbonyl and $19e^-$ tricarbonyl species discussed latter. Dr. David Vinyard's simulation is in good agreeance with raw data and again indicated a cobalt (II) high spin trigonal bipyramidal or square pyramidal structure were the unpaired electrons are only coupled to the cobalt metal center. Other characterization techniques will be need to verify the spin state of the active catalyst given the uncommon ligand field. However, the EPR measurements seem to strongly indicate a high spin catalyst complex.

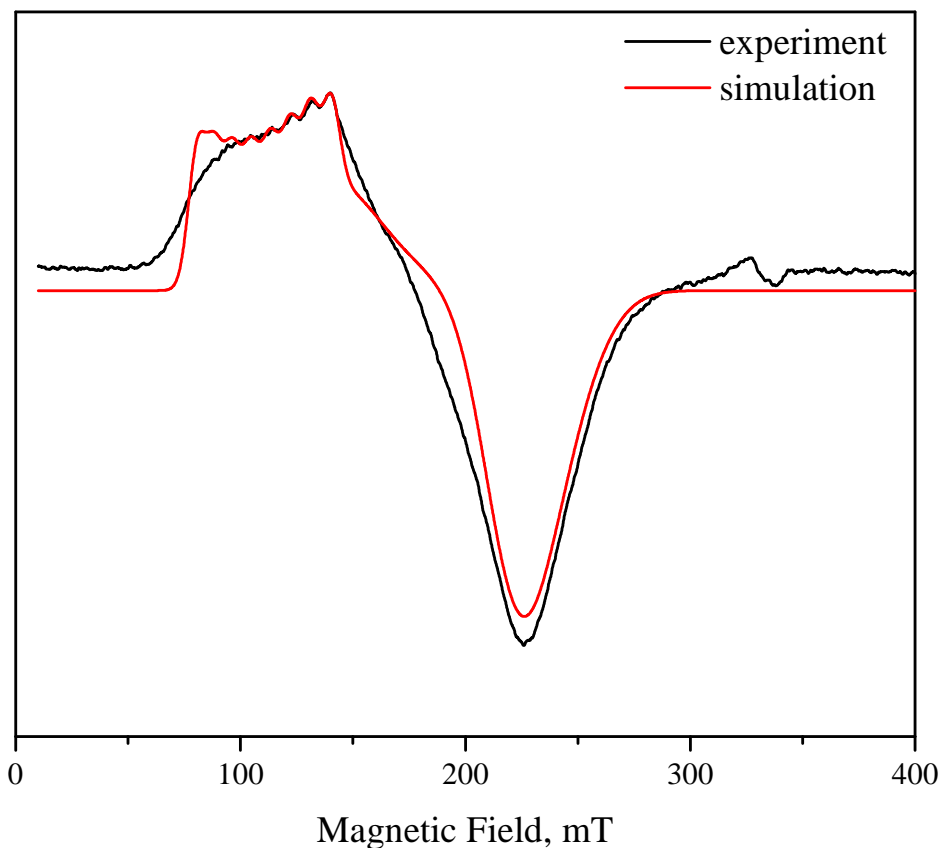


Figure 2.14. EPR spectrum of $[\text{HCo}(\text{CO})_2(\text{DPPBz})](\text{BF}_4)$ at 6.7 K (high pressure).

Fourier Transform Infrared Spectroscopy (FT-IR) is an analytical technique that provides insight into the type of bonds that are present in a sample. The metal carbonyl region in FTIR is well characterized with a plethora of examples for comparisons. This is especially useful in observing a hydroformylation catalyst because metal carbonyls have to form during catalysis.⁵ Furthermore, most functional groups including the ether bonds of t-glyme do not interfere with the carbonyl region resulting in an open window in the IR region for observing metal-carbonyl and metal-hydride IR bands. Metal-hydride bands are often weak and difficult to observe when carbonyl ligands are present.

In order to correctly characterize the active catalyst all observations have to be made under conditions that are representative of reactions conditions. A Mettler-Toledo ReactIR 45m instrument connected to a Parr high pressure IR cell was used along with a SiComp (silicon ATR) probe.

In Figure 2.15 a 101.5 hr catalyst study of the cationic cobalt catalyst (10 mM) and its behavior at different temperatures in t-glyme solvent is summarized. The spectra shown are solvent subtracted with the solvent spectra collected from pure solvent runs at the corresponding temperatures. The refractive index of the silicon ATR crystal changes with temperature, so it is important to use solvent spectra collected at the same temperature for the solvent-subtraction.

The catalyst precursor doesn't quickly activate until it is heated to at least 120°C at which time the complexes $[\text{HCo}(\text{CO})_x(\text{DPPBz})]^+$ ($x = 1-3$) begin to quickly form: the 15e-, 17e- (two isomers), and 19e⁻ species shown on the top part of Figure 2.15. The proposed corresponding carbonyl bands are at 2086, 2046, 2025, 2011, and 1990 cm^{-1} . The highest energy 2086 cm^{-1} band is proposed to be due to the 19e- tricarbonyl species, along with bands (shoulders) at 2046 and 2011 cm^{-1} . At higher temperatures the 17e- dicarbonyl complex is likely the major species with carbonyl bands around 2025 and 1990 cm^{-1} . The 15e- monocarbonyl is proposed to have a CO stretching frequency also around 1990 cm^{-1} .

These assignments are based on the idea that as more carbonyls bind the amount of π -backbonding that occurs at each carbonyl drops and results in carbonyl IR bands shifting to higher energy.⁷ Therefore, the tricarbonyl species should have the highest stretching frequency while the monocarbonyl species should have the lowest stretching frequency, and the dicarbonyl species should have frequencies in between. The monocarbonyl species should have only one stretching frequency while the di and tricarbonyl species should have more than one correlating

to symmetric and unsymmetrical vibrational modes. Only one of the tricarbonyl bands can be clearly seen (2086 cm^{-1}), the others are overlapping with those from the higher concentration dicarbonyl complex.

The dicarbonyl species probably exist as two square-pyramidal isomers with somewhat different stretching frequencies: one isomer with an equatorial and axial CO, while the other as two axial carbonyl ligands and an empty equatorial coordination site (see Figure 2.15). The dicarbonyl isomer with two axial CO ligands is proposed to form from the dissociation of the equatorial CO from the $19e^-$ tricarbonyl complex, which is an important part of our proposed mechanism discussed below. The facile conversion between the two isomers along with the multiple stretching modes results in the main cobalt-carbonyl set of bands between $2046\text{-}1990\text{ cm}^{-1}$. Therefore, with the current data the peaks at 2046 , 2025 and 2011 cm^{-1} are assigned to the dicarbonyl species. These assignments also correlates well with previously reported carbonyl frequencies for a phosphine modified cobalt +2 dicarbonyl hydride complex that showed bands at 2024 and 2051 cm^{-1} .⁸

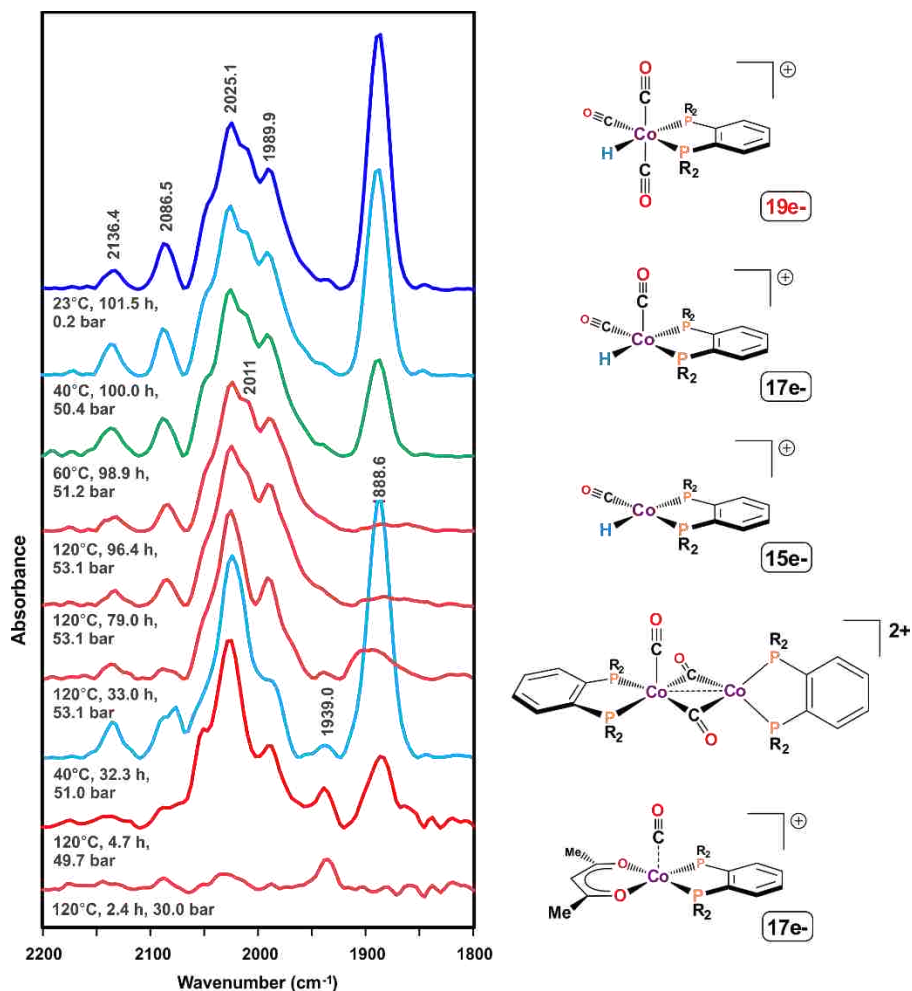


Figure 2.15. *In situ* FT-IR studies of $[\text{Co}(\text{acac})(\text{DPPBz})](\text{BF}_4)$.

We believe that the $[\text{HCo}(\text{CO})_x(\text{DPPBz})]^+$ ($x = 1-3$) species can react with itself to reductively eliminate H_2 and form a CO-bridged dicobalt(I) species, $[\text{Co}_2(\mu\text{-CO})_2(\text{CO})(\text{DPPBz})_2]^{2+}$, which has a proposed strong bridging CO band at 1888 cm^{-1} and probably at least one terminal band around 2025 cm^{-1} . The CO-bridged dicobalt complex readily reacts with H_2 and CO at temperatures above 50°C to reform the active monometallic catalysts. The system can be temperature cycled between $[\text{HCo}(\text{CO})_x(\text{DPPBz})]^+$ ($x = 1-3$) at higher temperatures and a mixture of the monomer and dicobalt complexes at lower temperatures. The monometallic cationic cobalt-bisphosphine catalyst shows no significant

change in the carbonyl region when stirring at 120°C and 53 bar for 65 hours. The band at 2136 cm⁻¹ is free CO dissolved in the solvent, and the band at 1939 cm⁻¹ is assigned to the 17e⁻ [Co(acac)(CO)(DPPBz)]⁺ complex. Also worth noting is that the characteristic HCo(CO)₄ band at 2116 cm⁻¹ is clearly not present further decreasing the likelihood of HCo(CO)₄ being formed and participating in the hydroformylation.⁹⁻¹²

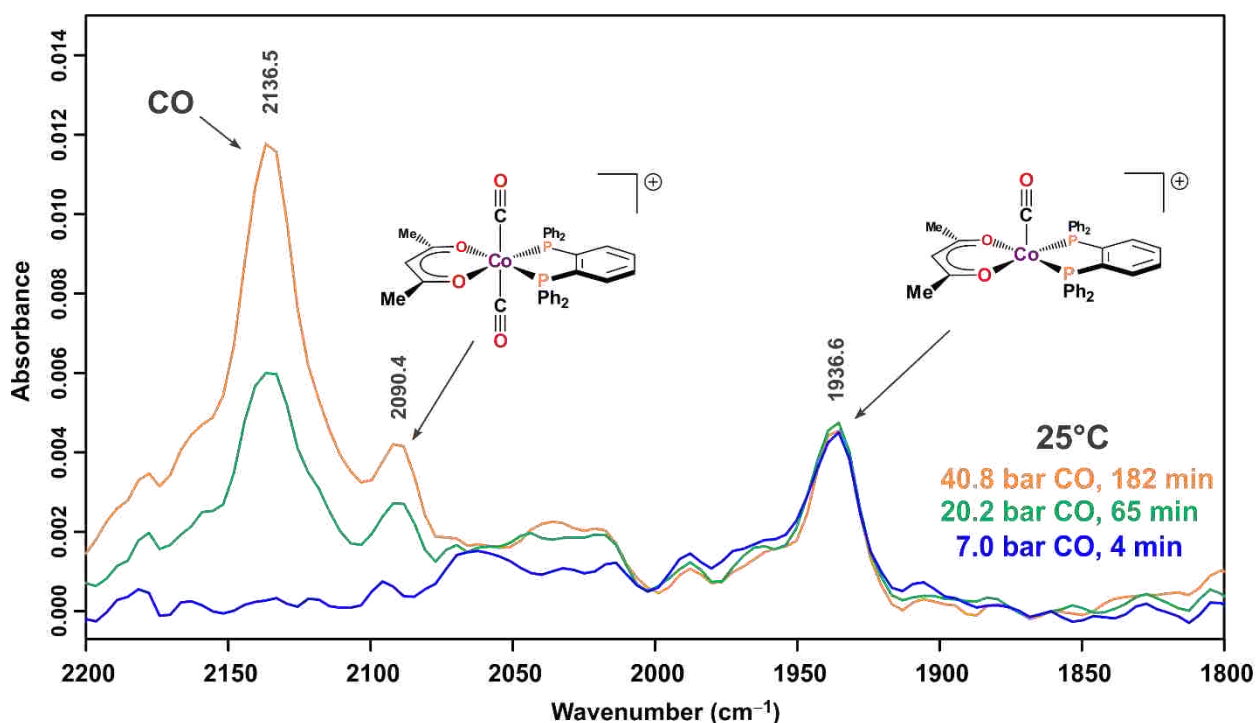


Figure 2.16. FT-IR Study of [Co(acac)(DPPBz)](BF₄) with CO.

In order to more carefully characterize a few of the FT-IR bands observed another study was conducted with 10 mM [Co(acac)(DPPBz)](BF₄), which was reacted with CO at various pressures in t-glyme solvent and at 25°C. The intention was to measure the stretching frequency of dissolved CO as well as the [Co(acac)(CO)(DPPBz)]⁺ complex. FT-IR solvent-subtracted spectra from this experiment are shown in Figure 2.16. No baseline corrections were performed on these spectra due to the relatively low intensities of the CO bands. The CO band at 2136 cm⁻¹

is free CO dissolved in the t-glyme solvent. This was confirmed by separate studies using only CO gas and t-glyme solvent at a variety of temperatures and pressures. The intensity of the free dissolved CO peak at 2136 cm^{-1} is very dependent on CO pressure and temperature. The CO band at 1937 cm^{-1} assigned to $[\text{Co}(\text{acac})(\text{CO})(\text{DPPBz})]^+$ forms immediately on exposure to CO gas but saturates quickly with additional CO pressure to the intensity shown in the spectra above and maintains its intensity as the CO pressure is varied. The lower intensity CO band at 2090 cm^{-1} is assigned to the 19e- dicarbonyl complex, $[\text{Co}(\text{acac})(\text{CO})_2(\text{DPPBz})]^+$, and does vary in intensity somewhat depending on the CO pressure and temperature.

The band at 1888 cm^{-1} in Figure 2.15 does raise concerns since it is well documented that a strong carbonyl band with the same frequency and similar intensity is seen for $[\text{Co}(\text{CO})_4]^-$. This is alarming because if $[\text{Co}(\text{CO})_4]^-$ is forming then $\text{HCo}(\text{CO})_4$ could also be formed and might be contributing to the hydroformylation catalysis. The reaction data shown earlier as well as the lack of a $\text{HCo}(\text{CO})_4$ IR band at 2116 cm^{-1} certainly points to $[\text{HCo}(\text{CO})_x(\text{P}2)]^+$ ($x = 1-3$) being the catalyst and not $\text{HCo}(\text{CO})_4$.⁹⁻¹² However, for further assurance additional analytical techniques were employed.

NMR is a powerful analytical tool but can be quite limited for paramagnetic complexes like our Co(II) precursor and catalyst, especially for observing atoms directly coordinated to the paramagnetic metal center. So if the cobalt of our active catalyst remains in a +2 oxidation state we should not observe any ^{31}P signals unless the oxidation state on the metal center changes and becomes diamagnetic.⁴ In an attempt to further rule out $[\text{Co}(\text{CO})_4]^-$ and $\text{HCo}(\text{CO})_4$ forming from our bisphosphine cationic Co(II) catalyst ^{31}P , ^1H and ^{59}Co NMR data was collected under reaction conditions. Dr. Thomas Weldeghiorghis, the head of LSU's NMR facility, helped tremendously with the ^{59}Co NMR experiment.

^{31}P NMR was run on a sample of $[\text{Co}(\text{acac})(\text{DPPBz})](\text{BF}_4)$ added to a high pressure 5 mm NMR tube (Wilmad) along with 0.75 mL of THF-d_8 . The tube was pressurized with 150 psig (10.4 bar) of H_2/CO and heated in an oil bath overnight at 120°C to activate the catalyst. ^{31}P NMR spectra were collected at 24, 40, 60, 80, 100 and 120°C . None of these spectra showed any ^{31}P resonances despite thousands of scans collected for each temperature. No decomposition to black cobalt metal or other precipitates was observed. This experiment was run three times with the exact same results observed. If the cobalt changed oxidation states to diamagnetic Co(I) or Co(III) with coordinated phosphine, we would expect to see ^{31}P peaks for these complexes.¹³⁻¹⁵ If the ligand was falling off of the metal center then we would expect ^{31}P peaks that correspond to free ligand in solution. The lack of ^{31}P NMR resonances strongly supports that the oxidation state on the cobalt is not changing to a diamagnetic system and that the ligand must remain bonded to the cobalt(II) center.

The ^{31}P NMR data also indicates that the dicobalt(I) complex proposed to form with a strong bridging carbonyl band at 1888 cm^{-1} is also paramagnetic. DFT calculations performed by Prof. Stanley and Dr. Jarod Younker (ExxonMobil) on the dicobalt(I) dimer show a structure with a 5-coordinate square pyramidal Co center and a tetrahedral Co(I) center (Figure 2.15). The tetrahedral Co(I) center should be paramagnetic with two unpaired spins ($I = 1$). Prof. Vineyard's EPR studies on the catalyst system, which did include the dicobalt dimer, was done on an EPR instrument that was only configured to detect systems with half-integer spins ($1/2$, $3/2$, etc). Integer spin systems, as proposed for the dicobalt(I) complex, require a different EPR resonance cavity that LSU doesn't currently have.

^1H NMRs were run similar to the ^{31}P NMR experiments using a high pressure 5 mm NMR tube (Wilmad) with $[\text{Co}(\text{acac})(\text{DPPBz})](\text{BF}_4)$ dissolved in 0.75 mL of THF-d_8 . The high

pressure NMR tube was pressurized with 150 psig (10.4 bar) of H₂/CO, however; the sample was not initially heated in an oil bath. Instead a ¹H NMR was collected of the sample prior to heating in an attempt to collect a spectrum of the catalyst precursor. Then the sample was placed in a 110°C oil bath for 6 hrs after which the sample was quickly transferred to the NMR that was preheated to 110°C for analysis. The resulting spectrum are shown in Figure 2.17 with the unactivated room temperature spectrum on the bottom in blue and the 110°C activated catalyst spectrum on top in green. Additionally, a room temperature spectrum of the activated catalyst was taken after cooling, which showed the same three major peaks with identical chemical shifts. This experiment was repeated under 350 psig (24.2 bar) with identical results.

In Figure 2.17 the three main peaks seen in both spectra are from residual protic THF in the deuterated solvent and dissolved hydrogen gas. The residual protic THF gives rise to two peaks with the protons adjacent to the oxygen observed at 3.6 ppm in the bottom spectrum and 1.76 in the top spectrum. The other two THF protons are observed at 1.76 ppm in the bottom spectrum and -0.10 ppm in the top spectrum. The dissolved hydrogen gas is at 4.58 ppm in the bottom spectra and 2.70 ppm in the top spectra. For all peaks a large shift of approximately 1.86 ppm is observed when going from the unactivated blue spectrum to the activated green spectrum. The large chemical shift between the two spectra implies a change in the magnetic susceptibility of the metal complexes present since all other parameters have been kept constant. Furthermore, this would suggest the spin state of the complex has changed from low-spin Co(II) catalyst precursor to high-spin Co(II) active catalyst. The inferred high spin active catalyst would agree well with the previous EPR studies that indicated a high spin catalyst. Additionally no hydride peak was observed for activated catalyst even when data was collected at room temperature indicating that diamagnetic HCo(CO)₄ is not present.^{9,10,13}

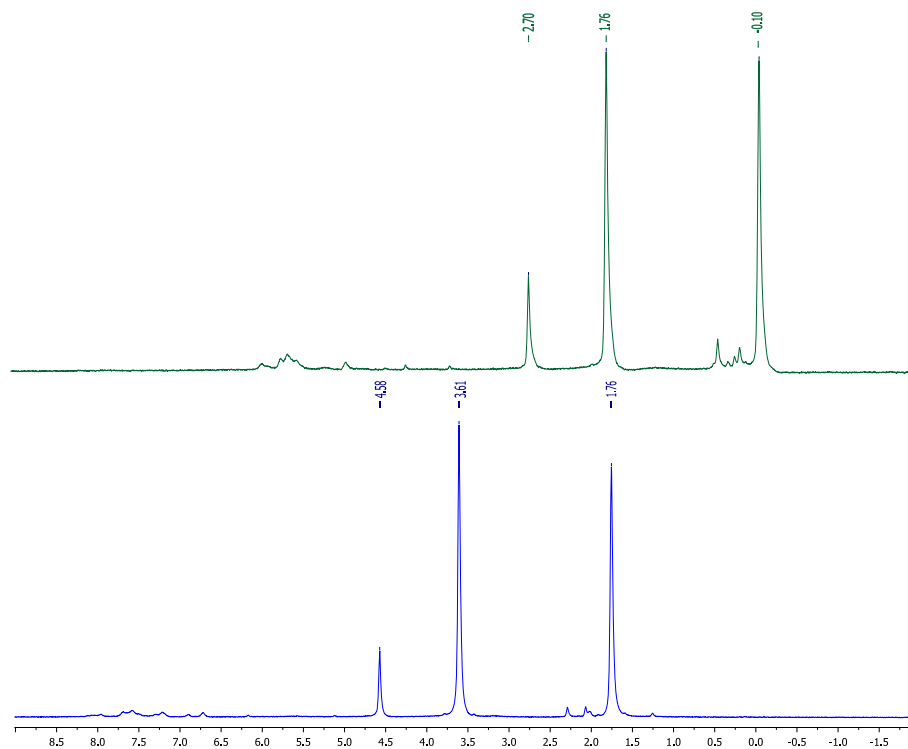


Figure 2.17. Proton NMR spectrum for $[\text{Co}(\text{acac})(\text{DPPBz})](\text{BF}_4)$ under 150 psig (10.4 bar) H_2/CO (blue) and after heating to 110°C to generate active catalyst (green).

^{59}Co NMR was run to further verify that $[\text{Co}(\text{CO})_4]^-$, as well as $\text{HCo}(\text{CO})_4$, were not being formed under reaction conditions. $\text{K}_3[\text{Co}(\text{CN})_3]$ was used as a reference compound and $\text{Na}[\text{Co}(\text{CO})_4]$ was used as a standard. Both were synthesized via literature preparations and prepped in D_2O . The active catalyst sample was prepared by dissolving $[\text{Co}(\text{acac})(\text{DPPBz})](\text{BF}_4)$ in 0.75 mL of THF-d_8 and adding to a high pressure quartz NMR tube (Wilmad). The tube was then pressurized to 27.6 bar (400 psig) with H_2/CO and heated in an oil bath to 120°C overnight to activate the catalyst.

In Figure 2.18 the ^{59}Co NMR data for $\text{Na}[\text{Co}(\text{CO})_4]$ (top) as well as the activated catalyst sample (bottom) are shown. In the case of the $\text{Na}[\text{Co}(\text{CO})_4]$ sample an easily observed peak at -3056ppm is observed, while no such peak is seen in the active catalyst sample despite thousands of additional scans. To rule out the possibility that paramagnetic impurities were washing out the

signal, excess CoCl_2 was added to the $\text{Na}[\text{Co}(\text{CO})_4]$ sample and the resulting spectra is shown in the middle of Figure 2.18. Addition of a large quantity of paramagnetic material did slightly shift and broaden the peak, however; the peak is still clearly visible making the loss of signal due to paramagnetic species highly unlikely. Broad peaks for $\text{HCo}(\text{CO})_4$ and Co_2CO_8 should also be visible in this region if they are being formed, but no such peaks are observed in the activated catalyst sample.

In fact, no ^{59}Co peaks were observed for the active catalyst sample across a spectral window from 5000ppm to -5000ppm . Furthermore, after the sample was depressurized a FT-IR of the catalyst solution showed the bridging CO band at 1888 cm^{-1} , as well as terminal CO bands between 2050 and 1950 cm^{-1} . The ^{59}Co NMR experiment essentially rules out possibility of $[\text{Co}(\text{CO})_4]^-$ being the species responsible for the 1888 cm^{-1} band in the FT-IR data.

Additionally the lack of ^{59}Co NMR peaks pretty much eliminates the likelihood of $\text{HCo}(\text{CO})_4$ being present and supports our proposed paramagnetic cationic $\text{Co}(\text{II})$ bisphosphine catalyst.¹⁶⁻¹⁷

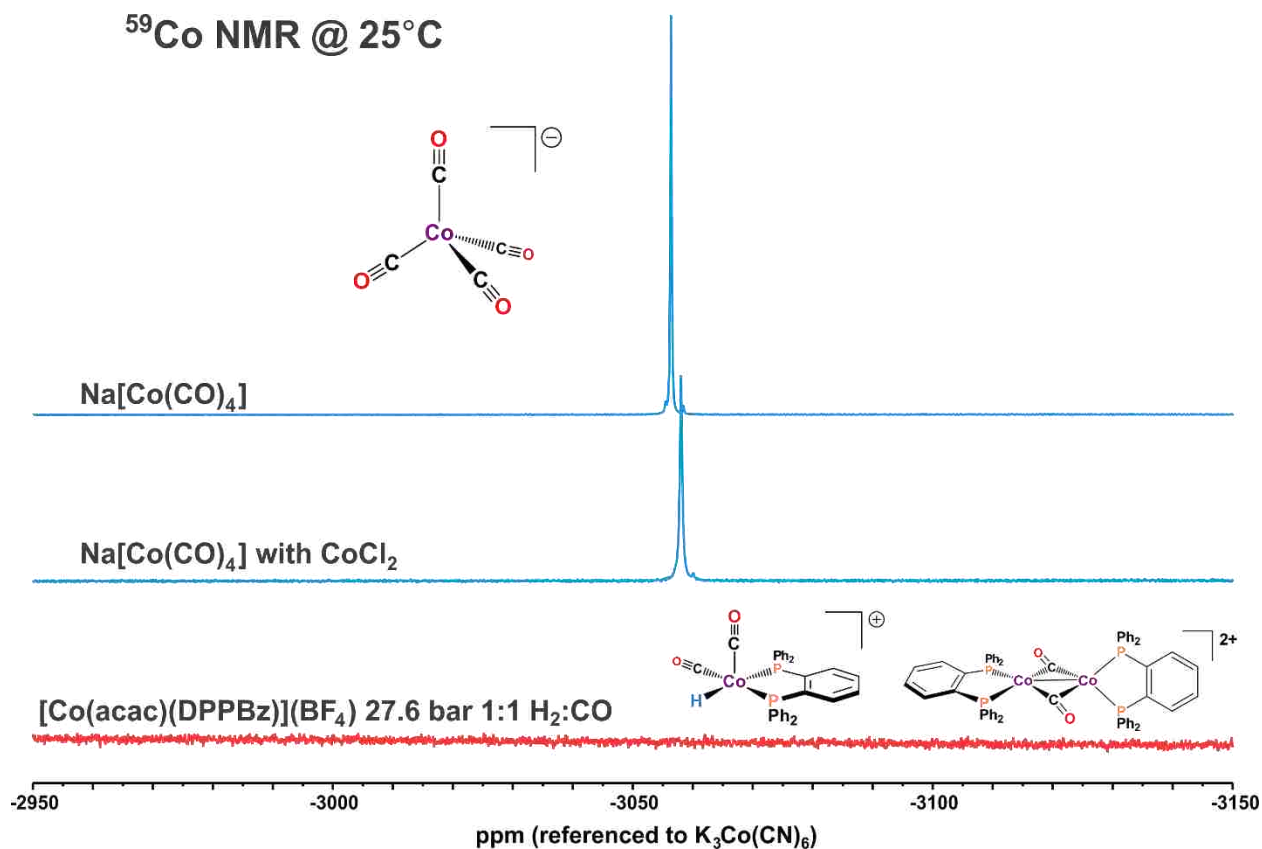


Figure 2.18. ^{59}Co NMR demonstrating that $[\text{Co}(\text{CO})_4]^-$ is not being generated from our catalyst. $\text{Na}[\text{Co}(\text{CO})_4]$ in D_2O (top spectrum), $\text{Na}[\text{Co}(\text{CO})_4]$ in D_2O with 5 equivalents of paramagnetic CoCl_2 added (middle spectrum) and $[\text{Co}(\text{acac})(\text{DPPBz})](\text{BF}_4)$ catalyst precursor in a high pressure quartz NMR tube under 27.6 bar of 1:1 H_2 :CO (bottom spectrum).

We were unable to get any crystals of the proposed active catalyst or the proposed dimer complex. However, one crystal structure we collected with the help of Dr. Frank Fronczek may provide some additional insight. Dr. Frank Fronczek is an expert X-ray crystallographer in the Department of Chemistry at LSU who collected and solved the crystal structure in Figure 2.19. A thermal ellipsoid plot of $[\text{Co}(\text{CO})_3(\text{DPPBz})](\text{BF}_4)$ using 50% probability ellipsoids is depicted in Figure 2.19 with the BF_4 counter anion and hydrogen atoms omitted for clarity. The crystal for this structure was grown in a high pressure quartz EPR (Wilmad) in 2-methyl-THF under H_2/CO pressure from the catalyst precursor $[\text{Co}(\text{acac})(\text{DPPBz})](\text{BF}_4)$ that had been activated at 120°C and then placed in the freezer. This structure almost perfectly represents one half of the proposed

dimer species. The cobalt metal center is in the +1 oxidation state, which would be rather unlikely to form via any pathway other than the cleavage of the proposed dimer species. The dimer species could have reacted with excess CO slowly over time as the H₂ gas depleted to yield two monomers with an additional CO ligand. The structure in Figure 2.19 supports, but does not prove the existence of the dimer species. However, the similarity in structure between the two compounds certainly makes for a compelling argument when considering how unlikely are the alternative pathways to forming [Co(CO)₃(DPPBz)]⁺.

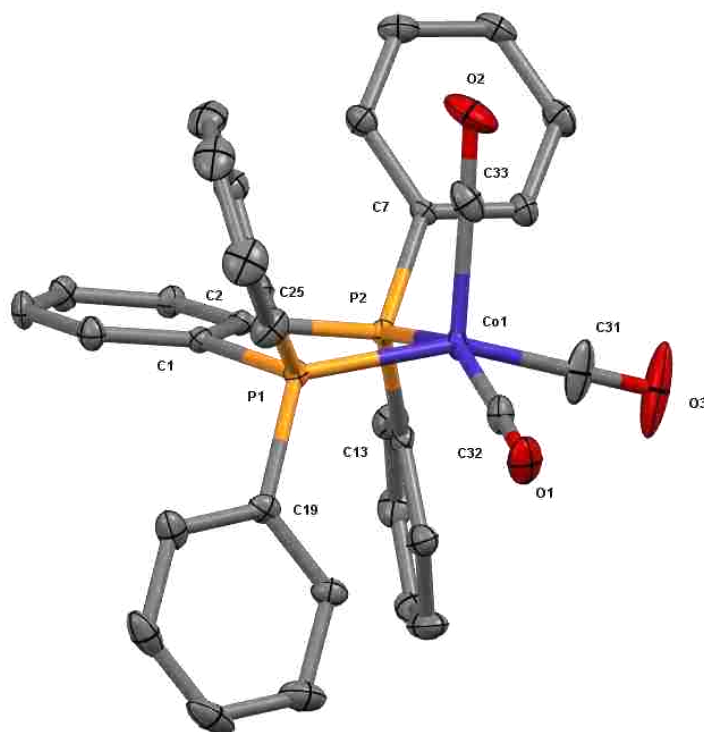


Figure 2.19. Thermal ellipsoid plot of [Co(CO)₃(DPPBz)]⁺. Hydrogens and the BF₄⁻ counter anion are omitted for clarity.

Taking all the data presented into account we have a good understanding of the active catalyst, which leads us to the discussion on the catalytic cycle for this cationic Co(II)

bisphosphine catalyst. Figure 2.20 shows the proposed catalytic cycle with the 15e⁻ complex in the top left corner. The [HCo(CO)(P₂)]⁺ 15e⁻ complex forms from the heterolytic cleavage of hydrogen gas to protonate off the acac ligand and add a hydride to the cobalt along with a carbonyl ligand. Most of the proposed reaction steps are entirely consistent with what is known for cobalt and rhodium hydroformylation catalysts. A key and unique feature is the ability to form 19e⁻ complexes via CO coordination, which helps weaken and dissociate the equatorial CO ligand.

The equatorial CO is thought to be the key to binding alkenes since the axial coordination sites are too sterically hindered to allow alkene coordination, especially internal branched alkenes. Once the equatorial CO dissociates and the alkene coordinates, the migratory insertion of a hydride and alkene occurs to form the 17e⁻ cobalt-alkyl species, which can coordinate another carbonyl to form the 19e⁻ complex shown in the bottom right of Figure 2.20. CO migratory insertion with the alkyl forms the 17e⁻ acyl complex. Next hydrogen is activated via a heterolytic cleavage to produce aldehyde and regenerate catalyst after CO coordination. The hydrogen activation step is proposed to be a heterolytic cleavage due to the low probability of doing an oxidative addition to a cationic Co(II) complex to form a cationic Co(IV) dihydride.⁵

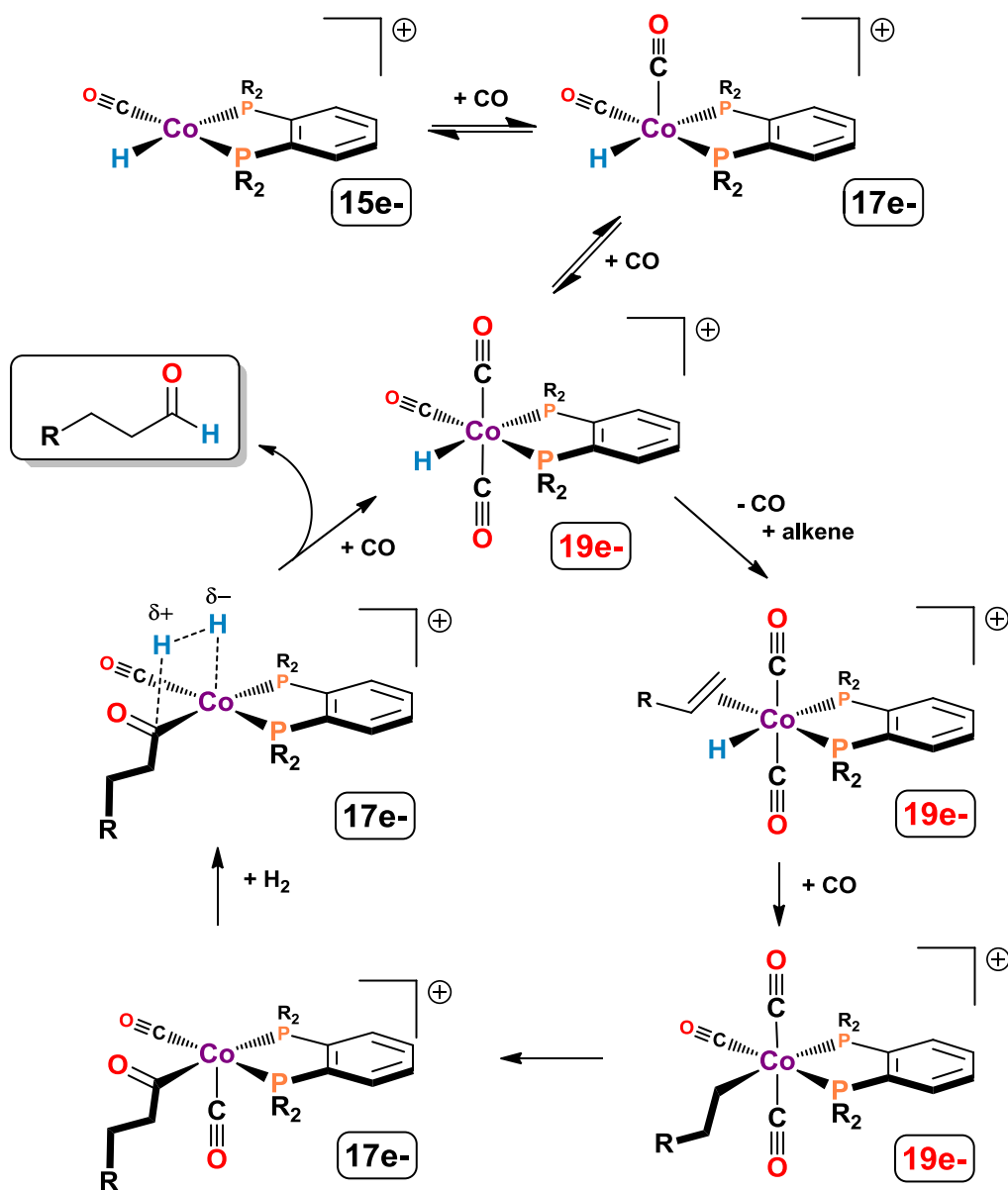


Figure 2.20. Proposed hydroformylation mechanism involving 19e- catalyst species.

There is a much lower energy cost to form a 19e- vs. a 20e- complex. Basolo and Trogler demonstrated that the carbonyl substitution chemistry for 17e- V(CO)₆ radical proceeds 10¹⁰ times faster than for 18e- Cr(CO)₆.¹⁸ The phosphine substitution reaction with the 17e- V(CO)₆ radical was shown to be associative and extremely facile proceeding through a 19e- transition

state. The 18e- $[\text{V}(\text{CO})_6]^-$ anion, in marked contrast, is inert towards phosphine substitution reactions.

2.5. References

1. Broussard, M., Juma, B., Train, S.G., Peng, W., Laneman, S.A., Stanley, G.G., A Bimetallic Hydroformylation Catalyst: High Regioselectivity and Reactivity Through Homobimetallic Cooperativity. *Science*, **1993**, 260, 1784-1788.
2. Laneman, S.A., Stanley, G.G., Homogeneous Bimetallic Hydroformylation Catalysis Two Metals Are Better Than One. *Advances in Chemistry*, **1992**, 230, 349-366.
3. Aubry, D.A., Monteil, A.R., Peng, W., Stanley, G.G., The unusual inhibition of a dirhodium tetraphosphine-based bimetallic hydroformylation catalyst by PPh_3 . *C. R. Chimie*. **2002**, 5, 1-8.
4. Schwarzhan, K.E., NMR Spectroscopy of Paramagnetic Complexes *Angew. Chem. internat. Edit.* **1970**, 9, 946.
5. Crabtree, R. *The Organometallic Chemistry of the Transition Metals*. Wiley: 2014.
6. Glidewell, C., *Metal Acetylacetonate Complexes: Preparation and Characterisation. In Inorganic Experiments*. Wiley-VCH: 2010.
7. Brito, J.A.; Archer, M., *Practical Approaches to Biological Inorganic Chemistry*. Elsevier: 2013
8. Krafft, M. J., Bubrin, M., Paretzki, A., Lissner, F., Fiedler, J., Zálíš, S. Kaim, W., Identifying Intermediates of Sequential Electron and Hydrogen Loss from a Dicarbonylcobalt Hydride Complex. *Angew. Chem. Int. Ed.*, **2013**, 52, 6781-6784.
9. Sternberg, H. W., Wender, I., Friedel, R. A., and Orchin, M. The chemistry of metal carbonyls. II. Preparation and properties of cobalt hydrocarbonyl. *J. Am. Chem. Soc.* **1953**, 75, 2717.
10. Edgell, W. F., Gallup, G., The bonding of the hydrogen atom in $\text{Co}(\text{CO})_4\text{H}$. *J. Am. Chem. Soc.* **1955**, 77, 5762.
11. Friedel, R. A., Wender, I., Shufler, S. L., Sternberg, H. W., Spectra and structures of cobalt carbonyls. *J. Am. Chem. Soc.* **1955**, 77, 3951.
12. Edgell, W. F., Magee, C., Gallup, G., The infrared spectrum of cobalt carbonyl hydride. *J. Am. Chem. Soc.* **1956**, 78, 4185

13. Haumann, M., Meijboom, R., Moss, J. R., Roodt, A., Synthesis, crystal structure and hydroformylation activity of triphenylphosphite modified cobalt catalysts. *Dalton Trans.* **2004**, 1679
14. Poilblanc, R., Attali, S., Arabi, M. S., Labroue, D., Maisonnat, A., de Montauzon, D., Cobalt carbonyl and its derivatives. *Oil Gas Sci. Technol.—Rev. IFP* **1974**, 29, 387.
15. Lee, K. Y., Kochi, J. K., Oxidation-reduction of carbonylcobalt cation-anion pairs in coupling to dimeric cobalt carbonyls. *Inorg. Chem.* **1989**, 28, 567.
16. Rathke, J. W., Klinger, R. J., Krause, T. R., Propylene hydroformylation in supercritical carbon dioxide. *Organometallics*, **1991**, 10, 1350.
17. Rathke, J. W., Klinger, R. J., Krause, T. R.. Thermodynamics for the hydrogenation of dicobalt octacarbonyl in supercritical carbon dioxide. *Organometallics*, **1992**, 11, 585.
18. Shi, Q., Richmond, T.G., Trogier, W.C., Basolo, F., Mechanism of Carbon Monoxide Substitution in Metal Carbonyl Radicals: Vanadium Hexacarbonyl and Its Phosphine-Substituted Derivatives. *J. Am. Chem. Soc.*, 1984, 106, 71.

Chapter 3. Catalyst Modifications

3.1. Introduction

Ligands were first used to modify hydroformylation catalysts in the early 1960s when Shell added phosphines to $\text{HCo}(\text{CO})_4$ drastically modifying the catalytic activity and stability. The same phenomenon was observed soon after by Wilkinson for rhodium which resulted in the development of the low-pressure (LPO) Rh/ PPh_3 technology. In both cases activity decreased while selectivity and stability increased. In the years following many different ligand modifications have been investigated with several noteworthy breakthroughs, although most of these investigations have been done with rhodium due to its higher activity and lower pressure requirements.¹

Early on rhodium was modified with the nitrogen, arsenic, antimony, and bismuth analogs of PPh_3 and were shown to produce significantly less active catalysts.² Therefore, ligands used for hydroformylation are mostly based on P(III) compounds with lone pairs. The phosphorus ligands are usually phosphines, which are ligands where the phosphorus has three carbon bonds, or phosphites where the phosphorus has three phosphine-oxygen bonds. Other more exotic ligands exist but they are of minor importance. Ligands that bind to a metal center through one Lewis base are considered monodentate. If the ligand binds to the metal using two Lewis base donors connected by a bridging group, then the ligand is bidentate. Tridentate and tetradentate ligands exist as well but have low activity for monometallic hydroformylation catalysts.¹

Modifications to the oxidation state or charge of the metal is much less common than ligand modifications. Prof. Stanley's work with a dicationic dirhodium complex is one of the only such examples where catalyst hydroformylation catalyst has a formal charge on the metal

center and operates in an unusual oxidation state for most of the catalytic cycle. This is surprising because monometallic cationic Rh(I) starting materials with PPh₃ ligands generate poor hydroformylation catalysts. The reason is that cationic Rh(III) dihydride complexes are produced when H₂ oxidatively adds to the cationic Rh(I) precursor. The cationic Rh(III) dihydride complexes are good at alkene hydrogenation and isomerization, but not good at hydroformylation. However, the work done by the Stanley group clearly shows that localized cationic charge on the metal center can compensate for stronger donating phosphines to produce labile carbonyls and active hydroformylation catalysts when working with dirhodium complexes.³

3.2. Effects of Complex Charge on Catalytic Activity

In order to probe the importance of cation charge on the metal center for high catalyst activity neutral and dicationic complexes were tested. Table 3.1 shows the effects of modifying the charge on the cobalt center. Clearly the +1 charge is a sweet spot resulting the highest activity by far. In the case of the dicationic system activation may be occurring via some cobalt-cobalt disproportionation reaction pathway that is producing some of the highly active monocationic complex. This makes for a good explanation since the rate of the dicationic precursor seem to be approximately half that of the monocationic precursor, possibly corresponding to a disproportion activation pathway in which about half of the precatalyst is turned into active catalyst. Additionally the identical L:B ratios support the possibility that in both runs the same active catalyst is present. No activity is seen for the neutral catalyst most likely due to the high steric congestion of the complex preventing activation. This makes for a slightly unfair comparison between the neutral and monocationic catalyst systems so another test is needed to truly discern the difference between them.

Table 3.1. Comparison of Different Charges on a Co-DPPBz catalyst.

Catalyst	TOF (min ⁻¹)	L:B	Aldehyde (%)	Isomer (%)	Alkane (%)
Co(acac) ₂ (DPPBz)	0	NA	0	0	0
[Co(acac)(DPPBz)](BF ₄)	66.0	1.1	33.0	39.5	0
[Co(DPPBz)](BF ₄) ₂	28.2	1.1	14.1	22.4	0

Reactions run in t-gylme solvent at 160°C under 725 psig (50 bar) of 1:1 H₂:CO with 1m M catalyst, 0.1 M heptane and 1 M 1-hexene. TOF = turnover frequency, L:B = aldehyde linear:branched ratio, Isomer = alkene isomerization. Results are based on a 5 min sample analyzed by GC/MS.

Table 3.2 shows another comparison of the effect metal center charge has on catalyst activity. Again the most active catalysts by far is the monocationic catalyst doubling the rates seen for the neutral catalyst. Unlike Table 3.1 the neutral catalyst, which is essentially the Shell phosphine-modified catalyst system, has no problem activating since the phosphine ligands are constantly dissociating and rebinding to open up coordination sites to facilitate activation. The monocationic starting complex may indeed produce a cationic $[\text{HCo}(\text{CO})_x(\text{PBu}_3)]^+$ ($x = 1-4$), catalyst that is similar to our chelated bisphosphine-based system. The higher activity and lower selectivity clearly indicates that we have not formed a neutral Shell phosphine-modified catalyst. The dicationic system can use the more basic PBu₃ to help the heterolytic cleavage of H₂ on the dicationic cobalt center to generate the monocationic $[\text{HCo}(\text{CO})_x(\text{PBu}_3)]^+$ ($x = 1-4$) catalyst and a protonated $[\text{HPBu}_3]^+$. This, however, decreases the amount of PBu₃ phosphine present that negatively affects the stability of the monometallic catalyst leading to catalyst deactivation and release of PBu₃. The lower amount of monocationic $[\text{HCo}(\text{CO})_x(\text{PBu}_3)]^+$ ($x = 1-4$) catalyst and additional PBu₃ can lead to deprotonation of the monocationic catalyst producing some slower, but more selective neutral Shell-like catalyst. The L:B seen for the dicationic system is higher

than the one observed for the monocationic system but lower than the neutral system suggesting a possible combination of the two catalyst systems.

Table 3.2. Comparison of Different Charges on a Co-PBu₃ catalyst.

Catalyst	Time	TOF (min ⁻¹)	L:B	Aldehyde (%)	Alcohol (%)	Isomer (%)	Alkane (%)
Co(acac) ₂ + 3eq Bu ₃ P	10 min	4.5		8.9	0	37.2	0.5
	1 hr		6.1	24.6	4.0	60.3	1.0
Co(acac)(BF ₄) + 3eq Bu ₃ P	10 min	9.1		18.2	0	48.6	0.7
	1 hr		1.2	44.4	5.1	45.6	1.4
Co(BF ₄) ₂ + 3eq Bu ₃ P	10 min	0.5		1.1	0	9.0	0
	1 hr	2.8	2.8	13.7	0	55.4	0.7

Reactions run in t-gylme solvent at 180°C under 750 psig (50 bar) of 1:1 H₂:CO with 2 mM cobalt, 6 mM PBu₃ ligand, L:Co = 3:1, 0.1 M heptane and 1 M 1-hexene. 1-hexene:Co = 500. TOF = turnover frequency, L:B = aldehyde linear:branched ratio, Isomer = alkene isomerization. Samples analyzed by GC/MS.

Also worth emphasizing is the considerable difference in the L:B selectivity between the neutral catalyst at 6.1 and monocationic systems at 1.2. This alone suffices to show that the two catalyst systems must be different. Since the neutral catalyst is the phosphine modified HCo(CO)₄, i.e., HCo(CO)₃(PBu₃), this supports that Co(acac)(BF₄) is not reacting to produce HCo(CO)₄ or HCo(CO)₃(PBu₃) during catalysis even under these harsh conditions. The monocationic characteristic of this Co(II) catalyst appears to be as important factor in the high catalytic activity observed.

3.3. Alternative Ligands

A large variety of ligands have been used to modify hydroformylation catalyst over the years, however; one basic comparison that should always be made is the catalyst without a ligand. Table 3.3 shows a comparison between the cationic cobalt catalyst with and without a

chelating bisphosphine ligand as well as the original unmodified $\text{HCo}(\text{CO})_4$ catalyst, which is formed in situ from Co_2CO_8 . The cationic cobalt precatalyst without a ligand shows no catalytic activity reinforcing the fact that $\text{HCo}(\text{CO})_4$ is not forming from this starting material under these conditions. $\text{HCo}(\text{CO})_4$ formed from Co_2CO_8 does show high initial activity, although still less than the $[\text{Co}(\text{acac})(\text{DEPBz})](\text{BF}_4)$ catalyst precursor. However, the activity is short-lived since $\text{HCo}(\text{CO})_4$ is not stable under these conditions resulting in the loss of activity via catalyst degradation verified by the presents of cobalt metal in the autoclave. Again based on the difference in activity and stability between $\text{HCo}(\text{CO})_4$ and $[\text{Co}(\text{acac})(\text{DEPBz})](\text{BF}_4)$ the active catalyst present in the $[\text{Co}(\text{acac})(\text{DEPBz})](\text{BF}_4)$ runs cannot be $\text{HCo}(\text{CO})_4$.

Table 3.3. Comparison of hydroformylation catalyst with and without a ligand.

Catalyst	Time	TOF (min^{-1})	L:B	Aldehyde (%)	Alcohol (%)	Isomer (%)	Alkane (%)
$[\text{Co}(\text{acac})(\text{DEPBz})](\text{BF}_4)$	10 min	21.2		42.5	1.0	51.8	1.1
	2 hr		0.95	77.9	11.4	8.4	2.0
$[\text{Co}(\text{acac})(\text{dioxane})_4](\text{BF}_4)$	10 min	N/A	N/A	0	0	0	0
	2 hr		N/A	0	0	0	0
Co_2CO_8	10 min	14.4		28.8	0	56.7	0.8
(extensive decomposition to Co metal)	2 hr		0.93	39.1	6.0	55.6	1.1

Reactions run in t-gylme solvent at 160°C under 450psi of 1:1 $\text{H}_2:\text{CO}$ with 2mM Cobalt, 0.1M heptane and 1M 1-hexene. TOF = turnover frequency, L:B = aldehyde linear:branched ratio, Isomer = alkene isomerization. Samples analyzed by GC/MS.

Now that the need for a phosphine ligand has been verified the next question to address is what ligands work best for this new cationic cobalt(II) catalyst motif. As a way of verifying that phosphorus based ligands are superior to nitrogen based ligands for the cationic cobalt catalyst a complex using tetramethylethylenediamine (TMEDA), $\text{Me}_2\text{NCH}_2\text{CH}_2\text{NMe}_2$, as a ligand was

made. The $[\text{Co}(\text{acac})(\text{TMEDA})](\text{BF}_4)$ complex was evaluated for hydroformylation activity and produced no catalytic activity after several hours under 725 psig (50 bar) 1:1 $\text{H}_2:\text{CO}$ at 160°C . Clearly the phosphorus based ligands are far superior for hydroformylation even when using a cationic cobalt precursor.

If the $[\text{Co}(\text{acac})(\text{TMEDA})](\text{BF}_4)$ complex is left soaking for a prolonged period of time hydroformylation does commence along with metal decomposition reactions noted by metal plating observed in the autoclave. However, given the long induction period, the low steric hindrance of the ligand, the strong basic nature of the ligand and the metal decomposition observed the most likely scenario is that under these conditions some preforming reaction to form $\text{HCo}(\text{CO})_4$ occurs to eventually give hydroformylation activity. Again this preforming reaction seems to be facilitated by the strong base TMEDA since the precatalyst without a ligand does not form any active catalyst under these conditions even after soaking for 18 hrs, much longer than the time taken for the reaction with TMEDA to become active.

Next the question of whether monodentate or bidentate ligands produce more active catalysts was raised. The answer can be clearly seen between Tables 3.1 and 3.2 where the initial turnover rate for the bidentate ligand complex was approximately 7 times faster than the monodentate ligand despite the slightly higher pressure and higher temperature. The bidentate ligands proved to always be significantly faster than the monodentate ligands regardless of the ligand concertation. Logically this makes sense for monodentate phosphines because regardless of the phosphine:cobalt ratios some catalyst will always have too many or not enough ligands bound at any given time reducing the percentage of the catalyst in an active form. Because the catalyst precursor is prepared with the bidentate phosphine the catalyst has the correct number of phosphine ligands always coordinated, favoring the most active and stable catalyst complexes.

Tridentate and tetradentate ligands have not been evaluated at this time, although they have produced far less active monometallic catalysts for hydroformylation.¹

Also worth noting is that the less electron-rich PPh₃ ligand never produced active catalyst regardless of concentration. This is in stark contrast to the neutral phosphine modified Shell cobalt catalyst research that showed that less donating phosphines produced more active catalysts with lower selectivities.⁴ The ability of a cationic Co(II) center to tolerate more electron-donating bisphosphine ligands and maintain high activity is consistent with all our data.

Normally when using chelating ligands excess ligand is added to the reaction to account for ligand dissociation. In all of the runs presented no excess phosphine is added to the reaction since the phosphine dissociation rate is assumed to be very low. However to verify that ligand dissociation is low and that excess phosphine is not needed a run was done in which excess phosphine was added. The addition of two extra equivalents of DPPBz resulted in an 18 fold reduction in turnover frequency clearly showing that the phosphine dissociation rate must be very low. Ligand inhibiting effects are shown in Table 3.4 where the effect of the addition of 1 eq of Bu₃P and 10% by volume of acetonitrile on catalytic performance are evaluated. The addition of coordinating ligands does result in a considerable reduction of catalyst activity, but little effect on the aldehyde L:B selectivity.

Table 3.4. Additive Effects on Hydroformylation with [Co(acac)DPPBz](BF₄).

Additive	Initial TOF (min ⁻¹)	L:B	% Aldehyde	% Alcohol	% iso	% hydro
----	45.4	1.1	45.4	0	38.1	0.8
10% CH ₃ C≡N	23.1	0.8	23.1	0	19.7	0.4
1 eq P(<i>n</i> -butyl) ₃	23.8	1.1	23.8	0	26.0	0.5

Reactions run in *t*-glyme solvent at 160°C under 750 psi (50 bar) of 1:1 H₂:CO with 1 mM [Co(acac)DPPBz](BF₄) catalyst, 0.1 M heptane and 1 M 1-hexene. TOF = turnover frequency, L:B = aldehyde linear:branched ratio, Isomer = alkene isomerization. Results are based on a 10 min sample analyzed by GC/MS.

3.4. Effects of Modifying Chelating Bisphosphine Ligands.

In an attempt to further probe the relationship between the bidentate bisphosphine ligands and catalyst activity two parameters were modified. First the bite angle of the ligand was augmented by varying the carbon chain length on the ligand backbone. Table 3.5 outlines the effect of changing bite angle has on the cationic cobalt(II) catalyst. Figure 3.1 shows the ligands used in the following reactions.

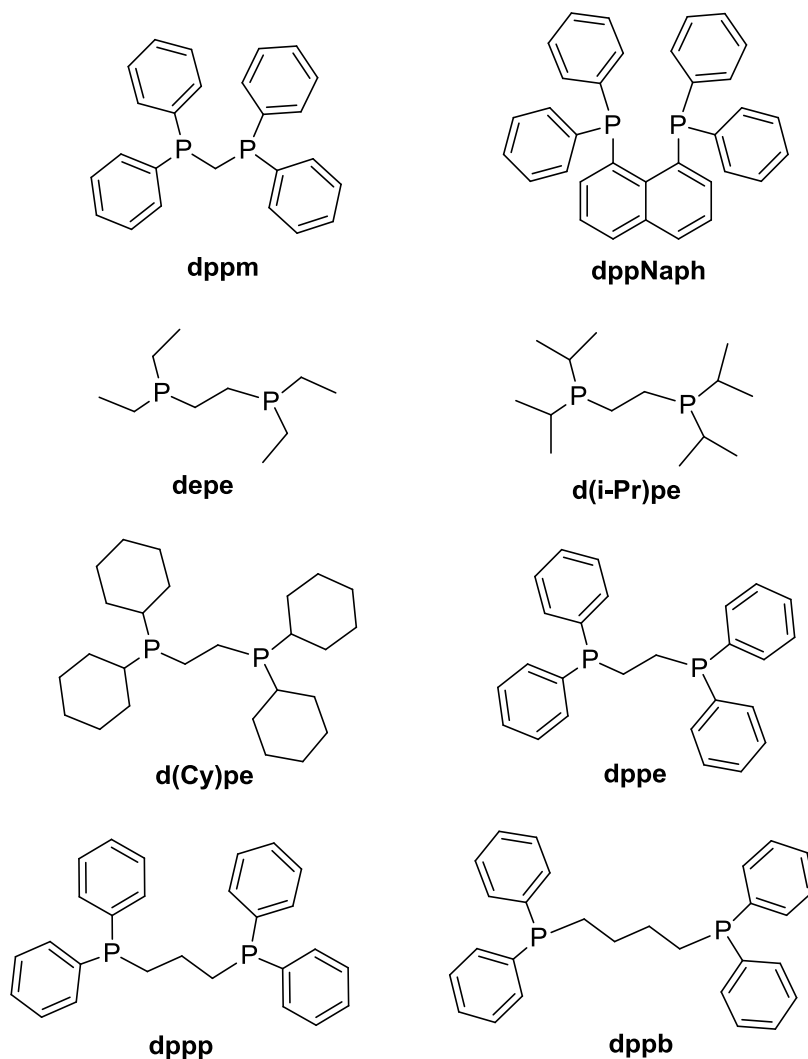


Figure 3.1. Ligands used in Tables 3.5 ad 3.6

The $[\text{Co}(\text{acac})(\text{dppe})](\text{BF}_4)$ two carbon backbone complex is by far the best catalyst of this group converting significantly more 1-hexene to aldehyde. The three carbon backbone

complex $[\text{Co}(\text{acac})(\text{dppp})](\text{BF}_4)$ is slower due to the increased flexibility in the propylene bridge, which makes for a weaker chelate effect. However, there is a more subtle and important steric effect that is occurring. The dppp chelate generally orients two of the phenyl rings down into axial 6-membered ring orientations, while the other two phenyl rings orient into outward directed equatorial positions. Figure 3.2 shows space filling models of $\text{Ni}(\kappa^2\text{-S-benzoate})(\kappa^2\text{-dppp})$ showing the two axial coordination sites.⁷ One site is fairly open, while the other axial binding site is blocked by the axial phenyl rings on the dppp ligand. We propose that the dppp ligand can twist its 6-membered chelate ring to open up both axial coordination sites, but often one site is blocked, which limits the amount of 19e- tricarbonyl catalyst, $[\text{HCo}(\text{CO})_3(\text{P}_2)]^+$, that can form. The 19e- tricarbonyl complex is important for labilizing the equatorial Co-CO to allow alkene to coordinate. Once again, as you can see from the space-filling models of the nickel-dppp complex, the axial coordination site is not accessible to sterically hindered alkenes. We proposed that the $[\text{HCo}(\text{CO})_x(\text{dppp})]^+$ ($x = 1-3$) catalyst has more difficulty forming the 19e- tricarbonyl and, therefore, has lower activity than the dppe ligand, which has more open axial coordination sites.

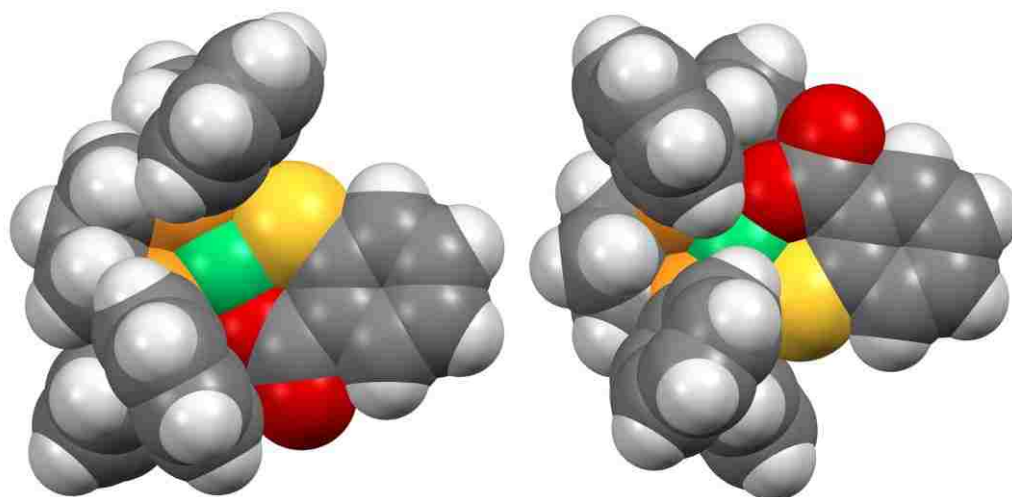


Figure 3.2. Space-filling models of $\text{Ni}(\kappa^2\text{-S-benzoate})(\kappa^2\text{-dppp})$ showing the two axial coordination sites. The nickel center is colored green.

This is made clear by the complete lack of activity seen for the other three carbon backbone complex, $[\text{Co}(\text{acac})(\text{dppNaph})](\text{BF}_4)$, that has a rigid planar backbone. We propose that the $[\text{Co}(\text{acac})(\text{dppNaph})](\text{BF}_4)$ complex can't even form the dicarbonyl catalyst, much less the tricarbonyl, which deactivates it for hydroformylation. The distortion of the dppNaph ligand to block both axial coordination sites is illustrated in Figure 3.3 with space filling models of the two axial binding sites for $\text{NiCl}_2(\text{dppNaph})$.⁸

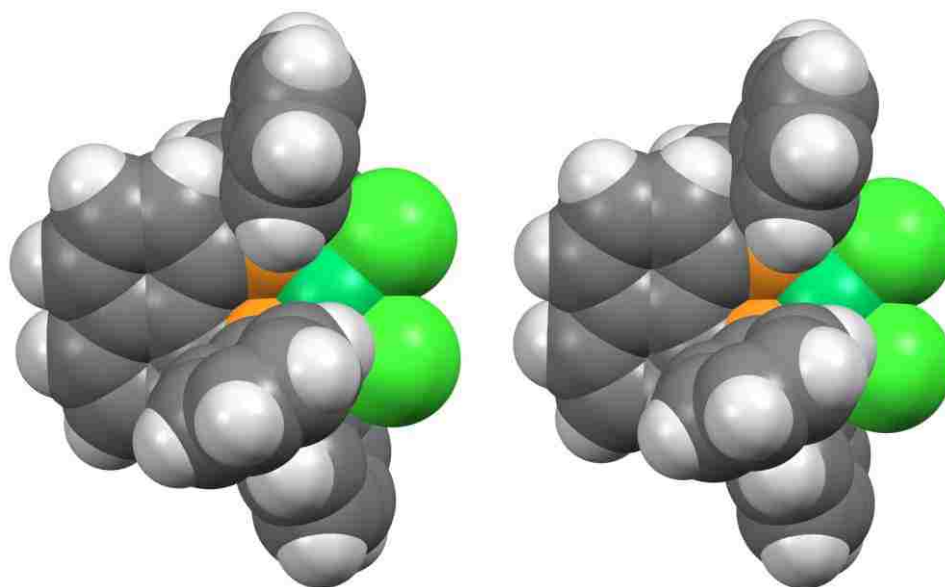


Figure 3.3. Space filling models showing the blocked axial binding sites for $\text{NiCl}_2(\text{dppNaph})$. Both sites are identical and related by a 2-fold rotation axis. The nickel center is square-planar and green, while the two chloride ligands are a different shade of green.

The four carbon backbone complex $[\text{Co}(\text{acac})(\text{dppb})](\text{BF}_4)$ suffers from a weak chelate effect and the same kind of phenyl ring blocking of at least one of the axial coordination sites that makes forming the 19e- tricarbonyl cobalt catalyst complex difficult.^{5,6,9} Finally, the dppm complex doesn't show any activity since it probably acts as a bridging ligand due to the higher energy of the 4-membered chelate ring.

Table 3.5. Effects of Bisphosphine Bite Angle on Hydroformylation Activity for 1-Hexene.

Catalyst	L:B	Aldehyde (%)	Isomer (%)	Alkane (%)
[Co(acac)(dppm)](BF ₄)	NA	0	0	0
[Co(acac)(dppe)](BF ₄)	1.3	45.6	17.9	0
[Co(acac)(dppp)](BF ₄)	1.3	29.3	13.5	0
[Co(acac)(dppNaph)](BF ₄)	NA	0	0	0
[Co(acac)(dppb)](BF ₄)	1.4	8.6	5.9	0

Reactions run in t-gylme solvent at 140°C under 725 psig (50 bar) of 1:1 H₂:CO with 1 mM catalyst, 0.1 M heptane and 1 M 1-hexene. L:B = aldehyde linear:branched ratio, Isomer = alkene isomerization. Results are based on a 20 min sample analyzed by GC/MS.

Another ligand modification to be probed is the effect of steric bulk on catalyst performance. In order to test this an ethyl backbone bisphosphine ligand motif was used. The R groups on the phosphines were varied from an ethyl group with low steric bulk to an isopropyl and cyclohexyl groups with high steric effect. Table 3.6 shows the role of increasing steric demand on catalyst activity. As the steric bulk is increased for an ethyl to a cyclohexyl or an isopropyl the rate is drastically reduced. The cyclohexyl-substituted catalyst precursor took over 40 mins to activate. The most likely explanation for this delay is that the cyclohexyl groups are blocking the axial binding sites on the complex inhibiting activation of the catalyst precursor by hydrogen. In Figure 3.4 this can be visualized by viewing the space filling model for the crystal structure from chapter 2 of [Co(acac)DPPBz](BF₄) with the BF₄ anion and coordinated THF solvent removed for clarity. Clearly the phenyl groups can move out of the way and facilitate catalyst activation, however; the higher steric demand imposed by the cyclohexyl groups block off more of the binding pocket resulting in slower activation. Figure 3.4 shows an interesting effect. In order to accommodate the larger THF that coordinates in the one axial site, the phenyl rings on that site open more than usual, which causes the phenyl rings on the opposite side to rotate and block that axial site. DFT calculation show that two smaller CO ligands can bind at

the same time to both axial sites on the cobalt with the DPPBz ligand, especially if the catalyst becomes high-spin and has longer Co-P bond distances.

Table 3.6. 1-Hexene Hydroformylation using $[\text{Co}(\text{acac})(\text{P}_2)](\text{BF}_4)$ with different R groups on bisphosphine Ligands.

Catalyst Precursor	L:B	Aldehyde (%)	Isomer (%)	Alkane (%)
$[\text{Co}(\text{acac})(\text{depe})](\text{BF}_4)$	1.2	50.8	20.9	0
$[\text{Co}(\text{acac})(\text{dppe})](\text{BF}_4)$	1.3	45.6	17.9	0
$[\text{Co}(\text{acac})(\text{d}(\text{Cy})\text{pe})](\text{BF}_4)^*$	1.2	36.1	17.1	0
$[\text{Co}(\text{acac})(\text{d}(\text{i-Pr})\text{pe})](\text{BF}_4)$	1.3	20.8	11.9	0

Reactions run in t-gylme solvent at 140°C under 725 psig (50 bar) of 1:1 H_2 :CO with 1 mM catalyst, 0.1 M heptane and 1 M 1-hexene. L:B = aldehyde linear:branched ratio, Isomer = alkene isomerization. Results are based on a 20 min sample analyzed by GC/MS. * $[\text{Co}(\text{acac})(\text{d}(\text{Cy})\text{pe})](\text{BF}_4)$ catalyst did not activate until 44 min after alkene was injected, sample was taken after an additional 20 mins.

In addition to explaining the slow activation of $[\text{Co}(\text{acac})(\text{d}(\text{Cy})\text{pe})](\text{BF}_4)$ the inhibition of carbonyl ligand addition to the axial binding site by more sterically hindered bisphosphine ligands also helps to explain the rate trends in Table 3.6. Again the rate of hydroformylation decreases with increasing steric bulk on the ligand. This is nicely explained by the sterically demanding ligands blocking out the axial binding sites. The inhibition of CO binding to the axial site on the metal center would reduce the catalyst activity since the binding of two axial CO ligands to form a $19e^-$ tricarbonyl complex is proposed to be crucial to the catalytic activity.

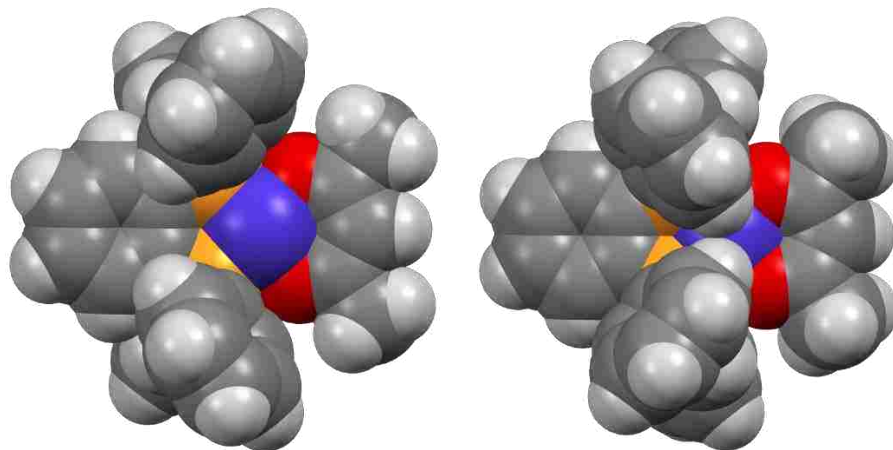


Figure 3.4. Space filling model of $[\text{Co}(\text{acac})\text{DPPBz}](\text{BF}_4)$ showing the two axial views. The THF molecule coordinated to the cobalt is not shown on the left-side view.

Furthermore, the constant low L:B selectivity can also be explained by observing the space filling model of $[\text{Co}(\text{acac})\text{DPPBz}](\text{BF}_4)$ in Figure 3.4. The phenyl groups shown are exhibiting very little steric pressure on the equatorial binding sites where the acac ligand is bonded. Swapping the phenyl groups out for isopropyl or cyclohexyl groups would not have much of an effect on the equatorial plane as most of the additional steric bulk is directed into the axial region. This is why no increase in L:B aldehyde selectivity is observed for the higher steric bulk of these ligand modifications. Alternative ligand modifications that forced the additional steric bulk into the equatorial plane while leaving the axial plane unaffected would be needed to produce higher L:B selectivity while retaining high catalyst activity. Such a ligand is under investigation but has not been made to date.

3.5. References

1. Franke, R., Selent, D., Börner, A., Applied Hydroformylation. *Chem. Rev.* **2012**, 112, 5675–5732.
2. Carlock, J.T., A comparative study of triphenylamine, triphenylphosphine, triphenylarsine, triphenylantimony and triphenylbismuth as ligands in the rhodium-catalyzed hydroformylation of 1-dodecene. *Tetrahedron*, **1984**, 40,185–192.

3. David A. Aubry, Alexandre R. Monteil, Wei-Jun Peng, George G. Stanley, The unusual inhibition of a dirhodium tetrphosphine-based bimetallic hydroformylation catalyst by PPh₃. *C. R. Chimie*, **2002**, 5, 473–480.
4. Slaugh, L. H.; Mullineaux, R. D., Novel Hydroformylation Catalyst. *J. Organomet. Chem.* **1968**, 13 (2), 469.
5. L.J.McCaffrey, W.Henderson, B.K.Nicholson, J.E.Mackay, M.B.Dinger, Platinum(II), palladium(II), and nickel(II) thiosalicylate complexes. *J.Chem.Soc.,Dalton Trans.* **1997**, 2577.
6. T.Niksch, H.Gorls, M.Friedrich, R.Oilunkaniemi, R.Laitinen, W.Weigand, Synthesis and Characterisation of 2,2-Bis(hydroxymethyl)-1,3-diselenolato Metal(II) Complexes Bearing Various Phosphanes *Eur.J.Inorg.Chem.* **2010**, 74
7. Kamer, P.C.J., Van Leeuwen, P.W.N.M., Reek, J.N.H., Wide Bite Angle Diphosphines: Xantphos Ligands in Transition Metal Complexes and Catalysis. *Acc. Chem. Res.* **2001**, 34, 895-904.
8. Freixa, Z., van Leeuwen, P.W.N.M., Bite angle effects in diphosphine metal catalysts: steric or electronic? *Dalton Trans.* **2003**, 1890–1901.
9. Crabtree, R. *The Organometallic Chemistry of the Transition Metals*. Wiley: 2014.

Chapter 4. Reaction Condition Optimization

4.1. Introduction

Reaction conditions can have substantial impact on catalyst activity, stability, and selectivity in hydroformylation. Much of this stems from two of the three reagents, H₂ and CO, being gases. Since gas concentration is dependent on solvent, temperature and pressure all of these factors have a noticeable impact on catalytic performance.¹

In the case of the unmodified HCo(CO)₄ hydroformylation catalyst the concentration of carbon monoxide and, therefore; the partial pressure plays a pivotal role in catalyst activity and stability. The carbon monoxide acts as a stabilizing ligand so when CO concentrations drop below a certain minimum the catalyst begins to degrade into cobalt metal. However, hydroformylation is usually inverse first order in CO concentration. Therefore, the high concentration of carbon monoxide has to be countered with higher operating temperatures in order to maintain acceptable overall rates. This requires operating conditions that strike a balance between reaction rates and temperature-pressure ratios to maintain catalyst stability. The result is rather harsh conditions with hydroformylation temperatures for HCo(CO)₄ between 150°C to 190°C and pressures between 250 and 350 bar.²

Phosphine-modified rhodium catalysts face similar issues with phosphine dissociation, which increases as the temperature increases. This results in less selective and less stable catalyst species being formed at higher temperatures. For this reason PPh₃-based rhodium hydroformylation is normally run with a phosphine to metal ratio in range of 400 to 1600:1.³

Hydroformylation catalysts are most active, selective, and stable across a certain set of operating conditions, which includes solvent and concentration of the catalyst and reactants. That

is why testing the catalyst while varying these conditions is important for better understanding the catalyst system and to discover the optimum reaction conditions.¹

4.2. Effects of Varying Temperature

Reaction rates almost always increase with temperature due to kinetics and activation barriers. The key is to find the upper and lower temperature limits for a given reaction. Most important is the upper temperature limit where catalyst decomposition starts.⁴ Table 4.1 shows the effects of varying temperature for the hydroformylation of 1-hexene using the catalyst precursor [Co(acac)DPPBz](BF₄). The catalyst precursor was activated at 160°C under 50 bar of H₂/CO for five minutes for the lower temperature runs. This was to ensure that the only variable being observed was the effect of temperature on the active catalyst and not the effect of temperature on activating the catalyst. The table clearly shows an increase in the rate of hydroformylation as temperature is increased from 120°C to 160°C by a factor of approximately 2.5. The inverse is observed for the rate of hydrogenation with no alkane observed for 120°C. Alkene isomerization increased with increasing temperature rising from 7.6% at 120°C to 18.9% at 160°C.

Table 4.1. Temperature effects for the Hydroformylation of 1-Hexene using [Co(acac)(DPPBz)](BF₄).

Temp (°C)	Pressure (bar)	Initial TOF (min ⁻¹)	Aldehyde (%)	Aldehyde L:B	Alkane (%)	Isomerization (%)
120	50	26.5	59.4	1.7	0	7.6
140	50	43.6	71.3	1.3	0.3	17.9
160*	50	66.0	76.8	1.1	1.4	18.9

Reaction run with 1 mM catalyst, 1 M 1-hexene, and 0.1 M heptane standard in tetraethylene glycol dimethyl ether (t-glyme) solvent under 1:1 H₂:CO. TOF = initial turnover frequency based on a sample taken at 5 min. Other results based on sampling after 1 hour. *TOF = initial turnover frequency based on a 2 min sample. Samples analyzed by GC/MS.

Table 4.2 mirrors Table 4.1 except the catalyst precursor used is based on the more electron-donating DEPbZ ligand, [Co(acac)(DEPBz)](BF₄). [Co(acac)(DEPBz)](BF₄) shows higher activity at lower temperatures than the DPPBz-based catalyst. The assumption was that full catalyst activation occurs at lower temperatures for the more electron-rich DEPbZ-catalyst and that 140°C was sufficient to fully activate the catalyst. This is why only the 120°C run was activated at 160°C.

Table 4.2 shows the results for the hydroformylation of 1-hexene using the DEPbZ-based catalyst: aldehyde production and alkene isomerization increase with increasing temperature, which was also observed with the DPPBz-catalyst and most other hydroformylation catalysts. The small difference in the initial hydroformylation rate between 160°C and 140°C is attributed to basing the initial TOF at 160°C on a 5 minute sample instead of a 2 minute sample like in table 4.1. The delay in sample collection meant that 38.4% of the alkene had been converted to aldehyde which is well outside of the acceptable conversion percentage to base an initial rate on. When such a large percentage of the alkene has already been consumed the concentration drops significantly enough to impact the rate law and reduce the overall observed rate at that time. Therefore, the expected rate for a 2 minute ample would be much higher and most likely produce a closer fit to that shown in Table 4.1.

Table 4.2. Temperature effects on [Co(acac)DEPBz]BF₄.

Temp (°C)	Pressure (bar)	Initial TOF (min ⁻¹)	Aldehyde (%)	Aldehyde L:B	Alkane (%)	Isomerization (%)
120*	50	25.4(5.0)	74.6(5.4)	1.6	0	7.9(1.1)
140	50	61.5(6.1)	84.7(1.2)	1.3	0	10.0(1.2)
160**	50	76.8(2.0)	78.2(4.9)	1.1	1.3(0.3)	19.5(1.0)

All reactions were run for 2 hrs with 1.0 M 1-hexene, 1.0 mM catalyst, and 0.1 M heptane as internal standard under 1:1 H₂/CO in tetraethylene glycol dimethyl ether (t-glyme) solvent. TOF = initial turnover frequency based on a 5 min sample. Values in parentheses are standard deviations based on four consistent catalytic runs. * The reaction mixture was heated to 160°C for 5 mins to activate catalyst then cooled to operating temperature before the alkene was injected. ** Some catalyst decomposition occurred as noted by black cobalt metal deposition inside the autoclave. Samples analyzed by GC/MS.

The reduction in overall aldehyde produced at the end of the run from 140°C to 160°C in Table 4.2 is most likely due to some catalyst decomposition noted at 160°C by black cobalt metal plating out on the walls of the autoclave. This is thought to be due to impurities in the ligand produced during the synthesis of the DEPBz ligand, which is prepared in our lab. However, decomposition at 160°C has been noted for other ligands that like DEPBz are more electron rich than DPPBz. More testing is needed to determine whether the decomposition of the Co-DEPBz catalyst is due to impurities or ligand-catalyst electronic factors.

Tables 4.1 and 4.2 both show an increase in aldehyde L:B is observed at lower temperature decreases, which can be attributed to two factors. One is that the increase in aldehyde L:B is due to a reduction in alkene isomerization at lower temperatures. This would lead to more 1-hexene being present and increase the statistical probability of producing linear aldehyde resulting in higher L:B. Another possibility is that the lower temperatures allow for higher carbon monoxide concentrations in solution, which favors hydroformylation over alkene isomerization.

Lower isomerization rates at lower temperatures almost surely contributes to the higher aldehyde L:B selectivity. However; to test whether carbon monoxide concentration was also a factor, a test alkene was chosen that could not be isomerized. This allows us to focus on the hydroformylation activity of the catalyst by removing the competing alkene isomerization catalysis. Table 4.3 shows the effect of temperature on the activity and L:B selectivity for the hydroformylation of 3,3-dimethyl-1-butene. There is a dramatic increase in catalyst activity on going from 120° to 140°C, and a small decrease in L:B selectivity from 99.0% at 120°C to 98.3% at 140°C. Longer reaction times were required for 120°C to convert enough alkene to get a clear branched aldehyde signal on the GC-MS for accurate calculations of the L:B ratio. Based

on the results from Table 4.3 the carbon monoxide concentration does influence L:B selectivity, but it is a fairly minor effect.

Table 4.3. Temperature Effect on the Hydroformylation of 3,3-Dimethyl-1-butene using [Co(acac)(DPPBz)](BF₄).

Temp (°C)	Pressure (bar)	Time (hr)	Aldehyde (%)	Aldehyde L:B
120	30	6	39.7	97
140	30	2	64.1	57

All reactions run with 1.0 M 3,3-dimethyl-1-butene, 1.0 mM catalyst, 0.1 M heptane as internal standard under 1:1 H₂/CO in tetraethylene glycol dimethyl ether (t-glyme) solvent. Product analysis determined by GC/MS.

4.3. Effects of Pressure

Pressure can be directly correlated to concentration when all other parameters are kept constant. The concentration of reagents can directly affect the rate of a given reaction and, therefore; affect the overall product distribution. Hydroformylation is a good example of this concept as modifying the partial pressures of hydrogen and carbon monoxide can drastically effect product distribution by enhancing the rate of some reactions while inhibiting others.⁴

Table 4.4 shows the effects of varying pressure on the catalyst generated from [Co(acac)DPPBz](BF₄). As the pressure increased the initial TOF, aldehyde L:B ratio, and overall aldehyde production all increased. Increasing the H₂/CO pressure decreased alkene isomerization and alkane production.

Table 4.4. Pressure Effects on the Hydroformylation of 1-Hexene using [Co(acac)DPPBz](BF₄).

Pressure (bar)	Temp (°C)	Initial TOF (min ⁻¹)	Aldehyde (%)	Aldehyde L:B	Alkane (%)	Isomerization (%)
30*	160	52.5	49.0	0.94	1.4	45.7
50	160	66.0	76.8	1.1	1.4	18.9
70	160	94.8	84.0	1.3	1.2	12.1
90	160	103.2	87.3	1.4	1.0	9.1

Reaction run with 1 mM catalyst, 1 M 1-hexene, and 0.1 M heptane standard in tetraethylene glycol dimethyl ether (t-glyme) solvent under 1:1 H₂:CO. TOF = initial turnover frequency based on a sample taken at 2 min. Other results based on sampling after 1 hour. *Some catalyst decomposition occurred as noted by black cobalt metal deposition inside the autoclave. Samples analyzed by GC/MS.

In order to see whether the trends observed in Table 4.4 were valid for other ligands, pressure effects were studied for the more electron-rich Co-DEPBz catalyst in Table 4.5. Unlike results with the DPPBz complex, evaluation of the DEPBz catalyst did not show a steady increase in rate. Instead a volcano type of plot is observed for rate where hydroformylation rate increases with pressure. However, there is a turning point after which the rate starts to decrease with increasing pressure. From a chemical standpoint this can be partially explained by the lower temperature used for this study (140°C) compared to the DPPBz-catalyst in Table 4.3 (160°C). The lower temperature for the DEPBz-catalyst study produces higher hydrogen and carbon monoxide concentrations in solution for a given pressure. Additionally the ligand being evaluated is a better electron donor that facilitates more π -backbonding to the carbonyls and stronger Co-carbonyl bonds. This should favor formation of the 19e- tricarbonyl complex that we have proposed is important in labilizing the equatorial carbonyl ligand that allows alkene coordination to the catalyst. But as the CO concentration increases in solution, it will start competing effectively with alkene coordination to the cobalt to fill this empty site and eventually become rate limiting.

Table 4.5. Pressure Effects on the Hydroformylation of 1-Hexene using [Co(acac)(DEPBz)](BF₄).

Pressure (bar)	Temp (°C)	Initial TOF (min ⁻¹)	Aldehyde (%)	Aldehyde L:B	Alkane (%)	Isomerization (%)
30*	140	40.0(5.1)	73.7(1.5)	1.0	0.5(0.4)	21.8(1.7)
50	140	61.5(6.1)	84.7(1.2)	1.3	0	10.0(1.2)
70	140	36.7(3.5)	79.3(2.2)	1.6	0	10.7(0.9)
90	140	21.7(2.3)	82.5(2.6)	1.8	0	8.1(0.6)

All reactions run for 2 hrs with 1.0 M 1-hexene, 1.0 mM catalyst, and 0.1 M heptane as internal standard under 1:1 H₂/CO in tetraethylene glycol dimethyl ether (t-glyme) solvent. TOF = initial turnover frequency based on a 5 min sample. Product analysis determined by GC/MS. * The reaction mixture was heated to 160°C for 5 mins to activate catalyst then cooled to operating temperature before the alkene was injected.

Other than rate all other trends for tables 4.5 and 4.4 qualitatively match with alkene isomerization and hydrogenation rates decreasing with increasing pressure, while aldehyde L:B selectivity increases as the pressure increases. 3,3-dimethyl-1-butene was used to probe the pressure effect on hydroformylation without having to worry about competing alkene isomerization reaction. Table 4.6 shows the results of this study using the Co-DPPBz catalyst system. As the pressure is increased from 30 to 40 bar a small increase in the aldehyde L:B selectivity is observed due to the increased carbon monoxide concentration. The higher pressure has a small effect on rate for this substrate, unlike that seen for 1-hexene.

Table 4.6. Pressure Effect on the Hydroformylation of 3,3-Dimethyl-1-butene using [Co(acac)(DPPBz)](BF₄).

Temp (°C)	Pressure (BAR)	Time (hr)	Aldehyde (%)	Aldehyde L:B
140	30	2	64.1	57
140	40	2	65.7	73

All reactions run with 1.0 M 3,3-Dimethyl-1-butene, 1.0 mM catalyst, 0.1 M heptane as internal standard, 1:1 H₂/CO in Tetraethylene glycol dimethyl ether (t-glyme) solvent. Product analysis determined by GC/MS.

4.4. Solvent Effects

Solvents are commonly needed in homogenous catalysis with some exceptions where the catalyst is soluble in pure reactant. Solvents can play a major role in catalysis enhancing, inhibiting, or altering catalyst activity. One good example of the role solvents can play is the dirhodium catalyst developed by the Stanley group. Table 4.7 shows how the addition of water to acetone affected the hydroformylation activity of several rhodium catalyst systems. The dirhodium catalyst was most effected by the addition of water with over a 50% increase in rate, as well as higher L:B selectivity and lower side reactions. Furthermore, all of the monometallic rhodium catalysts tested showed a similar solvent dependence with the addition of water increasing their rates, albeit to a lesser extent.⁵

Table 4.7. Addition of H₂O to Acetone Solvent for the Hydroformylation of 1-Hexene for Various Rh Catalysts at 90°C and 90 psig (6.2 bar) 1:1 H₂/CO.

Catalyst	H ₂ O (%)	Initial TOF (min ⁻¹)	Aldehyde L:B	Isomerization (%)
[<i>rac</i> -Rh ₂ (nbd) ₂ (<i>et,ph-P4</i>)](BF ₄) ₂	0	20	25	2.5
[<i>rac</i> -Rh ₂ (nbd) ₂ (<i>et,ph-P4</i>)](BF ₄) ₂	30	30	33	<0.5
Rh/PPh ₃ ^b	0	13	9.1	<0.5
Rh/PPh ₃ ^b	30	17	14	1.0
Rh/Bisbi ^c	0	25	70	<0.5
Rh/Bisbi ^c	30	37	80	2.0
Rh/Naphos ^c	0	27	120	1.5
Rh/Naphos ^c	30	35	100	2.2
Rh/Xantphos ^c	0	13	80	5.0
Rh/Xantphos ^c	30	28	60	<0.5

Conditions: Rh catalysts (1 mM) with 1-Hexene (1 M) at 90 °C and 6.2 bar 1:1 H₂/CO in acetone and with 30% added water by volume. Added^b 0.4 M PPh₃ (400 equiv), 1 mM Rh(acac)(CO)₂.^c 5 equiv of ligand.

The new cationic cobalt catalyst also has a preference for certain types of solvents. In general the ideal solvents seem to be unreactive solvents in which the catalyst precursor has a high degree of solubility. As with many catalysts, we should avoid solvents with strong metal coordination capabilities (e.g., acetonitrile) that can block empty coordination sites on the metal center needed to coordinate alkene and H₂.

Tetraethylene glycol dimethyl ether (t-glyme) was the solvent used for all initial catalyst screening. This solvent was chosen because the catalyst precursors were reasonably soluble and it is considered to be a relatively non-coordinating solvent. Other solvents such as acetone and dimethyl sulfoxide (DMSO) reacted with the catalyst and shut down catalytic activity completely. Acetophenone, decanol, and tetrahydrofuran (THF) solvents all worked to some extent for hydroformylation, but were not as good as t-glyme. Decanol drastically reduced the rate of hydroformylation as well as reducing the L:B aldehyde selectivity. Acetophenone gave similar results as t-glyme when the catalysis was run higher temperatures and pressures.

However, at lower temperatures around 110°C and modest pressures around 200 psig (13.8 bar), catalytic activity was shut down completely most likely due to solvent binding and saturating the catalyst complex.

THF was an especially strange solvent showing high catalytic activity even with catalyst precursors that had no activity in t-glyme. Table 4.8 shows the effects of using THF solvent with two catalyst precursors showing a clear distinction between the solvents. When using $[\text{Co}(\text{acac})(\text{DPPBz})](\text{BF}_4)$ as the catalyst precursor THF approximately cuts the hydroformylation rate in half. This is most likely due to THF binding to open coordination sites and saturating the active catalyst similar to what was previously seen with the addition of acetonitrile, a more strongly coordinating solvent.

Initially the $[\text{Co}(\text{acac})](\text{BF}_4)$ catalyst precursor seems to be well behaved in THF in that it had no catalyst activity after 1 hr as expected. However, when longer reaction times are evaluated using $[\text{Co}(\text{acac})](\text{BF}_4)$ as the catalyst precursor far more unusual effects are observed for THF. After 3.5 hrs an active hydroformylation catalyst is somehow produced. The extensive cobalt metal plating inside of the autoclave suggests that $\text{HCo}(\text{CO})_4$ is responsible for the activity observed under these conditions. Since no such activity is seen when $[\text{Co}(\text{acac})](\text{BF}_4)$ is tested in t-glyme despite significantly longer reaction times, the THF solvent must be assisting in some sort of preforming reaction in which $[\text{Co}(\text{acac})](\text{BF}_4)$ is reduced and converted to $\text{HCo}(\text{CO})_4$ under these conditions. These preforming reactions are much less likely to occur under the mild conditions that were used for NMR experiments with THF- d_8 since long induction times of 2-3 hrs were needed for the catalyst precursors to react with THF, even under the rather harsh conditions used in Table 4.8.

Table 4.8. Solvent Effects on the Hydroformylation of 1-Hexene using Different Cobalt Catalysts.

Catalyst	Solvent	Time	Aldehyde (%)	Aldehyde L:B	Alkane (%)	Isomerization (%)
[Co(acac)DPPBz](BF ₄)	THF	5 m	17.5	1.4	0	45.0
[Co(acac)DPPBz](BF ₄)	t-glyme	5 m	33.0	1.1	0	39.5
[Co(acac)](BF ₄)	THF	1 hr	0	0	0	0
[Co(acac)](BF ₄) (metal decomposition)	THF	3.5 hr	74.7	1.0	2.1	18.5
[Co(acac)](BF ₄)	t-glyme	18 hr	0	0	0	0

All reactions run with 1.0 M 1-hexene, 1.0 mM catalyst, 0.1 M heptane as internal standard, at 160°C under 725psi (50 bar) of 1:1 H₂/CO. Product analysis determined by GC/MS.

Clearly the best solvent found to date is the original test solvent t-glyme, which appears to have little if any interaction with the active catalyst. Ideally alkanes would be used as the solvent to favor maximum hydroformylation rates. Most hydroformylation catalysts are first order in alkene, including our cationic cobalt(II) bisphosphine system. Unfortunately the current catalyst precursors are not soluble in alkanes. Developing a catalyst precursor that is soluble in alkanes is currently being studied.

4.5. Catalyst Stability

All hydroformylation catalyst have a set of reaction conditions such as pressure, temperature and concentration for which they are active and reasonably stable. Stability is a major concern for any commercial catalyst since replacing catalyst is costly and decomposition products need to be disposed of or regenerated back into active catalyst. The low stability of some hydroformylation catalysts drastically reduces their commercial viability. One excellent example of this is the rhodium phosphite technology that has very high rates and extremely desirable L:B aldehyde selectivity, but is plagued by facile catalyst deactivations. Another good example is the original HCo(CO)₄ catalyst, which is highly active and a good catalyst for many difficult commercial alkene feeds. However, the active catalyst is only stable at high pressures,

which requires more robust reactors and engineering that drastically increases capital cost for building a hydroformylation plant and maintaining it.^{1,4}

There are several ways to assess the stability of a catalyst. The best way is to use a pilot plant in which a catalyst is operated and recycled for a month or more, just like in a full sized chemical plant. However, access to pilot plant facilities is limited and other approaches are often used in academia. One alternative approach is to test how many turnovers a catalyst can perform before deactivating. This can provide important insight into how long a catalyst might last in chemical plant before needing to be replaced.

Table 4.9 shows several high turnover hydroformylation runs with 1-hexene that were designed to test the stability of the catalyst. Initially the catalyst concentration was reduced to increase the overall potential number of turn overs to 100,000 of which 58,200 were achieved after 20 hrs. This was an impressive feat since the catalyst concentration was low and the reaction run in a batch autoclave reactor. Conditions like these put a good deal of strain on the catalyst as trace impurities and deactivation pathways that would normally not seriously impact larger amounts of catalyst used in our standard concentration runs (e.g., 1 mM) can now completely deactivate low concentrations of catalyst used in these high turnover runs.

With good results after lowering the catalyst loading the next test increased the alkene concentration to further increase the maximum turnover number. In order to increase the alkene concentration the catalyst dissolved in t-glyme was pressure injected into hot alkene and solvent in the autoclave, instead of the normal run conditions where the opposite is done. A 1-hexene concentration of 6 M in t-glyme solvent was used with the Co-DPPBz catalyst concentration of 6 μ M, which represents one million turnovers. After 41 hrs of reaction, 179,000 turnovers of aldehyde was produced. Once again, the catalyst was still functioning normally when the

reaction was stopped. This was astonishing for a batch reactor test and prompted a test to truly push the catalyst stability limits.

The catalyst loading was dropped to 3 μM with 6 M 1-hexene, increasing the maximum turnover number to two million. After two weeks over half of the alkene was converted to give an approximated turnover number of 1.2 million. The turnover number was determined by using the heptane standard and including the aldehyde condensation products (i.e., heavy ends that were mostly dimers and some trimers). The final product distribution was: 2% 1-hexene, 1.2% alkane, 40.8% iso-hexenes, 33.4% aldehyde (over half 2-methyl hexanal), 1.1% alcohol, and 21.5% heavy ends.

Table 4.9. High Turnover Hydroformylation Catalysis Runs using 1-Hexene.

Catalyst	Time (hr)	Avg TOF (min^{-1})	Aldehyde (TON)	L:B	Isomer (%)	Alkane (%)
DEPBz (55.2 bar) [Co] = 0.01 mM [1-hexene] = 1 M	3	58.6	10,600		19.3	0.3
	20	48.6	58,200	1.2	34.4	1.0
DPPBz (50 bar) [Co] = 6 μM [1-hexene] = 6 M	24	64.8	93,000		24.2	0.4
	41	74.6	179,000	0.9	34.2	0.5
DPPBz (50 bar) [Co] = 3 μM [1-hexene] = 6 M	336 (2 weeks)	59.5	1,200,000 (includes 21.5% heavy ends)	0.9	40.8	1.2

All catalytic runs were done in tetraethylene glycol dimethyl ether (t-glyme) solvent with 0.1M heptane as internal standard at 160°C using 1:1 H_2 :CO.

Another way to test catalyst stability is to monitor catalyst degradation. Since the active catalyst species is paramagnetic and the monitoring needs to be done under reaction conditions

most traditional analytical techniques such as NMR are not useful. However, one analytical tool that is very useful is IR as the carbonyl peaks will shift position and change in intensity if any catalyst deactivation is occurring. Figure 4.1 shows the IR spectra in the carbonyl region over a 63 hour period.⁶

The ReatIR data shown in Figure 4.1 is from the same 101 hour study discussed in Chapter 2 with the focus now being on the time frame from 33.0 hrs to 96.4 hrs. Prior to the 33.0 hr spectrum shown the catalyst solution had been heated to 140°C and cooled to room temperature twice before being heated to 120°C for even longer term stability testing. The IR spectra of the catalyst carbonyl region shows very little change from 33.0 to 96.4 hrs, indicating excellent catalyst stability under H₂/CO without any alkene substrate present.

As the catalyst activates the carbonyl bands at 1939 cm⁻¹ ([Co(acac)(CO)(DPPBz)]⁺) and 1888 cm⁻¹ ([Co₂(μ-CO)₂(CO)(DPPBz)₂]²⁺) disappear constant with both species being converted to the [HCo(CO)_x(DPPBz)]⁺, x = 1-3, catalyst. Likewise the increase in active catalyst concentration also increases the intensity of the 19e- tricarbonyl peak at 2084 cm⁻¹. The peak at 2026cm⁻¹ also begins to show shoulders as the concentration of active catalyst increases and an equilibrium distribution of monocarbonyl, dicarbonyl and tricarbonyl species is reached. Taking into account these changes the stability of the catalyst under these conditions appears to be excellent over the 63.4 hr period at 120°C. The complete lack of catalyst deactivation was further verified after this catalyst solution for the 100 hr ReactIR study was later tested for hydroformylation activity in the autoclaves with no noticeable loss in activity or selectivity.

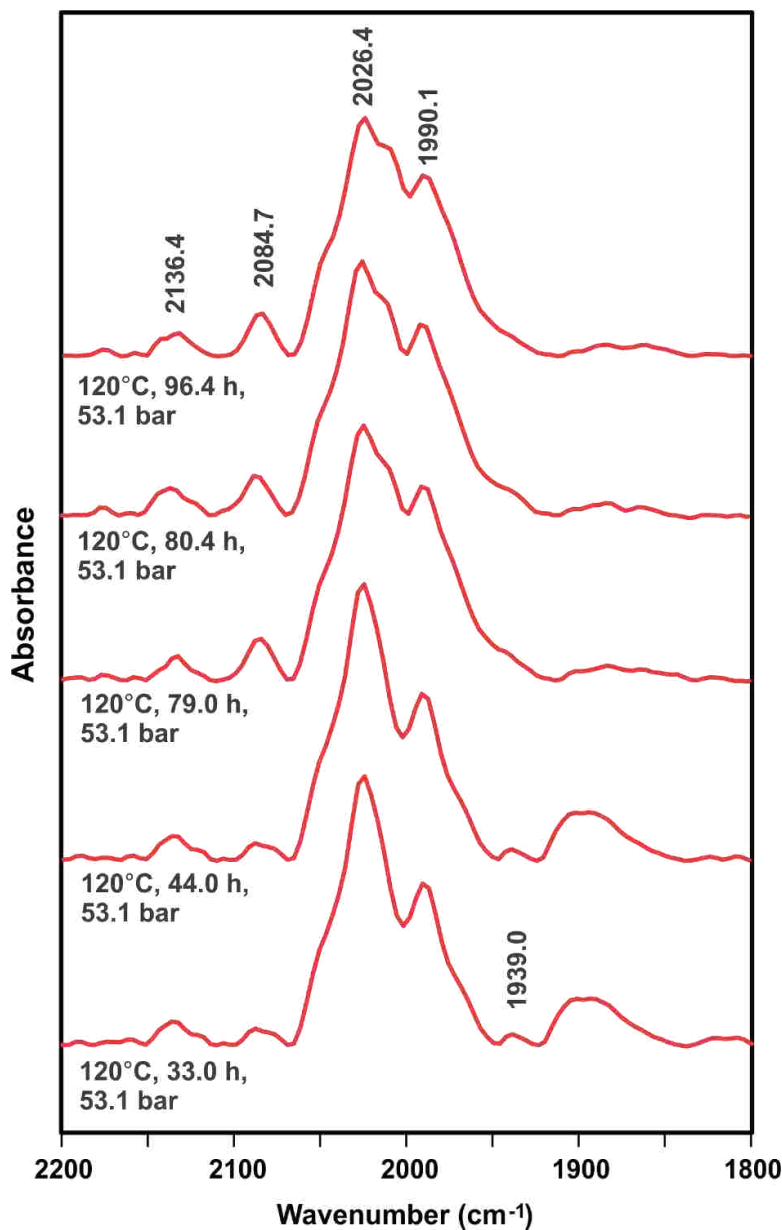


Figure 4.1. Extended FT-IR study of $[\text{Co}(\text{acac})(\text{DPPBz})](\text{BF}_4)$ under H_2/CO : 33 to 94 hours. 10 mM catalyst precursor dissolved in tetraethylene glycol dimethyl ether (t-glyme), 1:1 H_2/CO , temperatures and pressures as indicated on spectra

While testing the limits of catalyst stability a few catalyst decomposition products were observed under less than ideal reaction conditions. One such species was a double ligand cobalt (+1) complex with a single carbonyl ligand, $[\text{Co}(\text{CO})(\text{DPPBz})_2]^+$. This complex precipitated out of the reaction solution as orange-red crystals that were characterized by NMR, IR and X-ray

crystallography. The crystal structure is shown below in Figure 4.2 as a thermal ellipsoid plot using 50% probability ellipsoids. The BF_4 counter anion and hydrogen atoms are omitted for clarity. Only the first carbon atom of the phenyl rings on the phosphorus centers are shown for clarity. These crystals and decomposition product has only been observed in autoclaves when the catalyst being tested has poor solubility. Additionally this complex has only been observed twice in the ReactIR once on the bottom Teflon seal connecting the probe to the Parr reactor and again when the catalyst was first soaked in pure carbon monoxide overnight before being activated with H_2/CO .

In the first case only a small amount of microcrystalline material was observed on the Teflon seal in a location that experienced higher temperatures than the solution being studied as well as an environment that would be have a low H_2/CO gas concentration. There is an extremely small gap between the SiComp probe that inserts in from the bottom of the high-pressure IR cell and the main stainless steel housing. The flat Teflon O-ring seals the bottom of the IR probe to the main cell body to make a pressure seal. Whatever solution you put into the high-pressure cell seeps down between the probe and cell body to the Teflon O-ring. Thus, it is very important to fully disassemble and clean the cell after each study. A FT-IR was run on the orange-red microcrystalline material on the Teflon O-ring, showing a strong CO stretch at 1910 cm^{-1} .

In the second case a large number of orange-red crystals were found after activating the DPPBz-based catalyst precursor with H_2/CO , but then allowing it to sit overnight under pure carbon monoxide before purging and refilling with H_2/CO . Once again, a FT-IR on this material showed a strong CO band at 1910 cm^{-1} showing that it was the Co(I) double-DPPBz ligand complex. Since the CO band at 1910 cm^{-1} is normally never observed during our ReactIR studies

under H₂/CO, there must be some effect induced by soaking the catalyst in pure carbon monoxide for an extended period. The most likely explanation is that even after purging the reactor down to remove CO some CO remained dissolved in solution such that when the reactor was charged with H₂/CO the resulting gas ratio was not 1:1 but rich in CO. The higher CO concentration under these conditions induced ligand dissociation to form large quantities of the double ligand complex seen in Figure 4.2.

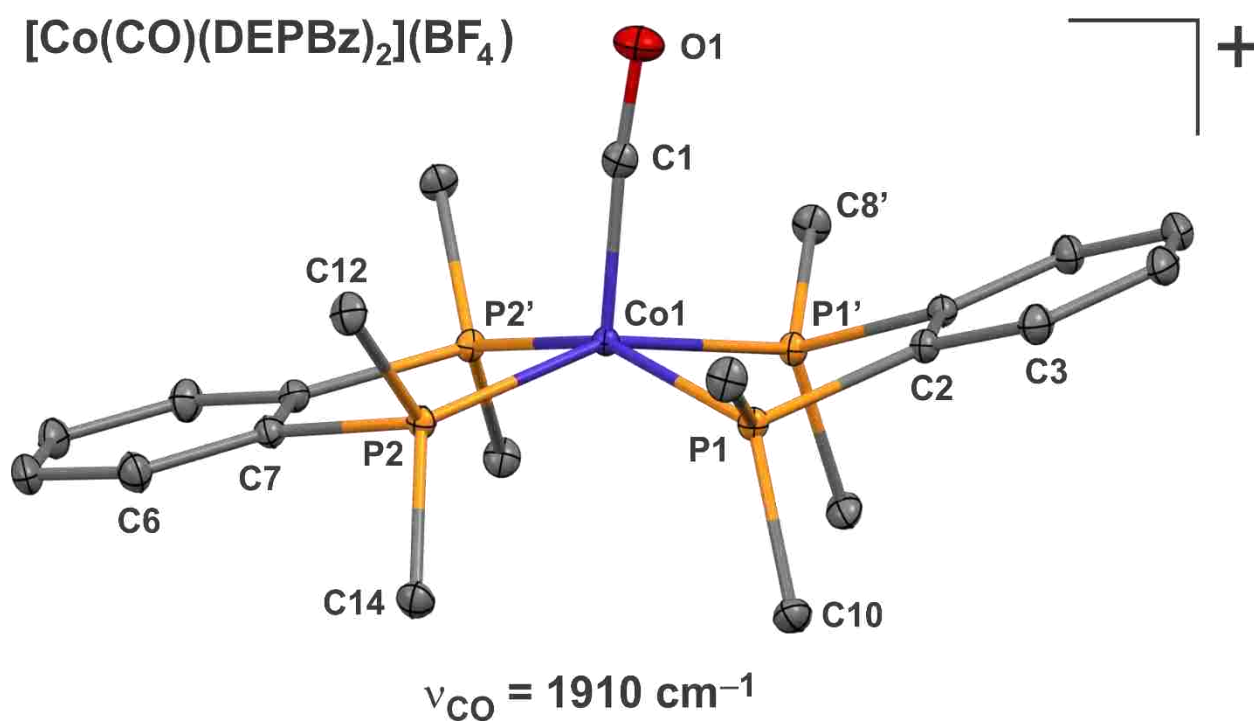


Figure 4.2. Thermal ellipsoid plot of [Co(CO)(DPPBz)₂]⁺.

Figure 4.3 shows the FTIR spectra of the double ligand decomposition product, [Co(CO)(DPPBz)₂](BF₄), that was collected as orange-red crystals. There is a single large carbonyl stretching frequency at 1910cm⁻¹ which is quite distinct from the carbonyl stretching frequencies observed in the ReactIR for what is believed to be active catalyst. The ³¹P NMR for this complex was collected in deuterated acetonitrile showing a signal peak with a 61.9 ppm

chemical shift. The ^1H NMR was also collected showing three main peaks at 3.57, 3.50, and 3.32 ppm corresponding to the phenyl groups of the ligand. Several small peaks were also observed from 8.0 ppm to 6.5 ppm and are attributed to the phenyl backbone of the DPPBz ligands.

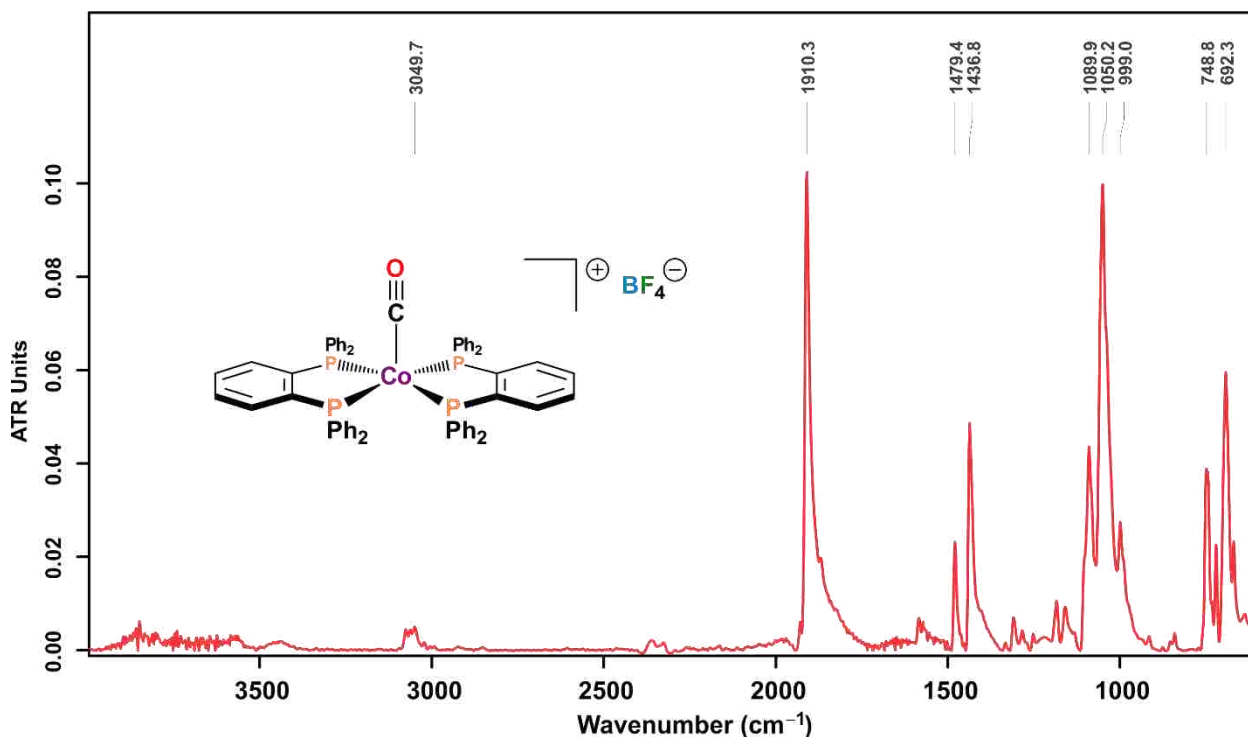


Figure 4.3. FT-IR of [Co(CO)(DPPBz)₂](BF₄).

4.6. References

1. Börner, A., Franke, R., *Hydroformylation Fundamentals, Processes, and Applications in Organic Synthesis*. Wiley-VCH, 2016.
2. Hebrard, F., Kalck, P., Cobalt-Catalyzed Hydroformylation of Alkenes: Generation and Recycling of the Carbonyl Species, and Catalytic Cycle. *Chem.Rev.*, **2009**, 109, 4272-4282.
3. Franke, R., Selent, D., Börner. A., Applied Hydroformylation. *Chem. Rev.* **2012**, 112, 5675–5732.
4. Beller, M., Albert Renken, A., van Santen, R.A., *Catalysis: From Principles to Applications*. Wiley, 2012.
5. Aubry, D.A., Bridges, N.N., Ezell, K., Stanley, G.G., Polar Phase Hydroformylation: The Dramatic Effect of Water on Mono- and Dirhodium Catalysts. *J. Am. Chem. Soc.* **2003**, 125, 11180-11181.

6. Crabtree, R. *The Organometallic Chemistry of the Transition Metals*. Wiley: 2014.

Chapter 5. Hydroformylation Using Cationic Cobalt Catalysts with Different Alkenes

5.1. Introduction

Historically there have been four generations of hydroformylation catalyst technologies starting with the unmodified cobalt and rhodium carbonyl catalysts, $\text{HCo}(\text{CO})_4$ and $\text{HRh}(\text{CO})_4$. Then phosphine-modified cobalt catalysts were discovered by Shell in the early 1960s. Next the phosphine modified rhodium catalysts were discovered by Wilkinson in the mid-1960s, which ushered in a new era of low pressure oxo technology. Finally, the most recent generation of chelating bisphosphine and bulky bisphosphite-modified rhodium catalysts were developed and offer exceptionally high L:B aldehyde selectivities and, for the bulky bisphosphite ligands, very high activity. The chelating phosphine/phosphite ligands, unfortunately, suffer from rhodium-induced ligand fragmentation reactions that limit catalyst lifetimes. Each generation offers some improvement over the previous class of catalysts, usually fulfilling a product application or major engineering improvement.¹

The first generation of hydroformylation catalysts are the unmodified $\text{HCo}(\text{CO})_4$ and $\text{HRh}(\text{CO})_4$ catalyst systems. These are the most active hydroformylation catalysts but they require very high partial pressures of CO to maintain stability limiting their applications. Low to modest L:B aldehyde selectivities (1 to 4) are seen for these catalysts, but their high activity allows them to react with internal branched alkenes and still produce linear aldehyde via highly active alkene isomerization ability. Access to internal alkenes is advantageous since many industrial alkene feeds are not pure alpha olefins and the internal alkene feeds often have fewer uses and are low cost. The activity of these catalysts towards internal and branched alkenes is unrivaled even today, which is why the high-pressure $\text{HCo}(\text{CO})_4$ and $\text{HRh}(\text{CO})_4$ catalysts are still in use today.²

The second generation of hydroformylation systems are phosphine ligand modified cobalt catalysts, $\text{HCo}(\text{CO})_3(\text{PR}_3)$. These were discovered by Shell in the 1960s and are still in use today being tightly tied to Shell's Higher Olefin Process (SHOP) where ethylene is oligomerized and converted via hydroformylation into detergent grade long chain linear alcohols. The phosphine-modified cobalt catalysts differ significantly from $\text{HCo}(\text{CO})_4$ in that significantly lower pressures can be used and much higher product L:B ratios of 8:1 are produced despite starting with internal alkenes. The coordinated phosphine ligand increases the hydricity of the catalyst and makes it a much better hydrogenation catalyst, which has good and bad aspects. $\text{HCo}(\text{CO})_3(\text{PR}_3)$ can hydrogenate the aldehydes produced from hydroformylation into alcohols, which is the desired product. Unfortunately, the increased hydrogenation activity also hydrogenates the alkene leading to high alkane side products on the order of 10-20%.^{1,3}

The third generation of hydroformylation catalysts are the phosphine modified rhodium catalysts that proved to be extremely active under mild conditions. The Rh/ PPh_3 catalyst system produces high L:B selectivity of 8 to 20:1 depending on the 1-alkene and concentration of PPh_3 used. Propylene hydroformylation to eventually produce 2-ethylhexanol is the single largest product from Rh/ PPh_3 hydroformylation. This process is typically operated at 110°C and 10 bar of 1:1 H_2/CO . Rh/ PPh_3 catalysts are used exclusively with 1-alkenes since the catalyst is not very active for alkene isomerization and, therefore, unsuitable for reacting with internal alkenes to produce linear products.^{1,4}

The fourth generation of hydroformylation catalysts are the larger bite-angle chelating bisphosphine and bulky bisphosphite modified rhodium catalysts that are highly selective for producing linear aldehyde products, offering L:B selectivities of 50-150:1 for 1-alkenes. The bulky bisphosphite ligands were developed by Union Carbide (now Dow Chemical) in the mid-

1980s and make rhodium hydroformylation catalysts with extremely high activity and selectivity. They also offer reasonably high alkene isomerization activity making them suitable for internal alkenes. 2-butene, for example, can be hydroformylated with a rhodium-bisphosphite catalyst to produce 25:1 L:B aldehyde. Unfortunately, both the bisphosphine and bisphosphite-based rhodium catalysts suffer from ligand degradation reactions that result in short catalyst lifetimes. The short catalyst lifetimes have significantly limited the industrialization of these catalysts.^{1,4}

5.2. Alfa Olefin Hydroformylation

Alfa olefins (α -olefins, 1-alkenes) are classified as any alkene in which the double bond is terminally located. Technically this means that branching or other functionalization could occur elsewhere, however; normally α -olefins are assumed to be linear and unfunctionalized. Commercially the most important α -olefin used as a hydroformylation feedstock is propylene. Propylene accounts for approximately 70% of hydroformylation products produced annually.¹

Table 5.1 shows the hydroformylation results for $[\text{Co}(\text{acac})(\text{DPPBz})](\text{BF}_4)$ and α -olefins of various lengths. The highest hydroformylation activity is seen for 1-hexene, as expected since 1-hexene is the smallest alkene studied here and, therefore, should be the fastest from a kinetic viewpoint with any hydroformylation catalyst. This reactivity trend continues with 1-octene more active than 1-decene. Due to the high isomerization activity of the catalyst the L:B selectivity drops with increasing alkene chain length. No alkane side-product is observed for 1-octene or 1-decene mostly likely due to the overall lower activity of the alkene.⁵

Table 5.1. Hydroformylation Activity of [Co(acac)(DPPBz)](BF₄) with some α -Olefins.

Alkene	Aldehyde (%)	Aldehyde L:B	Alkane (%)	Isomers (%)
1-Hexene	76.8	1.1	1.4	18.9
1-Octene	63.2	0.9	0	34.1
1-Decene	58.2	0.8	0	36.9

All reactions were run for 1hr with 1M alkene, 1mM [Co(acac)DPPBz]BF₄ catalyst, and 0.1M heptane as internal standard at 160°C under 725psi 1:1 H₂:CO. Samples were analyzed by GC/MS.

Figure 5.1 shows the aldehyde product distribution for the hydroformylation of hexene, octene, and decene (Table 5.1) in red for the corresponding aldehyde location. The fact that terminal double bonds are more active for hydroformylation is well known and can clearly be seen in Figure 5.1 where the aldehydes in the 1 and 2 position make up the majority of the product distribution for all alkenes. Interestingly for the 1-decene product distribution the catalyst seems to have very little preference between producing the aldehyde product in the 3 or 5 carbon positions. Clearly the additional steric hindrance of the more internal double bonds have little effect on the catalyst activity and where the aldehyde ends up on internal carbons for longer chain alkenes.

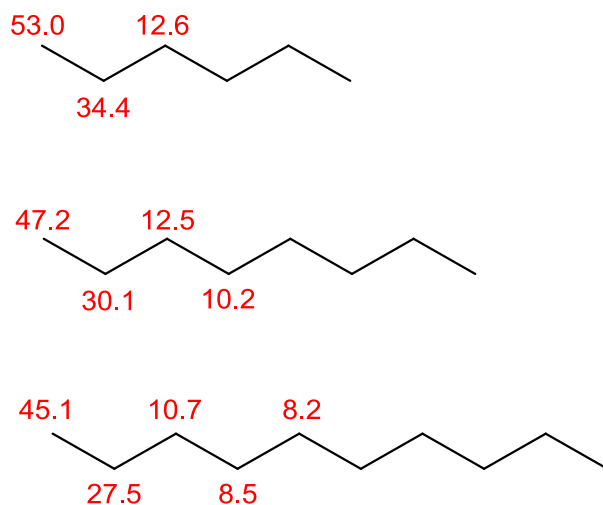


Figure 5.1. Aldehyde selectivity for $[\text{Co}(\text{acac})(\text{DPPBz})](\text{BF}_4)$ for the hydroformylation of 1-hexene, 1-octene, and 1-decene (Table 5.1).

Given the high isomerization activity of the cationic cobalt catalyst an alkene that could not be isomerized was needed to test the hydroformylation activity of the catalyst relative to several rhodium hydroformylation catalysts. The alkene chosen for this test was 3,3-dimethylbutene and for benchmark comparisons two of the most active rhodium based hydroformylation catalysts were used. Table 5.2 shows the comparison between several cationic cobalt based catalyst and the benchmark rhodium catalyst. The observe rate constant ($k(\text{obs})$) was calculated from H_2/CO gas consumption data with the cobalt runs based on 2 hr samples and the rhodium runs based on 20 min samples. The cobalt catalysts were activated at 160°C for 5 mins then cooled to operating temperature to ensure all of the catalyst was activated. The ligands used as well as the alkene tested in Table 5.2 are shown in Figure 5.2.

Table 5.2 shows that the rhodium catalysts are clearly more active for hydroformylation using 3,3-dimethylbutene, as expected. However, comparing the rate constant observed for the most active cobalt catalyst and the rhodium catalyst reveals that the rhodium catalyst is only about 10 times faster than the DEPbZ-based cationic cobalt(II) catalyst. This is quite impressive

when one considers that all other cobalt hydroformylation catalysts are regarded as being hundreds of times less active than rhodium.^{1,5} The cobalt is run under higher temperatures and pressures in Table 5.2 so we believe it is safe to say that rhodium is 20 times faster than our cationic cobalt(II) bisphosphine catalyst system.

Table 5.2. Hydroformylation of 3,3-Dimethylbutene by Cobalt and Rhodium Catalysts.

Catalyst	Temp (°C)	Press (bar)	Time (min)	Aldehyde (%)	Aldehyde L:B	Alkane (%)	$K(\text{obs}) \times 10^{-4}$ ($M \text{ sec}^{-1}$)
[Co(acac)(DPPBz)]BF ₄	140	30	120	60.0(3.8)	58	0.8(0.02)	1.4(2)
[Co(acac)(dppe)]BF ₄	140	30	120	64.1(3.5)	57	1.0(0.1)	1.5(1)
[Co(acac)(depe)]BF ₄	140	30	120	77.1(1.0)	54	1.2(0.05)	2.1(1)
[Co(acac)(DEPBz)]BF ₄	140	30	120	84.8(1.7)	51	1.2(0.1)	2.6(1)
RH:Biphenphos (1:3)	120	15	20	96.4(0.2)	All linear	3.3(0.06)	25(1)
Rh:PPh ₃ (1:400)	120	10.3	20	91.1(2.1)	34	0.3(0.04)	21(2)

All reactions were run with 1.0 M 3,3-dimethylbutene, 1.0 mM catalyst, 0.1 M heptane as internal standard, and 1:1 H₂/CO. Cobalt reactions were run in t-glyme solvent. Rh(acac)(CO)₂ was used as the catalyst precursor and run in toluene with the following excess phosphine:Rh ratios: 3:1 for the chelating biphenphos ligand, and 400:1 for PPh₃:Rh.

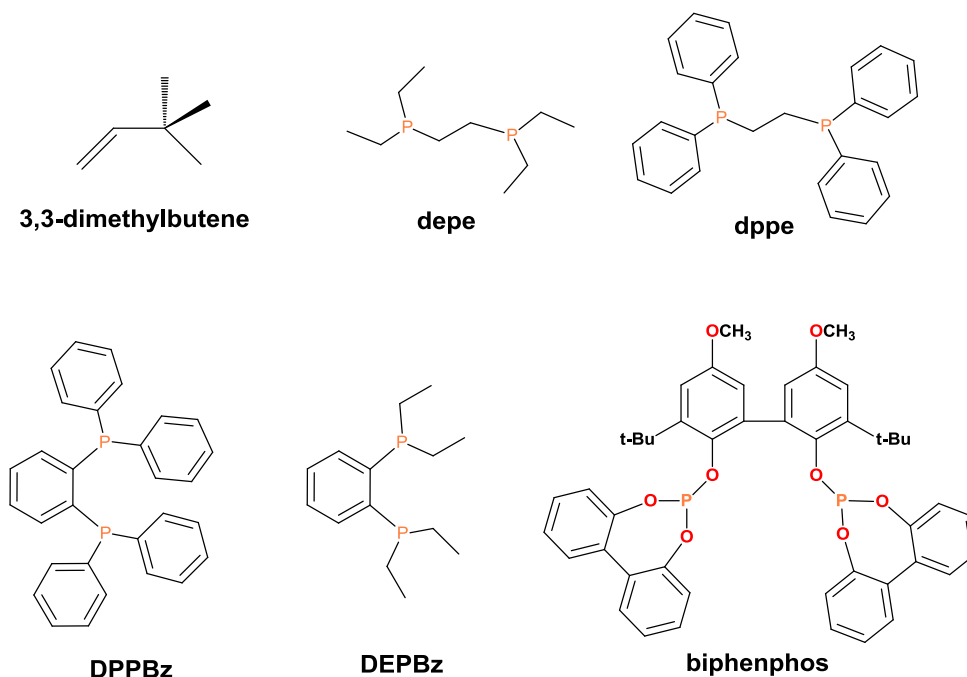


Figure 5.2. Alkene and ligands used for rhodium rate comparisons

Ligand effects can also be observed in Table 5.2 with the with the more electron rich and less sterically hindered ethyl arm phosphines giving higher rates than the bisphosphine ligands with phenyl groups. This is clear when looking at the observed rate constants for the dppe and depe catalyst as well as the DPPBz and DEPBz catalyst since swapping the phenyl groups out for ethyl groups resulted in a significant rate enhancement. This is most likely due to the more electron donating bisphosphine ligands enhancing CO binding and favoring the proposed 19e- tricarbonyl catalyst that labilizes the equatorial Co-CO ligand for alkene coordination. This is another dramatic difference between this cationic cobalt(II) catalyst and rhodium-phosphine catalysts. Electron-donating phosphine ligands are very poor ligands for rhodium hydroformylation catalysts. We observe exactly the opposite for this cationic Co(II) bisphosphine catalyst, which, once again, supports our 19e- catalyst proposal. The less bulky alkylated bisphosphine ligands also reduce steric hindrance allowing the bulky 3,3-dimethylbutene alkene to coordinate more easily. But we believe the electronic-effect is considerably more important.

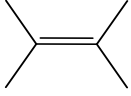
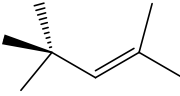
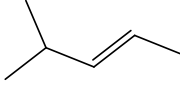
5.3. Internal and Branched Olefin Hydroformylation

Internal and branched olefins are often overlooked in academic hydroformylation research as they generally give low reaction rates, poor L:B aldehyde selectivity, and are less compatible with the far more studied rhodium technologies. Industrial internal branched alkene feeds are often a complex mix of isomers and chain-lengths. This requires the selection of pure model alkenes for this type of academic study in order to get better rate and selectivity data. Ideally these model alkenes will provide some insight into how the catalyst would handle industrial feeds.⁶

Table 5.3 presents three model internal branched alkenes that were evaluated using our cationic cobalt(II) bisphosphine catalyst, the Rh/PPh₃ industrial catalyst, and the Rh/biphenphos bulky bisphosphite system. The [Co:depe]⁺ (depe = Et₂PCH₂CH₂PEt₂) catalyst system was chosen because the alkylated bisphosphine ligands generate the most active hydroformylation catalysts that operate under the mildest conditions. Although Table 5.2 demonstrated that the [Co:DEPBz]⁺ catalyst is the most active, DEPBz is not commercially available and needs to be synthesized in our group. The DEPBz synthesis is challenging and time-consuming, so it is more efficient to purchase depe ligand.

The first alkene in Table 5.3, 2,3-dimethyl-2-butene (tetramethylethylene), is the most difficult to hydroformylate, and clearly shows the limitations of the rhodium catalysts as even after 6 hrs no alkene transformations were observed including alkene isomerization or hydrogenation. The [Co:depe]⁺ catalyst was able to convert almost a quarter of the alkene into aldehyde as well as converting an additional 10% into a more active 1-alkene isomer. The pressure difference between the cobalt and rhodium reactions is considerable and must be taken into account when comparing activity. Comparing catalyst at different pressures is difficult and normally if two catalyst had roughly equivalent activities, but one was evaluated at a higher H₂/CO pressure, then that catalyst would be considered less active. However, in this case the lower pressure cannot make up for a complete lack of activity observed with the rhodium catalyst; especially when considering that the rhodium catalyst are not stable under the higher pressure of the cobalt reaction.

Table 5.3. Results for Difficult to Hydroformylate Internal Branched Alkenes.

Alkene	Catalyst	Temp (°C)	Press (bar)	Aldehyde (%)	Aldehyde L:B	Alkane (%)	Isomer (%)
	[Co:depe] ⁺	140	30	24.9	All linear	0	10.0
	Rh:biphenphos	120	15	0	--	0	0
	Rh:PPh ₃	120	10.3	0	--	0	0
	[Co:depe] ⁺	140	30	26.9	All linear	3.7	33.5
	Rh:biphenphos	120	15	0.8	All linear	0	2.8
	Rh:PPh ₃	120	10.3	0	--	0	0
	[Co:depe] ⁺	140	30	54.7	4.4	0	32.1
	Rh:biphenphos	120	15	81.7	28	1.9	14.8
	Rh:PPh ₃	120	10.3	62.0	0.4	0	8.4

All reactions were run for 6 hrs with 1.0 M alkene, 1.0 mM catalyst, 0.1 M heptane as internal standard, and 1:1 H₂/CO. [Co:depe]⁺ = [Co(acac)depe]BF₄ and the cobalt reactions were run in t-glyme solvent. Rh(acac)(CO)₂ was used as the catalyst precursor and run in toluene with the following excess phosphine:Rh ratios: 3:1 for the chelating biphenphos ligand, and 400:1 for PPh₃:Rh.

The second alkene, 2,4,4-trimethyl-2-pentene, is also a very difficult alkene to hydroformylate. The rhodium triphenylphosphine catalyst, once again, did not show any catalyst activity. The rhodium bisphosphite catalyst was able to produce some aldehyde but with very low conversions achieving only 8 turnovers. The cationic cobalt(II) bisphosphine catalyst again showed significantly higher activity than the rhodium catalysts converting 26.9% of the alkene into aldehyde and another 33.5% into the more active 1-alkene isomer, while still maintaining exceptionally high linear selectivity (no branched aldehyde detected). The cobalt catalyst again is vastly superior relative to the rhodium catalysts for the hydroformylation of a bulky internal alkene.

The third alkene *trans*-4-methyl-2-pentene is a significantly easier to hydroformylate substrate compared to the first two alkenes. This is clearly shown in the data as both rhodium catalysts are now converting considerable portions of the alkene to aldehyde. The Rh/PPh₃ catalyst is able to convert 62.0% of the alkene although the low isomerization activity of this

catalyst also results in a very low L:B selectivity of 0.4. The rhodium bisphosphite catalyst proves to be much more active and selective for internal alkenes converting 81.7% of the alkene into aldehyde with a L:B selectivity of 28. But the rhodium bisphosphite catalyst did show clear signs of catalyst degradation with the rates dropping drastically over the first few hours and was inactive after three hours.

The $[\text{Co:depe}]^+$ catalyst had the lowest rate converting only 54.7% of the alkene into aldehyde but with the second best L:B selectivity of 4.4. Also worth noting is that the cationic cobalt(II) catalyst is not being evaluated under ideal conditions while the rhodium catalyst are much closer to optimum reaction conditions. The rhodium phosphite catalyst clearly gave the highest selectivity, however; given the short catalyst lifetime a convincing argument can be made for the cationic cobalt still being the better catalyst since modest selectivities are still achieved under reasonably modest conditions while retaining a high degree of catalyst stability. The $[\text{Co:depe}]^+$ catalyst clearly outperformed both rhodium catalysts for the first two alkenes and on the basis of L:B selectivity even beat the Rh/PPh_3 for the last and easiest to hydroformylate alkene.

The new cationic cobalt(II) bisphosphine catalyst presented here represents the fifth generation of hydroformylation catalysts. Having high hydroformylation activity under mild reaction conditions for a cobalt based catalyst is unprecedented. Unlike the phosphine-modified rhodium catalysts, this catalyst has not shown any signs of cobalt-induced phosphine ligand fragmentation reactions. Thus, the $[\text{HCo}(\text{CO})_x(\text{P}_2)]^+$ catalyst system has remarkable catalyst stability without any added excess phosphine ligand. The high alkene isomerization activity offers considerable advantages for difficult to hydroformylate internal branched alkenes. Currently only low L:B selectivities are accessible with 1-alkenes, but modification of the

bisphosphine ligand provides an important handle for dramatically increasing the selectivity.

Given the early stages of development this new cationic catalyst system has enormous potential to outperform many other hydroformylation catalysts currently in use today.

5.4. References

1. Franke, R.; Selent, D.; Börner, A. Applied Hydroformylation. *Chem. Rev.* **2012**, 112, 5675.
2. Hebrard, F.; Kalck, P. Cobalt-Catalyzed Hydroformylation of Alkenes: Generation and Recycling of the Carbonyl Species, and Catalytic Cycle. *Chem. Rev.* **2009**, 109, 4272.
3. Tucci, E.R. Organophosphorus Complexes of Cobalt Carbonyl as Hydroformylation Catalyst. *I&CE*. 1969, 8, 286.
4. Cornils, B.; Herrmann, W. A. Applied Homogeneous Catalysis with Organometallic Compounds. Wiley: 2002.
5. Bhaduri, S.; Mukesh, D. *Homogeneous Catalysis: Mechanisms and Industrial Applications*. Wiley: 2014.
6. Börner, A., Franke, R., *Hydroformylation Fundamentals, Processes, and Applications in Organic Synthesis*. Wiley-VCH, 2016.

Chapter 6. Experimental Procedures

6.1. General Considerations

All reactions and preparations were performed under an inert atmosphere of nitrogen in either a Vacuum Atmospheres or MBraun Glovebox or using standard Schlenk techniques. All solvents were reagent grade or higher. When dealing with air-sensitive reagents, the solvents were degassed with nitrogen prior to use. Chemicals used were purchased from Aldrich or Strem Chemicals and used as received (degassed with nitrogen as needed).

^{31}P , ^{59}Co , and ^1H NMR spectra were recorded on either a Bruker AV-400 or AVIII-400 spectrometer. All ^1H NMR spectra were referenced internally to either added TMS (0.0 ppm) or to the residual solvent peak. All ^{31}P NMR spectra were referenced externally to 85% H_3PO_4 (0.0 ppm). ^{59}Co NMR were referenced to $\text{K}_3[\text{Co}(\text{CN})_6]$ (0.0 ppm). NMR data processing was done using Bruker Topspin 3.4 or MestReNova 11.0 software packages. Mass spectra were collected on an Agilent 6210 or 6230 Electrospray TOF instruments via direct injection of the sample dissolved in a 60:40 solvent system of acetonitrile and 0.1% formic acid/water.

FT-IR were collected on a Bruker Tensor 27 instrument equipped with a TDGS room-temperature detector. Bruker OPUS v8.0 software was used for data collection and processing. High-pressure/temperature FT-IR spectra were collected on a Mettler-Toledo ReactIR model 45m equipped with a liquid-nitrogen cooled MCT detector. This was connected with a fiber optic conduit to a Mettler-Toledo/Parr high pressure IR cell that used a SiComp (silicon ATR) probe. The high-pressure IR cell was modified with a Teflon gasket for the SiComp probe seal to the main cell body. This all-Teflon gasket makes a much better pressure seal compared to the original gasket that came with the IR cell. The head-piece of the IR cell was modified with Swagelok quick-connects equipped with solvent-resistant Markez O-rings to facilitate assembly

and cleaning. Mettler-Toledo iC IR v7.0 software was used for data collection. Bruker OPUS software was used to do baseline corrections on the data collected from the ReactIR system.

EPR spectra were recorded on a Bruker EMX spectrometer equipped with a standard ER-4102 resonator and an Oxford ESR-900 helium flow cryostat. Acquisition parameters were frequency, 9.475 GHz; modulation amplitude, 10 G; modulation frequency, 100 kHz; time constant, 164 ms; conversion time, 41 ms; sweep time, 84 s. EPR spectra were simulated using the “pepper” function in EasySpin version 5.2.20 (1).

Single-crystal X-ray structures were collected on Bruker APEX II diffractometers using Mo Ka radiation. The $[\text{Co}(\text{CO})(\text{DPPBz})_2](\text{BF}_4)$ structure was collected and solved by Dr. Frank Fronczek (LSU). The $[\text{Co}(\text{acac})(\text{DPPBz})](\text{BF}_4)$ structure was collected at ExxonMobil Baytown and solved by co-author Dr. Alex Carpenter.

Catalytic reactions were done in 160 mL Parr autoclaves modified with Swagelok quick-connects with solvent-resistant Markez O-rings for gas and other related connections to the autoclave, which allowed easy disassembly and cleaning. A Parr 4870 controller is interfaced with four autoclave systems and a Windows PC computer running SpecView v2.5 software to collect and analyze the temperatures, pressures, stirring rates, and times of catalytic runs. A schematic diagram of one autoclave system is shown in Figure 6.1 and a photograph of two autoclaves that share the three gas reservoirs in one hood is shown in Figure 6.2.

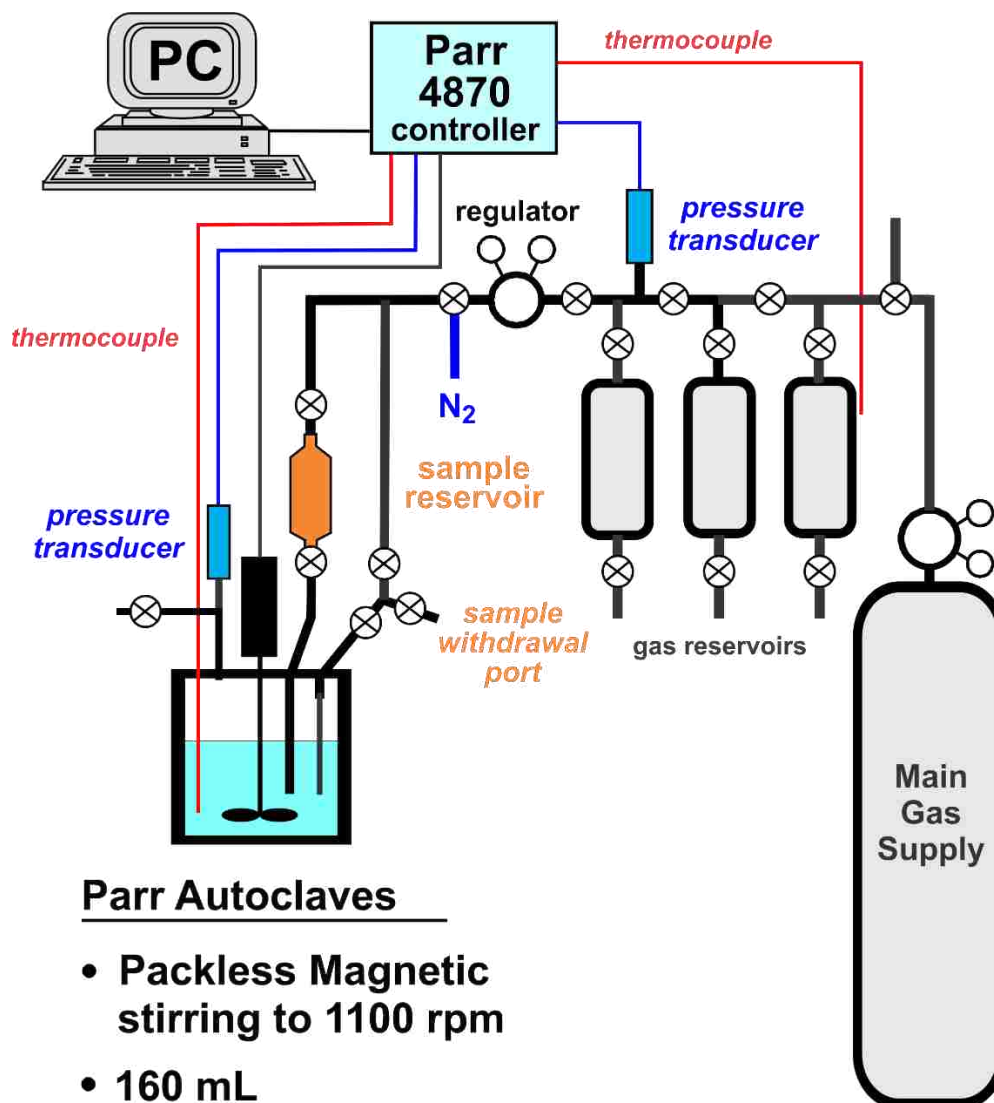


Figure 6.1. Schematic drawing of one of the Parr autoclave systems.

Schematic drawing of one of the Parr autoclave systems used in this study. The Parr 4870 controller is connected to four such autoclaves that can each be independently operated and data collected on the Windows PC using SpecView v2.5 software. Catalyst precursor solution is typically loaded directly into the autoclave via cannula from a Schlenk flask after flushing with N_2 or H_2/CO gas. Alkene is loaded into the sample reservoir, which is then pressurized with the system. The sample reservoir can be heated, if needed, via the use of heat tape and a temperature controller. Once the alkene is pressure added to the autoclave at reaction conditions, the H_2/CO gas is introduced via both inlets into the autoclave solution. Samples can be removed for analysis during a catalysis run via the sample withdrawal port. By closing the top and bottom valves of the sample port, gas pressure can be released via the side valve. Opening the bottom valve allows catalyst solution to be pressure pushed into the sampling area. Closing the bottom valve and opening the side valve allows a small sample to be removed. The catalyst solution remaining can then be returned to the autoclave by re-opening the top and bottom valves.

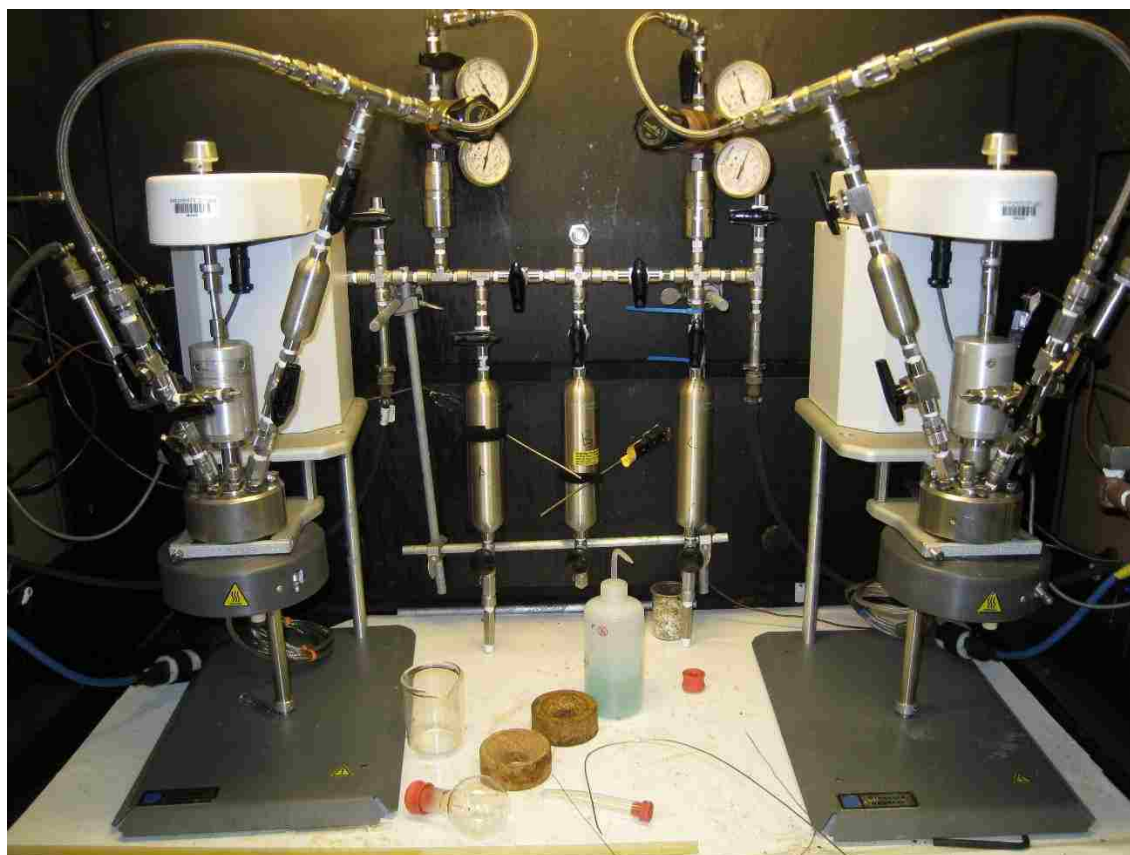


Figure 6.2. Photograph of two of the Parr autoclave systems.

Photograph of two of the autoclave systems used for hydroformylation studies reported. Each autoclave has a design shown in Fig. S1 and share the three gas reservoirs that can be dedicated to one or the other autoclave system. Autoclaves are located in a fume hood with a CO detector mounted at the front of the hood. They are connected to a Parr 4870 process controller, along with two other autoclaves in a separate hood.

6.2. General Hydroformylation Procedure

All runs reported with the exception of the million turnover run were run under conditions outlined below. The autoclave was first purged out with nitrogen then pressure was reduced under vacuum. After evacuated the alkene injection arm was sealed off from the rest of the autoclave. The alkene injection arm was charged with the desired amount of alkene via cannula using standard air free techniques. The catalyst solution which consist of the catalyst and

standard dissolved in a given solvent was transferred from a sealed flask to the autoclave via cannula using standard air free techniques. Next a steel hose was purged with H₂/CO gas while being attached to the alkene injection arm and the sampling arm. Once the hose was connected the regulator was set to the desired pressure and the sampling arm was opened to the autoclave. The pressure in the autoclave was set to the desired pressure using an electronic pressure transducer connected to a Parr process controller. The sample arm was then closed to reseal the autoclave after which the autoclave was set to the desired temperature. The autoclave was allowed to heat until the desired temperature was reached after which the autoclave pressure was reduced to approximately 90% of the desired pressure via the venting arm. The reaction was initiated by opening the sealed autoclave to the alkene injection arm. This was immediately followed by opening the valve between the alkene injection arm and the gas feed line. Finally the valve between the sampling arm and the gas feed line was opened. Samples were taken by closing the valve between the sampling arm and the gas feed line and opening the release valve on the sampling arm. The resulting solution was collected in a vial to be transferred to a GC vial for analysis.

The million turn over run was run identical to the standard run outlined above with one exception. The alkene injection arm was charged with catalyst solution and the autoclave was charged with pure alkene.

6.3. [Co(acac)(dioxane)_x]BF₄ Synthesis

5g of cobalt (II) acetylacetonate along with 150ml of dioxane (0.13M) is added to a 500ml two neck schlenk flask equipped with a condenser. The solution is heated to 60°C while stirring until all cobalt (II) acetylacetonate has dissolved. Then the solution is allowed to cool to 50-45°C before 3.3 g (1.05 equivalents) of tetrafluoroboric acid in ether is added to the solution

via cannula. Note the tetrafluoroboric acid ether complex has to be relatively fresh. We have noticed that if the acid is more than a month or two old the acid does not yield clean enough product. The resulting solution is allowed to stir overnight while returning to room temperature. The pink precipitate is collected on a glass frit and washed with ether. The resulting pink powder is then dried under vacuum overnight to remove excess dioxane. In order to obtain a final molecular weight for synthesis applications an NMR has to be done using D₂O as a solvent. The dioxane and acetylacetonate peaks are integrated and their respective areas correlated as shown below. The molecular weight of the starting material complex is calculated and used for further synthesis. Note that over time more dioxane will be lost by the solid so the calculated molecular weight does not stay constant over long periods of time. The molecular weight should be recalculated if more than a day or two has passed since the last calculation.

$$\# \text{ of Dioxanes} = \frac{6(\text{Area of Dioxane peaks})}{8(\text{Area of Acetylacetonate peaks})}$$

6.4. [Co(acac)(ligand)]BF₄ Synthesis

[Co(acac)(ligand)]BF₄ of a desired ligand is made by adding 0.1g of ligand dissolved in dichloromethane (DCM) (15mM) to 1 equivalent of [Co(acac)(dioxane)_x]BF₄ salt dissolved in acetone (10mM) slowly via pipet while stirring. The resulting solution is allowed to stir for 30mins and the solvent is then removed under vacuum. If the resulting solid is sticky (this occurs when large quantities of dioxane are left) then dissolve the material in DCM before removing the solvent under vacuum again. The resulting powder should be red to brown depending on the ligand bound.

6.5. Co(acac)₂DPPBz Synthesis

Co(acac)₂DPPBz is made by adding 0.174g of 1,2-bis(diphenylphosphino)benzene (DPPBz) dissolved in dichloromethane (DCM) (15mM) to a solution of 0.1g of Co(acac)₂ in

acetone (10mM) slowly via pipet while stirring. The resulting solution is allowed to stir for 30mins and the solvent is then removed under vacuum. The resulting powder should be a pale green.

6.6. [CoDPPBz](BF₄)₂ Synthesis

[CoDPPBz](BF₄)₂ is made by adding 0.131g of 1,2-bis(diphenylphosphino)benzene (DPPBz) dissolved in dichloromethane (DCM) (15mM) to a solution of 0.1g of [Co(H₂O)₆](BF₄)₂ in acetone (10mM) slowly via pipet while stirring. The resulting solution is allowed to stir for 30mins and the solvent is then removed under vacuum. The resulting powder should be a bright yellow.

Vita

Drew Hood is the only son of Layne Hood and Bridget Richie born in October of 1990 in Lake Charles, LA. He attended McNeese State University and received a Bachelor of Science in Mathematics in May of 2014. He became part of the Louisiana State University's graduate school to study chemistry in 2015. Drew is expecting to graduate from LSU with a Doctor of Philosophy in chemistry in May of 2019.